New Developments in Isoelectric Focusing and Dielectrophoresis for Bioanalysis

by

Noah Graham Weiss

A Dissertation Presented in Partial Fulfillment
of the Requirements for the Degree
Doctor of Philosophy

Approved November 2011 by the
Graduate Supervisory Committee:

Mark Hayes, Chair
Antonio Garcia
Alexandra Ros

ARIZONA STATE UNIVERSITY

December 2011

ABSTRACT

Bioanalytes such as protein, cells, and viruses provide vital information but are inherently challenging to measure with selective and sensitive detection. Gradient separation technologies can provide solutions to these challenges by enabling the selective isolation and pre-concentration of bioanalytes for improved detection and monitoring. Some fundamental aspects of two of these techniques, isoelectric focusing and dielectrophoresis, are examined and novel developments are presented.

A reproducible and automatable method for coupling capillary isoelectric focusing (cIEF) and matrix assisted laser desorption/ionization mass spectrometry (MALDI-MS) based on syringe pump mobilization is found. Results show high resolution is maintained during mobilization and β-lactoglobulin protein isoforms differing by two amino acids are resolved. Subsequently, the instrumental advantages of this approach are utilized to clarify the microheterogeneity of serum amyloid P component. Comprehensive, quantitative results support a relatively uniform glycoprotein model, contrary to inconsistent and equivocal observations in several gel isoelectric focusing studies. Fundamental studies of MALDI-MS on novel superhydrophobic substrates yield unique insights towards an optimal interface between cIEF and MALDI-MS. Finally, the fundamentals of isoelectric focusing in an open drop are explored. Findings suggest this could be a robust sample preparation technique for droplet-based microfluidic systems.

Fundamental advancements in dielectrophoresis are also presented. Microfluidic channels for dielectrophoretic mobility characterization are designed

which enable particle standardization, new insights to be deduced, and future devices to be intelligently designed. Dielectrophoretic mobilities are obtained for 1 μm polystyrene particles and red blood cells under select conditions. Employing velocimetry techniques allows models of particle motion to be improved which in turn improves the experimental methodology. Together this work contributes a quantitative framework which improves dielectrophoretic particle separation and analysis.

To the women in my life, my mother for guiding me to this point and my wife for ensuring I arrived in success.

ACKNOWLEDGMENTS

I begin with a special thanks to my advisor Dr. Mark Hayes. The experiences, challenges, and guidance you have given me during my time at ASU have transformed me into a new person. I thank you for your time, support, and belief in me.

Next I give thanks to my family. First and foremost I thank my beautiful wife and best friend Julie who has helped me tremendously through my entire graduate school journey. Thank you for keeping me grounded and for making every day special. Thanks to my mother who makes me aware of my strengths, challenges me on my weaknesses, and has provided me with so many great opportunities. Thanks to my father who is my inspirational scientist and must have planted scientific seeds in my brain many years ago. Thanks to my big brothers Seth and Jefferson who have taught me so much about the world and have been wonderful supporters in my life.

I could not have succeeded in graduate school without my peers. Thank you to Dr. Michelle Meighan for your friendship and for taking me under your wing in the early years of graduate school. Thank you to Dr. Josie Castillo for being a role model and for paving the way one step ahead of me. Thank you to Stacy Kenyon for being a good office mate and even better friend. Thank you to Paul Jones for late afternoon discussions (or was it venting?) over the origins of dielectrophoresis. Thank you to Dr. Prasun Mahanti for helping me understand things outside of my comfort zone. I am very fortunate to have been surrounded by such hard working and fun people.

There are many other people who deserve special recognition. Thank you to my committee members Dr. Alexandra Ros and Dr. Antonio Gartcia for your contributions toward my graduate education and for challenging me on my work. Thank you to those who contributed to my research projects: Nicole Zwick for guidance in isoelectric focusing, Dr. Randall Nelson for providing MALDI-MS facilities, Jason Jarvis for assistance in MSIA and ESI-MS, Dr. Tom Picraux for nanowire synthesis, Dr. Timo Park for help in superhydrophobic surfaces, Dr. Ana Egatz-Gomez for help in droplet isoelectric focusing, Dr. Rafat Ansari and Jim King for providing NASA facilities and mentorship, Dr. Kang P. Chen for and Dr. Tom Taylor for assistance in dielectrophoretic mobility framework, Saleh Gani for help in particle tracking, and finally the CSSER cleanroom staff for assistance in fabrication and for keeping my research projects alive.

Finally, I would like to acknowledge funding from the Jump Start Research Grant sponsored by the Graduate and Professional Students Association (GPSA). In addition, I am especially grateful to the GPSA for conference travel grant sponsorships which tremendously enriched my graduate school experience.

I would not be where I am today without help from all of these people. Thank you all dearly for your guidance and support.

TABLE OF CONTENTS

LIST OF TABLES

LIST OF FIGURES

Figure Page

Chapter 1

Introduction

1.1 Role of separation science in analytical chemistry

One of the most important principles of analytical chemistry is selectivity. Selectivity is defined as the "degree to which a method is free from interference by other species contained in the sample matrix" [1]. The integrity of any chemical measurement depends on a mechanism to selectively interrogate the desired component in a mixture. Selective probing techniques exploit a unique chemical or physical property associated with the analyte of interest. For example, energy states (spectroscopy and electrochemistry), mass to charge ratio (mass spectrometry), chemical reactivity (titrations), and ligand affinity (assay and biosensor) are frequently targeted to acquire selective chemical measurements. Often times, however, the targeted analyte does not have a distinctly unique property that can be targeted. In these instances chemical labels that react with the analyte of interest can be added to further enable improved selectivity. Common modifications include the addition of a fluorophore or chromophore (e.g., protein, DNA, or cell labeling) [2], isotope labeling [3], and enzyme or ligand linking [4] among many other techniques [5, 6]. Analytical measurements are limited by selectivity when probing mechanisms have insufficient selectivity, labeling methods are impractical, or mixed samples contain interfering species. The universal solution to overcome the limitation of analytical selectivity is chemical separations [7].

Separations allow for the isolation of pure components from mixtures so that a probes' response can be associated directly with a particular material. This opportunity was first realized and practiced through extractions where specific solvents could be used to isolate pure materials [7]. Today the field of separation science is now so advanced that enantiomers, protein isoforms, and single base differences in DNA are readily isolated from their very similar counterparts. In addition to purifying samples, separations can also serve as an analytical probe by monitoring outcomes spatially or temporally. The position or time in which a certain species is detected can be used to qualitatively identify it. Thus, separation science has and will continue to be an integral part of analytical chemistry by improving selectivity through purification and acting as an independent analytical probe.

1.2 Linear vs. gradient separations

For this dissertation, separation techniques are classified as being either linear or gradient. A linear separation is one characterized by a uniform transport force along the separation length. Chromatography and electrophoresis are common techniques exemplifying this where samples are loaded at one end, separation occurs due to differential transport rates, and species travel unidirectional towards the opposite end. Gradient separations on the other hand are characterized by having a multi-directional velocity gradient that varies across space. Some representative gradient separations include isoelectric focusing (IEF) and gradient dielectrophoresis (DEP).

The distinction between gradient and linear separations is important when considering the effects on analyte concentration relative to detection limits. “The most generally accepted qualitative definition of detection limit is that it is the minimum concentration or mass of analyte that can be detected at a known confidence level” [1]. In other words, analytical measurements become null when the amount of analyte falls below the detection limit. Thus, it is imperative to consider the effect a separation mechanisms has on the analyte concentration at the time of detection. This is particularly concerning for bioanalytes which are typically relatively dilute, costly or difficult to obtain, and exist in limited quantities.

In the case of linear separations, an analyte zone experiences a uniform transport force and is diluted over time through diffusion and other mechanisms such as multiple paths, heterogeneous flow profile, and mass transport effects (Fig. 1.1A). Sometimes conditions can be optimized to minimize these effects; however, even subtle dispersion processes can compromise the detection of bioanalytes which are near the detection limit threshold. Therefore, in many cases linear separations cannot be used when starting with relatively dilute or low total mass samples.

Gradient separations, in contrast, provide a restoring force to counteract the dispersion processes. The velocity profile varies across space such that analytes experience a net zero velocity in certain regions. They are transported to this focal point from all directions and they experience a restoring force if dispersion processes transport them away. In most instances the restoring force

can be used to increase the analyte concentration above starting levels (Fig. 1.1B). In addition, the position of the focal point in gradient separations depends on the properties of a particular analyte. Gradient separations are thus capable of simultaneously pre-concentrating and isolating individual components. Gradient separations are a highly advantageous alternative to linear separations when considering detection limits.

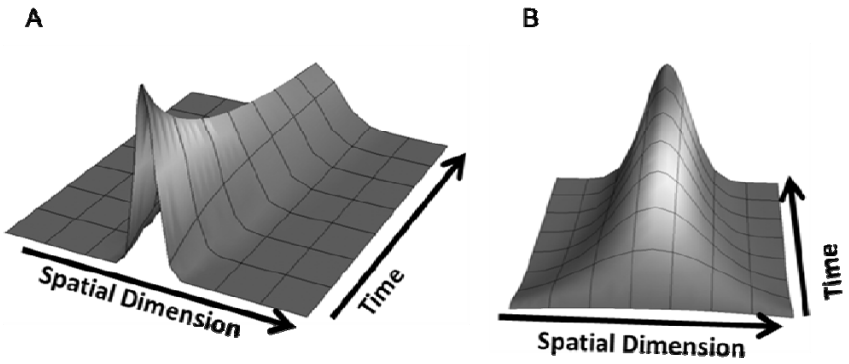

Figure 1.1. Linear vs. gradient separations. Hypothetical analyte concentrations as a function of time and space in (A) linear and (B) gradient separations.

1.3 The importance of bioanalytes

The trajectory of health care is headed towards that of personalized medicine [8-10]. This means the diagnosis, prognosis, and treatment of ailments is becoming increasingly more personalized and assessed on an individualized basis. Leading the charge for this movement are the 'omic' fields (genomics, proteomics, metabolomics, etc.) where unique expression patterns of biological molecules are observed between individuals. Thus, the reliance of multi-billion dollar industries such as diagnostics and pharmaceuticals on biomolecular

information is at an all-time high. Therefore, analytes of biological origin (bioanalytes) represent a vital source of information with enormous economic impact. Additionally, bioanalytes are critical to many other sectors including forensics, national security, food safety, and energy.

The value of bioanalytes is clear, however, their inherent complexity in terms of size, concentration, and diversity makes selective analysis very challenging. Ultimately, the understanding of biological systems and ability to discern relevant information directly depends on the availability of selective tools. Separation science has enormous impact towards this. Different types of bioanalytes are discussed below. In all instances, gradient separation technologies can improve bioanalysis by improving selectivity and pre-concentrating components.

1.3.1 Nucleic acids

DNA and RNA are highly valuable targets that describe the genetic code of organisms. These molecules provide key insights into biological mechanisms, enable biological engineering, and have enormous economic, social, and environmental impact. The properties of different nucleic acid strands are essentially identical because they are polymeric molecules assembled from only four different base nucleotides. Additionally, there are several thousand unique sequences of nucleic acid within a single cell. Therefore, separations are vital in the selective interrogation of nucleic acids [11]. Electrophoretic separations are the mostly widely used and are still being rigorously advanced today to enable rapid, highly specific DNA sequencing [12, 13].

1.3.2 Proteins

Proteins are the functional units of biology and are being increasingly sought after as targets to provide vital information about biological systems. Human cells have the capacity to express over 10,000 unique proteins which are polymeric molecules having anywhere from 20-2,000 of the twenty different amino acid monomers. This gives rise to shear diversity of the natural world and also makes analytical measurements very difficult. Therefore, in virtually all protein analyses a separation or purification step is employed to allow the proteins of interest to be targeted. Seemingly all separation techniques have been used for proteins, but most popular are immunoprecipitation [14], liquid chromatography [15], two-dimensional gel electrophoresis [16], and capillary electrophoresis [17].

1.3.3 Cells, organelles, and viruses

Larger bioparticles such as cells and viruses pose a unique separation challenge because of their size and dilute concentrations [18]. Many successful applications avoid employing separations altogether and selectively target cells/viruses with highly specific antibodies [19-21]. Although this approach is very successful, the use of antibodies is far from a universal solution because antibody production has its limitations and assays can require long times [22]. Therefore, technologies capable of performing cheap and fast purification and enrichment of cells and viruses are of high demand.

1.3.4 Other bioanalytes

In addition to those mentioned above many other bioanalytes provide vital information including: carbohydrates, lipids, bioparticle complexes, inorganic

materials, and metabolic derivatives. These molecular groups contain a diverse number of molecules having very similar structures. Thus, selective measurements are equally challenging for all types bioanalytes.

1.4 Overview of isoelectric focusing and dielectrophoresis

The bulk of this dissertation primarily employs two different gradient separation techniques: isoelectric focusing (IEF) [23] and dielectrophoresis (DEP) [24]. A brief introduction to these techniques is discussed here while Chapter 2 provides much more comprehensive detail. IEF relies on the force of electric fields on net charge while DEP is the force of electric field gradients acting on dipoles. pH gradients are employed in IEF while spatial gradients are employed in DEP to form velocity gradients. Besides these differences there are also many commonalities. Both techniques utilize an electric field within a defined geometry to move the sample components with a velocity that is dependent on their composition. Finally, these techniques are highly complementary in nature where DEP is best suited for large bioparticles (> 50 nm) and IEF is best suited for proteins (< 50 nm). Together they can enhance selectivity across the entire size spectrum of bioparticles while providing enrichment capabilities [25]. The applications within this dissertation are on protein separations in Chapters 3-6 and cell separations in Chapters 7-8.

1.5 Overview of MALDI-MS

Mass spectrometry (MS) exploits the separation of gas phase ions based on their mass and charge velocity dependence. Many different instruments exist and they can be distinguished by ionization source and ion selection method.

Methods for attaining ion selectivity include ion cyclone resonance, quadropole, fourier transform, and time of flight (TOF). There are also numerous ionization methods for introducing samples into the MS instrument. Matrix assisted laser desorption/ionization (MALDI) is a popular MS ionization mode for larger molecules including bioparticles [26]. In this technique, a laser is fired at a crystalline sample deposit enriched with an organic matrix. The matrix absorbs the laser light and becomes highly energetic leading to the vaporization and ionization of the analyte molecules. Studies of the fundamental processes reveal that multiple mechanisms may be involved and a precise understanding of the desorption/ionization dynamics remains out of reach [27, 28].

Like all MS analysis, MALDI-MS is useful because it allows for the structural and qualitative information to be determined. Usually singly charged ions are produced allowing the ions' mass to be directly determined. Therefore, MALDI-MS is highly valuable because it can provide very good resolution and unmatched qualitative detail of bioanalytes. Proteins are the most popular targets but all bioparticles are actively studied with MALDI-MS [29]. While the bulk of this dissertation emphasizes gradient separation techniques, MALDI-MS is a sub-topic because of its utility for bioanalyte detection.

1.6 Superhydrophobic surfaces

Hydrophobicity and hydrophilicity describes the degree to which a material is repelled and attracted to water, respectively. This property is quantified for solid surfaces by the contact angle of a resting water droplet between the solid-liquid and liquid-air equilibrium contact lines. Hydrophilic

materials have water contact angles less than 90°, hydrophobic between 90-150°, and superhydrophobic materials greater than 150°. Hydrophilic materials include polar materials such as glass and metals while hydrophobic materials include non-polar organic materials such as plastics and lipids. These are complex properties that depend on several factors including polarity, structure, and roughness [30, 31]. A roughened surface causes an enhancement in hydrophobicity or hydrophilicty compared to the same material having a smooth surface because of the increased interfacial surface area interacting with water. Therefore, superhydrophobic surfaces (SHS) are produced when a hydrophobic surface is roughened. SHS can be found among the leaves of many plant species where micro and nano scale fibers create roughened structures on the leaf [32]. There are several methods to synthetically roughen surfaces so that they become SHS [33].

Superhydrophobic surfaces provide a unique ability to control and manipulate aqueous droplets for some unique applications. Droplets have minimal surface area contact, maintain well defined spherical or ellipsoidal geometries, and have negligible surface adhesion. The field of droplet microfluidics utilizes these features to perform numerous automated, parallel, and small volume fluid manipulations. Using electric or magnetic fields, droplets can be moved, mixed, and split enabling means to perform chemical sample preparations in a unique format. Therefore, SHS play an important role in analytical chemistry and in bioanalysis by enabling new technologies. For this

dissertation SHS are utilized in Chapter 5 to study MALDI-MS signal dependencies and Chapter 6 to enable isolectric focusing in a drop.

1.7 Dissertation objectives

The purpose of this dissertation is to advance IEF and DEP to further enable high resolution bioanalysis. These techniques are related because they both rely on electric fields to move material in a composition specific manner, but they are suited best for different yet complimentary bioanalytes (IEF for proteins and DEP for cells). Together they provide a powerful platform for proteomic analysis: DEP provides means to isolate larger particle mixtures while IEF could subsequently separate protein substructures. However, both of these techniques are in need of a better understanding and technological advancement before such rich bioanalysis becomes commonplace.

Some weaknesses of IEF protein separations include poor detection capabilities and difficulty in automation. Chapter 3 presents some developments in coupling capillary IEF with mass spectrometric detection. In addition to improving the limits of detection, coupling to mass spectrometry enables unprecedented resolution in protein analysis. Furthermore, utilizing a capillary separation with MS detection lends itself to being completely automatable. These improvements are applied in Chapter 4 to characterizing a glycoprotein, serum amyloid P component (SAP), which allowed for an improved assessment of its microheterogeneity profile. In Chapter 6 droplet-based IEF (dIEF) is introduced as a potentially high-throughput, automatable sample preparation technique. Together the IEF related research in this dissertation demonstrates a number of

technological improvements which advance its suitability to protein analysis. Chapter 5 discusses findings and limitations of efforts to pre-concentrate analytes for MALDI-MS on a patterned superhydrophobic surface.

Current limitations in the field of dielectrophoresis include a lack of quantitative metrics and an understanding of behaviors within particle populations. Quantitative insights about dielectrophoretic responses of particles would greatly advance the field. Chapters 7-8 present a novel methodology for the determination of dielectrophoretic mobilities. Using simple, linear electric field gradients the dielectrophoretic motion of particles is quantitatively assessed. Advancements in the method and dielectrophoretic mobility findings are presented.

Cumulatively, the work presented here improves bioanalytical selectivity with advances in the complimentary techniques of isoelectric focusing and dielectrophoresis.

1.8 References

[1] Skoog, D. A., Holler, F. J., Crouch, S. R., *Principles of Instrumental Analysis 6th Ed.*, Thomson Brooks/Cole, Belmont 2007.

[2] Goncalves, M. S., *Chem. Rev.* 2009, *109*, 190-212.

[3] Jameson, C. J., *Isotopes in the Physical and Biomedical Sciences*, Elsevier Science Ltd., Amsterdam 1987.

[4] Maeda, M., *J. Pharm. Biomed. Anal.* 2003, *30*, 1725-1735.

[5] Chattopadhaya, S., Bakar, F. B. A., Yao, S. Q., *Curr. Med. Chem.* 2009, *16*, 4527-4543.

[6] Prange, A., Proefrock, D., *J. Anal. At. Spectrom.* 2008, *23*, 432-459.

[7] Giddings, J. C., *Unified Separation Science*, Wiley, New York 1991.

[8] Mancinelli, L., Cronin, M., Sadee, W., *AAPS PharmSci* 2000, *2*.

[9] Meyer, J. M., Ginsburg, G. S., *Curr. Opin. Chem. Biol.* 2002, *6*, 434-438.

[10] Bates, S., *Drug Discov. Today* 2010, *15*, 115-120.

[11] Smith, C. L., Cantor, C. R., *Methods Enzymol.* 1987, *155*, 449-467.

[12] Barron, A. E., Blanch, H. W., *Sep. Purif. Methods* 1995, *24*, 1-118.

[13] Sinville, R., Soper, S. A., *J. Sep. Sci.* 2007, *30*, 1714-1728.

[14] Firestone, G. L., Winguth, S. D., *Methods Enzymol.* 1990, *182*, 688-700.

[15] Paliwal, S. K., DeFrutos, M., Regnier, F. E., *Methods Enzymol.* 1996, *270*, 133-151.

[16] Lilley, K. S., Razzaq, A., Dupree, P., *Curr. Opin. Chem. Biol.* 2002, *6*, 46-50.

[17] Huang, Y. F., Huang, C. C., Hu, C. C., Chang, H. T., *Electrophoresis* 2006, *27*, 3503-3522.

[18] Radisci, M., Iyer, R. K., Murthy, S. K., *Int. J. Nanomedicine* 2006, *1*, 3-14.

[19] Langer, V., Niessner, R., Seidel, M., *Anal. Bioanal. Chem.* 2011, *399*, 1041-1050.

[20] Abdel-Hamid, I., Ivnitski, D., Atanasov, P., Wilkins, E., *Anal. Chim. Acta* 1999, *399*, 99-108.

[21] Clark, M. F., Lister, R. M., Barjoseph, M., *Methods Enzymol.* 1986, *118*, 742-766.

[22] Kozlowski, S., Swann, P., *Adv. Drug Deliv. Rev.* 2006, *58*, 707-722.

[23] Righetti, P. G., Drysdale, J. W., *J. Chromatogr.* 1974, *98*, 271-321.

[24] Pohl, H. A., *J. Appl. Phys.* 1951, *22*, 869-871.

[25] Meighan, M. M., Staton, S. J. R., Hayes, M. A., *Electrophoresis* 2009, *30*, 852-565.

[26] Karas, M., Hillenkamp, F., *Anal. Chem.* 1988, *60*, 2299-2301.

[27] Gluckmann, M., Pfenninger, A., Kruger, R., Thierolf, M., Karas, M., Horneffer, V., Hillenkamp, F., Stupat, K., *Int. J. Mass Spectrom.* 2001, *210*, 121-132.

[28] Chang, W. C., Huang, L. C. L., Wang, Y.-S., Peng, W.-P., Chang, H. C., Hsu, N. Y., Yang, W. B., Chen, C. H., *Anal. Chim. Acta* 2007, *582*, 1-9.

[29] Gross, J., Strupat, K., *Trends Analyt. Chem.* 1998, *17*, 8-9.

[30] He, B., Patankar, N. A., Lee, J., *Langmuir* 2003, *19*, 4999.

[31] Shibuichi, S., Onda, T., Satho, N., Tsujii, K., *J. Phys. Chem.* 1996, *100*, 19512.

[32] Barthlott, W., Neinhuis, C., *Planta* 1997, *202*, 1-8.

[33] Li, X.-M., Reinhoudt, D., Crego-Calama, M., *Chem. Soc. Rev.* 2007, *36*.

Chapter 2

Overview of Electrokinetic Techniques

2.1 Principle of charge, electric fields, and electrokinetic separation techniques

Molecules and larger units of matter (polymers, particles, etc.) have a highly diverse composition and distribution of elementary charged particles. The origin of this principle stems from the fact that every atom contains a different numbers of positive and negative charges in protons and electrons, respectively. In fact, this fundamental property of atomic charge gives rise to many other uniquely observable physical and chemical properties. Chemical reactivity and acid/base properties add to the higher order charge diversity by selectively altering chemical structures. Therefore, every molecule has a unique distribution of charge even if it is net neutral or an isomer. Naturally, this broad diversity suggests that charge distribution can be exploited to separate chemical mixtures. In principle, unique forces (F) can be exerted on different molecules by targeting either net charge (q) or dipole (p) using an electric field (E) based on the following equations:

$$F = q\,E \tag{1}$$

$$F = p \cdot \nabla E \tag{2}$$

Eq. (1) and Eq. (2) state differential forces can be applied to molecules composed of different charge or different dipoles by employing an electric field or electric field gradient, respectively. If a unique force can be generated for a particular

analyte than systems can be engineered which enable the isolation of that analyte from mixtures.

The electromagnetic force is one of the four fundamental forces of nature and for the purpose of this dissertation only the electric component will be introduced. An electrical or Coulombic force exists between charged particles and is described as follows:

$$F \propto \frac{q_1 q_2}{r^2} \tag{3}$$

The magnitude of force is proportional to the magnitude of each charge (q) and inversely proportional to the distance separating the charges (r) squared. The electric force can be modeled by stating each charge emits an unobservable electric field (E) which interacts with other charges as in Eq. (1). This is identical to the concept of an unobservable gravitational field which interacts with mass. Although the physicality of real systems is simplified by discussing electric fields, it is important to recognize the charges are the actual source of electric fields. A significant goal of this dissertation is to intelligently design electric fields so that Eqs. (1-2) can be applied to the separation of sample mixtures.

2.2 Engineering electric fields for separations

Various materials and geometries are used to shape and control electric fields throughout this dissertation. In all instances charged electrodes are used to initiate an electric field, insulating materials are used to direct electric fields, and conductive aqueous mediums are used to propagate the fields. These systems can be described as an electrochemical circuit where the following occurs: a voltage

generator produces a charged anode (voltage greater than ground) or cathode (voltage lower than ground), the opposite electrode is grounded, molecules lose electrons via oxidation at the anode, molecules and particles experience forces in accord with Eqs. (1-2) as applicable, and molecules gain electrons via reduction at the cathode.

Ohm's law states that the voltage drop across two points is proportional to the resistance between them. Therefore, points of greater electrical resistance will have the largest voltage drops and thus the highest electric fields. This is an important consideration because cross sectional area can be used to spatially alter electrical resistance and thus spatially alter electric fields. A generic illustration of these principles demonstrates that the electric field is uniform where the cross sectional area is uniform (Fig. 2.1). However, sharp boundaries produce localized field non-uniformities.

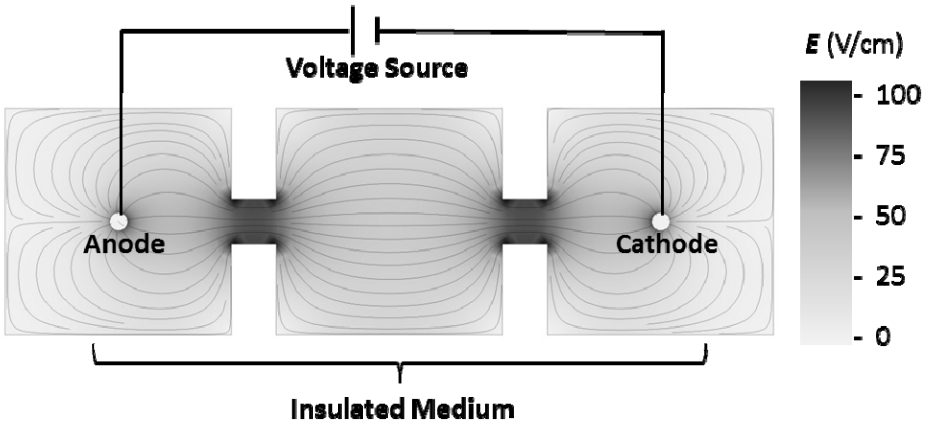

Figure 2.1. Generic illustration of an electric field. A conductive medium, with insulating material at the boundaries, contains an anode and cathode. The electric field was determined using finite elements methods in COMSOL software (arbitrary parameter inputs).

If the charge or polarization properties of a given species are understood then electric fields can be precisely engineered to achieve a particular outcome. The applied voltage and the geometry of the insulated medium determines the electric field. Therefore, these parameters can be intelligently adjusted to optimize a particular separation experiment. Uniform capillaries are used for most isoelectric focusing experiments because homogeneous electric fields are required. On the other hand, high resolution fabrication techniques are used to precisely vary the cross-section of a microfluidic channel for dielectrophoresis experiments. Finite elements multiphysics modeling software (COMSOL Multiphysics) is used to compute engineered electric fields (Fig. 2.1). Either the net transport of species can be modeled by inputting particle properties or the properties can be deduced by monitoring particle motion (Eqs. 1-2).

2.3 Electrokinetic separation techniques

2.3.1 Electrophoresis

Electrophoresis is historically the oldest and most common electrokinetic separation technique [1]. It exploits differences in charge via Eq. (1) and size via frictional drag force as the sample migrates through a gel or aqueous medium. Together the charge and size dependency are described by the single term electrophoretic mobility (μ_{EP}):

$$\mu_{EP} = \frac{q}{6\pi\eta r} \qquad \text{and} \tag{4}$$

$$v = \mu_{EP} E \tag{5}$$

where (η) is the medium viscosity, (r) is the effective particle radius, (v) is the electrophoretic velocity. In the case of larger particles (>100 nm) it is important to note that the net charge becomes complicated and is better described by electrical double layers [2]. The principles are the same although the effective net charge becomes altered because of this effect.

Typical electrophoresis experiments start with a localized injection of the sample at the start of separation medium. An electric field is subsequently applied. Analytes having different electrophoretic mobilities migrate with different velocities (Eq. 5) and are separated in space. Detection is conducted either spatially with imaging techniques (whole column scans or staining techniques) or temporally by fixed point detection (absorbance, fluorescence, etc.) whereby migrating species pass at different times [3, 4].

In addition to electrophoretic transport, systems with small cross sectional areas (<1 mm) and charged walls produce electroosmotic flow [5]. This fluid flow is the result of a body force exerted on the fluid which originates from an ionic double layer migrating via Eq. 1. Therefore, the net motion of an analyte is the sum of that from electrophoretic (μ_{EP}) and electroosmotic (μ_{EO}) components:

$$v = \mu_{Net} E = (\mu_{EO} + \mu_{EP})E \tag{5}$$

This is an important factor because it allows the simultaneous unidirectional transport of positive, neutral, and negative species without externally induced fluid flow.

Electrophoresis tends to have the least degree of band broadening of all linear separation techniques and therefore, can provide the highest resolution [6].

However, the subtle dispersion effects can still be problematic for dilute samples near detection limits. Thus, it is not surprising then that many gradient separation techniques have been developed to exploit differences in electrophoretic mobility while pre-concentrating analytes [7]. These include but are not limited to: isoelectric focusing [8], temperature gradient [9], dynamic field gradient [10], and counter flow techniques [11]. In addition, many microfluidic-based electrophoretic techniques have been developed which exploit unique features and operations [12]. Of these, isoelectric focusing is a main emphasis of this dissertation.

2.3.2 Isoelectric focusing

The development of isoelectric focusing has a relatively long history and has long been an alternative technique to electrophoresis [13]. It is essentially an electrophoresis experiment that is carried out with a buffered pH gradient along the separation medium. It takes advantage of the acid/base properties of biopolymers where net charge is altered by exchange of protons with the solution (mostly protein, but sometimes cells, DNA, and other applications). The pH gradient produces a velocity gradient for each analyte (Fig. 2.2). At the low and high pH extremes species tend to have net positive and net negative charge, respectively. Therefore, electrophoretic transport is towards a focal pH, the isoelectric point (pI), where a particular species has no net charge (Fig. 2.2). In the early years of the technique (1960-1970s), the most important development was finding suitable means to engineer stable pH gradients with synthetic buffer mixtures called ampholytes [14]. More recently, an alternative strategy has been

developed which uses immobilized and spatially patterned polymers called immobilized pH gradients (IPGs) [15]. With the development of these methods, isoelectric focusing has become a central tool for the separation of bioanalytes.

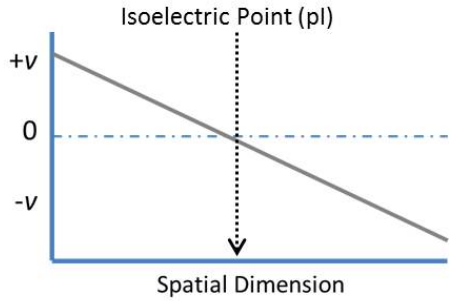

Figure 2.2. Illustration of isoelectric point. A hypothetical gradient velocity profile is plotted across space. The driving force from all directions is towards the position of zero velocity where the pH produces a net neutral molecule.

An isoelectric focusing experiment can be broken down into four distinct parts: 1) sample loading, 2) transient state, 3) steady state, and 4) detection (Fig. 2.3). To begin an experiment, the ampholyte and analyte solution is loaded across the whole length of the separation medium. Then the terminal ends are submerged in acid (anode) and base (cathode) solutions. In some instances the ampholyte is added first and the analytes are added later. Then the transient state is initiated by application of high voltage to cause electrophoretic migration of the sample components. During this phase the sample components migrate and the ampholyte buffers begin controlling localized regions of pH. This process has been observed to propagate from the terminal ends where the extreme pH zones, and thus highest charge states, are experienced [16]. After some period of time, the steady state phase is reached whereby sample components are separated from

one another and focused into their respective isoelectric points. This simplistic model is typically used although ampholytes have been observed to have much more complex distributions at steady state [17]. If the analytes were omitted in the initial sample loading then they are introduced at this point and undergo a separate transient state. The steady state is characterized by the mass transport balance between diffusion (D) and electrophoretic transport. This balance allows the steady state concentration (C) distribution about its isoelectric point (x_{pI}) for a given species to be described mathematically when one dimension (x) and a constant electrophoretic mobility gradient (ρ) are assumed [18].

$$C(x) = C_o\, e^{\frac{-\left(\rho E (x - x_{pI})^2\right)}{2D}} \tag{6}$$

Finally, detection is conducted once a steady state is reached. Gel mediums mostly employ staining and spatial imaging detection techniques. Capillary and microchannel systems typically utilize fixed point detection (temporal), and thus, require a mobilization phase where the contents are mobilized past the detector. The offline detection and analysis of collected fractions is an alternative approach for all mediums.

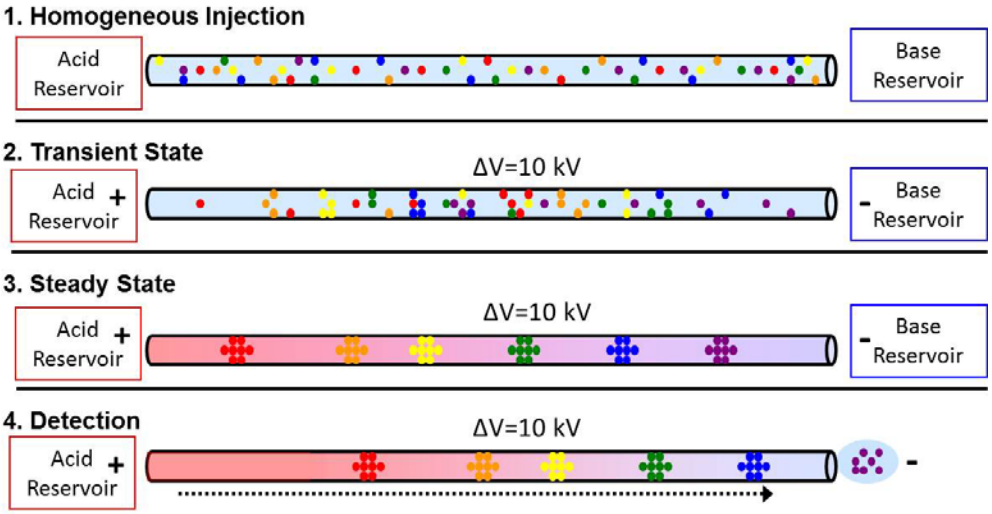

Figure 2.3. General depiction of isoelectric focusing. Schematic illustration of the four main stages of an isoelectric focusing experiment: 1) sample loading, 2) transient state, 3) steady state, and 4) detection. Detection is carried out via spatial scanning, mobilization for fixed point temporal detection, or fraction collection for offline detection.

2.3.2.1 Gel isoelectric focusing

Just like electrophoresis, isoelectric focusing first evolved from gel based mediums. Gel materials were initially desired because of their ease to engineer, low diffusion coefficients (minimal dispersion), and compatibility with simple imaging based detection techniques [13]. Overtime however, gel isoelectric focusing became very popular because of the establishment of two-dimensional gel electrophoresis techniques which multiplicatively increased resolution and peak capacity [19, 20]. With its broad use in two-dimensional separations, gel isoelectric focusing has become one of the most universally applied bioanalytical techniques and in particular is used in many proteomic applications. Agarose and polyacrylamide derivatives are the most common polymers used for gel production [21]. Furthermore, there is a large body of literature available for

selectively controlling the properties of gels including pore size, surface charge, and viscosity [20, 21].

Although the ability to engineer desired properties with gels is desirable, it also represents a source of limitation for isoelectric focusing. This flexibility requires manual manipulations and results in broad variations in gel properties and detection. These factors make it difficult to compare data sets, introduce errors into experiments, and cause varied results [22]. This is particularly true for isoelectric focusing because the pI has a strong dependence on temperature, structure, and equilibrium properties with the medium. Therefore, gel variations have strong influence on the outcomes of experiments. An example of this argument is detailed in Chapter 4. This limitation of gels serves as perhaps one explanation for the evolution of capillary based techniques in the 1980s.

2.3.2.2 Capillary isoelectric focusing

Compared to gel isoelectric focusing, capillary isoelectric focusing (cIEF) offers the advantage of better heat dissipation (allowing higher field strengths), faster run times (minutes versus hours), smaller sample handling (100 fold), and less manual manipulation [23]. It is not as good, however, when considering preparative scale applications and multi-dimensional coupling. It provides equivalent resolving power, but this is sometimes compromised with the added need for a mobilization step. Overall, the capillary format is very complimentary and has its own particular niche compared to gels [23]. More recently similar arguments would hold true for microfluidic based operations which offer certain advantages over capillaries [12].

The instrumentation is essentially the same except a small bore capillary (<200 μm) is used instead of a relatively large gel slab. Unless whole column detection is performed [16], the focused contents of the capillary are mobilized past a fixed point detector or eluted from the capillary for offline analysis. This can be done chemically [24], with electroosmotic flow [25], or pressure driven flow [26] and each approach offers different advantages and disadvantages [8].

2.3.2.3 Droplet-based isoelectric focusing

The field of droplet based microfluidics (DMF) is relatively new within the last 20 years. DMF offers the potential for high throughput, small volume analysis through the manipulation of discreet fluid volumes (droplets) [27]. Using either pressure, electrical, or magnetic fields droplets are actuated on hydrophobic surfaces or within immiscible fluids. This arrangement minimizes surface interactions which can be lead to sample losses and system fouling. There are many different manipulations demonstrated in DMF systems including: droplet merging and splitting [28-30], immunoassays [31], analytical electrochemistry [32], large particle isolations [33, 34], study of reaction kinetics [35], and many other sample preparations. However, one clearly lacking and difficult application is droplet based separations [36].

The mechanism of isoelectric focusing lends itself well to be applied to droplet based microfluidics. This is a unique format where the confining chamber (column, channel, slab gel, etc.) normally present in separations is not needed. A superhydrophobic substrate is used on one side and air acts as the insulating material on the remainder of the drop. Droplet based isoelectric focusing only

requires metal electrodes and means to generate stable pH gradients. Chapter 6 demonstrates the principles of this technique. This is a beneficial approach because aqueous capillary and micro-channel systems are impractical for preparative purposes and gel systems are often difficult to automate. The fundamentals examined in this technique enable automatable, high throughput separations that could be fully integrated into droplet microfluidic systems.

2.3.3 Dielectrophoresis

Dielectrophoresis (DEP) acts on particle dipoles (charge distribution) rather than net charge and is described by Eq. 2. Large electric field gradients (>1 $\times 10^5$ cm^4 V^{-2} s^{-1}) and large particle sizes (>20 nm) are needed for the magnitude of this force to be significant relative to thermal motion and other forces. This means DEP is best suited to target large DNA or protein, viruses, cells, and other large bioparticle complexes. This is a complimentary niche because other electrokinetic techniques are well suited for targeting smaller molecules. The DEP dependence on high field gradient demands that devices be engineered at micro scales to provide precise control and avoid excessive joule heating. Two approaches are predominant where either electrodes or insulating structures are patterned to produce the field non-uniformities.

Applied electric fields have the effect of moving charges and thus inducing dipoles across polarizable particles. The theory of dielectrophoresis is typically derived from a spherical particle with the assumptions that it is homogeneously and linearly polarizable. Thus, the dipole moment (p) depends on the field, and thus by substitution into Eq. 2 the DEP force depends on the

gradient of the field squared. This makes DEP uniquely different from other electrokinetic forces because the direction of the motion does not depend on the direction of the field but rather on the direction of the field gradient. The DEP motion is either towards that of greater or weaker field strength regardless of field orientation.

The DEP force can be exploited in different ways to achieve sample separation including bifurcation [33], differential deflection [37], or trapping [38]. Usually, other forces such as electrophoresis, electroosmosis, and hydrodynamic flow are also employed in order to transport material through the medium and/or produce velocity gradient focusing zones. DEP is a powerful approach because it targets the intricate parameter of polarizability while other electrokinetic techniques only target charge and size. The polarizability of a particle depends on shape, rigidity, and electrical properties among other particle properties. This sensitivity also makes it more difficult because precise control is needed over all physical parameters: pH, conductivity, temperature, surface properties, particle composition, and local electric fields.

2.4 References

[1] Andrews, A. T., *Electrophoresis: theory, techniques, and biochemical and clinical applications*, Oxford University Press, New York 1986.

[2] Schulz, S. F., Sticher, H., *Progr. Colloid. Polym. Sci.* 1994, *97*, 85-88.

[3] Swinney, K., Bornhop, D. J., *Electrophoresis* 2000, *21*, 1239-1250.

[4] Miura, K., *Electrophoresis* 2001, *22*, 801-813.

[5] Rice, C., Whitehead, R., *J. Phys. Chem.* 1965, *69*, 4017-4024.

[6] Giddings, J. C., *Unified Separation Science*, Wiley, New York 1991.

[7] Meighan, M. M., Staton, S. J. R., Hayes, M. A., *Electrophoresis* 2009, *30*, 852-565.

[8] Rodriguez-Diaz, R., Wehr, T., Zhu, M., *Electrophoresis* 1997, *18*, 2134-2144.

[9] Shackman, J. G., Munson, M. S., Ross, D., *Anal. Chem.* 2007, *387*, 155-158.

[10] Burke, J. M., Ivory, C. F., *Electrophoresis* 2008, *29*, 1013-1025.

[11] Meighan, M. M., Keebaugh, M. W., Quihuis, A. M., Kenyon, S. M., Hayes, M. A., *Electrophoresis* 2009, *30*, 3786-3792.

[12] Kenyon, S. M., Meighan, M. M., Hayes, M. A., *Electrophoresis* 2011, *32*, 482-493.

[13] Righetti, P. G., Drysdale, J. W., *J. Chromatogr.* 1974, *98*, 271-321.

[14] Just, W. W., *Methods Enzymol.* 1983, *91*, 281-298.

[15] Righetti, P. G., Bossi, A., *Anal. Biochem.* 1997, *247*, 1-10.

[16] Mao, Q., Pawllszyn, J., Thormann, W., *Anal. Chem.* 2000, *72*, 5493-5502.

[17] Sebastiano, R., Simo, C., Mendieta, M. E., Antonioli, P., Citterio, A., Cifuentes, A., Peltre, G., Righetti, P., *Electrophoresis* 2006, *27*, 3919.

[18] Svensson, H., *Acta Chem. Scand.* 1961, *15*, 325-341.

[19] Lilley, K. S., Razzaq, A., Dupree, P., *Curr. Opin. Chem. Biol.* 2002, *6*, 46-50.

[20] Issaq, H. J., Veenstra, T. D., *Biotechniques* 2008, *44*, 697.

[21] Ogden, R. C., A., A. D., *Methods Enzymol.* 1987, *152*, 61-87.

[22] Righetti, P. G., *Journal of Chromatography A* 2004, *1037*, 491-499.

[23] Hille, J. M., Freed, A. L., Watzig, H., *Electrophoresis* 2001, *22*, 4035-4052.

[24] Harper, S. B., Hurst, W. J., Lang, C. M., *J. Chromatogr. B.* 1994, *657*, 339-344.

[25] Horka, M., Ruzicka, F., Horky, J., Hola, V., Slais, K., *J. Chromatogr. B.* 2006, *841*, 152-159.

[26] Weiss, N. G., Zwick, N. L., Hayes, M. A., *J. of Chromatogr. A* 2010, *1217*, 179-182.

[27] Abdelgawad, M., Wheeler, A. R., *Adv. Mater.* 2009, *21*, 920-925.

[28] Garcia, A. A., Egatz-Gomez, A., Lindsay, S. A., Dominguez-Garcia, P., Melle, S., Marquez, M., Rubio, M. A., Picraux, S. T., Yang, D., Aella, P., Hayes, M. A., Gust, D., Loyprasert, S., Vazquez-Alvarez, T., Wang, J., *J. Magn. Magn. Mater.* 2007, *311*.

[29] Cooney, C. G., Chen, C.-Y., Emerling, M. R., Nadim, A., Sterling, J. D., *Microfluid. Nanofluid.* 2006, *2*, 435-446.

[30] Cho, S. K., Moon, H., Kim, C.-J., *J. Microelectromech. Syst.* 2003, *12*, 70-80.

[31] Sista, R. S., Eckhardt, A. E., Srinivasan, V., Pollack, M. G., Palanki, S., Pamula, V. K., *Lab Chip* 2008, *8*, 2188-2196.

[32] Lindsay, S. A., Vazquez-Alvarez, T., Egatz-Gomez, A., Loyprasert, S., Garcia, A. A., Wang, J., *Analyst* 2007, *132*, 412-416.

[33] Fan, S.-K., Huang, P.-W., Wang, T.-T., Peng, Y.-H., *Lab Chip* 2008, *8*, 1325-1331.

[34] Wang, Y., Zhao, Y., Cho, S. K., *J. Micromech. Microeng.* 2007, *17*, 2148-2156.

[35] Cygan, Z. T., T., C. J., Beers, K. L., Amis, E. J., *Langmuir* 2005, *21*, 3629-3634.

[36] Fair, R. B., *Microfluid. Nanofluidics* 2007, *3*, 245-281.

[37] Kang, Y., Li, D., Kalams, S. A., Eid, J. E., *Biomed. Microdevices* 2008, *10*, 243-249.

[38] Pysher, M. D., Hayes, M. A., *Anal. Chem.* 2007, *79*, 4552-4557.

Chapter 3

Capillary Isoelectric Focusing Coupled Offline to MALDI-MS with Syringe Pump Mobilization

3.1 Introduction

As already introduced in the previous chapters, protein analysis can provide insight into the health and disease state of humans. Protein analytics often requires the examination of complex samples and heterogeneous expression patterns, thus highly selective tools are critical. A key technique that can contribute towards the goal of protein analysis is capillary isoelectric focusing (cIEF) coupled offline to matrix assisted laser desorption/ionization mass spectrometry (MALDI-MS). The coupling of cIEF with MALDI-MS has been only demonstrated a few times [1-6] and is in need of further development in order to reach its full potential. The technical details presented here provide a basis for expanding the use of the technique to solve greater proteomic/analytical problems.

In cIEF, carrier ampholyte mixtures are used to establish a stable pH gradient inside a capillary suspended between an acid and base reservoir. Amphoteric analytes, typically proteins, will migrate with their local electrophoretic mobility until reaching the pH where their net charge is zero, defined as the isoelectric point (pI). Once steady state is achieved in cIEF, the focused analytes are typically mobilized for detection and/or fraction collection. Most commonly this is either through chemical, electroosmotic, or hydrodynamic mobilization [7]. Of these, hydrodynamic mobilization is arguably the best

choice for interfacing with fraction collection for MALDI-MS detection. It does not cause significant band broadening when the potential field is maintained [8], allows for predictable elution profiles unlike cathodic mobilization [9], and is compatible with internally coated capillaries known to improve cIEF performance [7]. In this work the syringe pump mobilization method is investigated.

Even though the syringe pump is designed to improve the ease of cIEF coupling to MALDI-MS, the additional hardware can cause failed runs if not handled properly. These malfunctions are most often attributed to a disruption of the electric field or fluid flow by a large particle or gas bubble. Such events can have detrimental effects to the electric and/or flow fields resulting in poor separations and null results. Particles arise from sample contamination or precipitation during the focusing process, and resolving this problem has been discussed elsewhere [7]. Gas bubbles are a consequence of electrolysis, joule heating, and hardware handling issues at the site of liquid/air interfaces. This is easily avoided in other mobilization modes since the capillary is suspended between reservoirs open to atmosphere. Air bubbles are more frequent and problematic in syringe pump mobilization due to the additional capillary lines, dynamic junctions, and the need for air tight pressure seals. The work here demonstrates the proper hardware and protocol necessary to make syringe pump mobilization compatible for cIEF and MALDI-MS interfacing. Following careful protocol, reproducible elution times of markers (RSD < 5%) and accurate pI determination of proteins is demonstrated.

3.2 Materials and methods

3.2.1 Chemicals and materials

Sinapinic acid, myoglobin (from equine skeletal muscle), β-lactoglobulin A & B mixture (from bovine milk), acetonitrile, trifluoracetic acid, fluorescent IEF markers (pI: 7.6, 6.8, 6.2, 5.5, 5.1, & 4), & BioChemika ampholyte pH 5-8 were obtained from Sigma-Aldrich (St.Louis, MO, USA). Pharmalyte pH 3-10 was obtained from Amersham Biosciences (Poscataway, NJ, USA). Fused silica capillaries with an electroosomotic flow suppression coating were obtained from Microsolv (Long Branch, NJ, USA). A Nanopure UV Ultra water system from Branstead/Thermolyne (Dubuque, IA, USA) was used to provide deionized nanopure water.

3.2.2 Capillary isoelectric focusing

cIEF was performed on an in-house system utilizing a 50 cm x 75 μm (id) coated capillary (proprietary) for electroosmotic flow suppression (Fig. 3.1). Absorbance detection (325 nm) was carried out 7 cm from the capillary end using a capillary flow cell, DH-2000 deuterium light source, and USB 4000 bench top spectrometer (Ocean Optics, Dunendin, FL, USA). For assessment of pI marker reproducibility, the sample solution was composed of 2% (w/v) Pharmalyte 3-10 and six fluorescent pI markers (pI: 4.0, 5.1, 5.5, 6.2, 6.8, & 7.6) adjusted between 6-50 μg/mL. For validation of cIEF-MALDI-MS, the sample solution contained 2% (w/v) carrier ampholytes of BioChemika 5-8, five fluorescent pI standards (pI: 5.1, 5.5, 6.2, 6.8, & 7.6) adjusted between 6-50μg/mL, myoglobin (70 μg/mL), and a mixture β-lactoglobulin A & B (70 μg/mL). The capillary was filled with

the sample solution using a pressure of 20 psi for approximately 25 seconds. Isoelectric focusing was run at 15 kV for 20 minutes in all experiments, using 10 mM phosphoric acid as the anolyte and 20 mM ammonium hydroxide as the catholyte and sheath flow. For the mobilization step, a syringe pump was used for capillary elution and sheath flow delivery at flow rates of 0.75 μL/min and 2.6 μL/min respectively. At the start of mobilization, the catholyte reservoir was removed to allow for fraction collection at the capillary tip. Fractions were collected in thirty second intervals, corresponding to 1.4 μL, by contacting a ground steel MALDI plate (96 well) to the developing droplet where the sheath and capillary flows combined. This configuration allowed for absorbance detection of pI markers and MALDI-MS detection of standard proteins. It took 25.3 minutes for mobilization to the online detector (43 cm) and 30 minutes to elute the entire sample out of the capillary (50 cm).

3.2.3 Hardware components for instrumentation

After sample injection, the focusing capillary is connected to the anolyte junction using a microtee joint and microferrules (Upchurch Scientific, Oak Harbor, WA, USA). The anolyte junction provides an air tight seal to the anolyte vial while allowing the focusing capillary to be easily removed for rinsing and sample injection. Initially it is filled with anolyte solution and is coupled to the anolyte vial by an 8 cm connecting capillary. The anolyte vial consists of a 3 mL vial with an airtight cap ensured by sealing with epoxy. It has an embedded platinum electrode, a capillary line connected to the syringe (in-line), and a capillary line connected to the anolyte junction (out-line).

The sheath flow configuration allows for fraction collection while maintaining an electrical connection across the capillary to minimize hydrodynamic flow band broadening. The focusing capillary is threaded coaxially through an 18 gauge stainless steel tube, and a micro tee fitting allows for allows for delivery of the sheath flow from the syringe pump. A ground wire attached to the outer part of the tube allows for the electrical circuit to be completed while performing syringe pump mobilization.

3.2.4 MALDI-MS

For cIEF-MALDI-MS experiments, a saturated solution of sinapinic acid in 70/30 0.1% trifluoracetic acid/acetonitrile was used as the MALDI-MS matrix. Immediately after collecting a fraction, 2 μL of matrix solution was added. The droplets were allowed to evaporate at room temperature and pressure until completely dry (~ 15 minutes). Mass spectral data was collected on a Bruker Daltonics (Billerica, MA, USA) Autoflex MALDI-TOF spectometer. The instrument was operated in linear, positive ion mode and the data was collected with a 20 kV extraction voltage and 250 ns delay time. Excitation of the SA matrix was achieved using a 337 nm nitrogen laser. Samples were evaluated at a m/z range of 4,000 to 40,000 and 500 shot spectrums were accumulated for each sample.

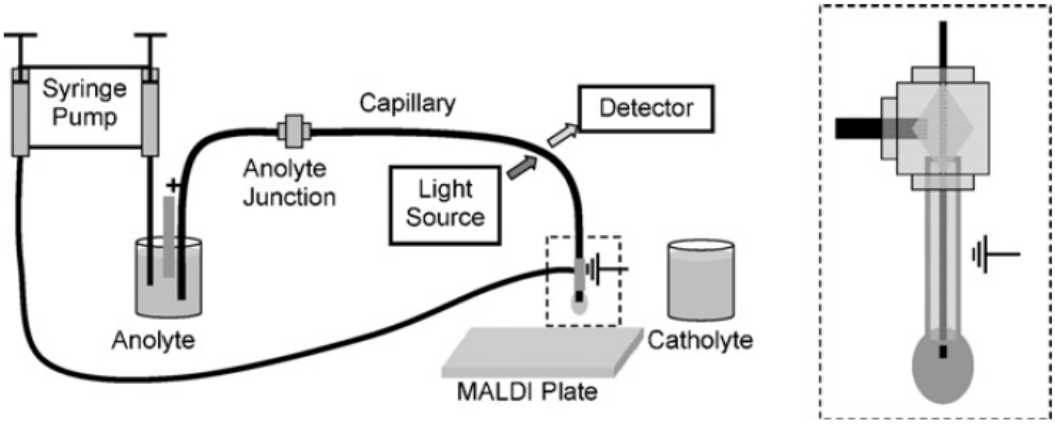

Figure 3.1. Schematic illustration of cIEF-MALDI-MS instrument. Syringe pump mobilization is used for mobilization. The anode and cathode are marked by the positive and ground symbols respectively. The inset illustrates the sheath flow arrangement allowing for fraction collection while maintaining the potential field.

3.3 Results and discussion

At the start of a cIEF separation it is critical to ensure that no bubbles become trapped inside the junctions or capillaries. Bubbles can disrupt the applied field and/or prevent capillary elution causing poor cIEF reproducibility. To avoid this problem the anolyte vial and the connecting capillaries are completely filled with anolyte solution. Similarly, the junctions are filled with excess anolyte solution to prevent air entrapment upon connection of the fittings. The time of atmosphere exposure should be minimized for each air/liquid interface to prevent any significant height induced hydrodynamic flow or evaporation which could introduce air into the system. It is also important to vent the anolyte vial after multiple trials to remove any gas generation due to long periods of electrolysis or Joule heating. Establishing these protocols is critical since applying pressure to a system with bubbles can cause compression rather than fluid transport; thus,

capillary contents will fail to elute so long as the applied pressure is compensated by a compressible bubble. The collapsing bubble phenomenon can be identified by unusually long or inconsistent elution times. Chaotic changes in the current can also signal interference in the focusing or mobilization steps due to bubbles.

Following this procedure, reproducible cIEF separations of pI markers are observed over several trials. A representative electropherogram shows well defined peaks (A_{325nm}) of six fluorescent pI markers in pH 3-10 (Fig. 3.2A). The poor resolution between pI 5.5 and 5.1 is not indicative of resolution loss due to hydrodynamic mobilization since the β lactoglobulin species exhibit better resolution although having a smaller pI difference (Δ pI ~0.2). The relative standard deviation of elution times for the pI markers are less than 5% for all peaks over ninety trials (Fig. 3.2B), which is comparable to non-coupled cIEF literature data [10]. However, the reproducibility of proteins would likely be less due to stronger surface interactions with the capillary wall [11]. It can be seen in the plot that the pH gradient does not exhibit uniform linearity over the entire range, and thus care must be taken in determining experimental pIs [12]. The elution times of the standard proteins was determined by MALDI-MS detection after correcting for the 4.1 minute delay between absorbance detection and fraction collection. The fraction having the highest MS signal was used for determining the experimental protein pI after the five pI marker elution times were fitted with a second order polynomial (R^2 =0.99). Using this approach, the pI of myoglobin, β-lactoglobulin B, and β-lactoglobulin A was found to be 7.0,

5.3, and 5.0 respectively. These pI determinations are in good agreement with literature values [1-2].

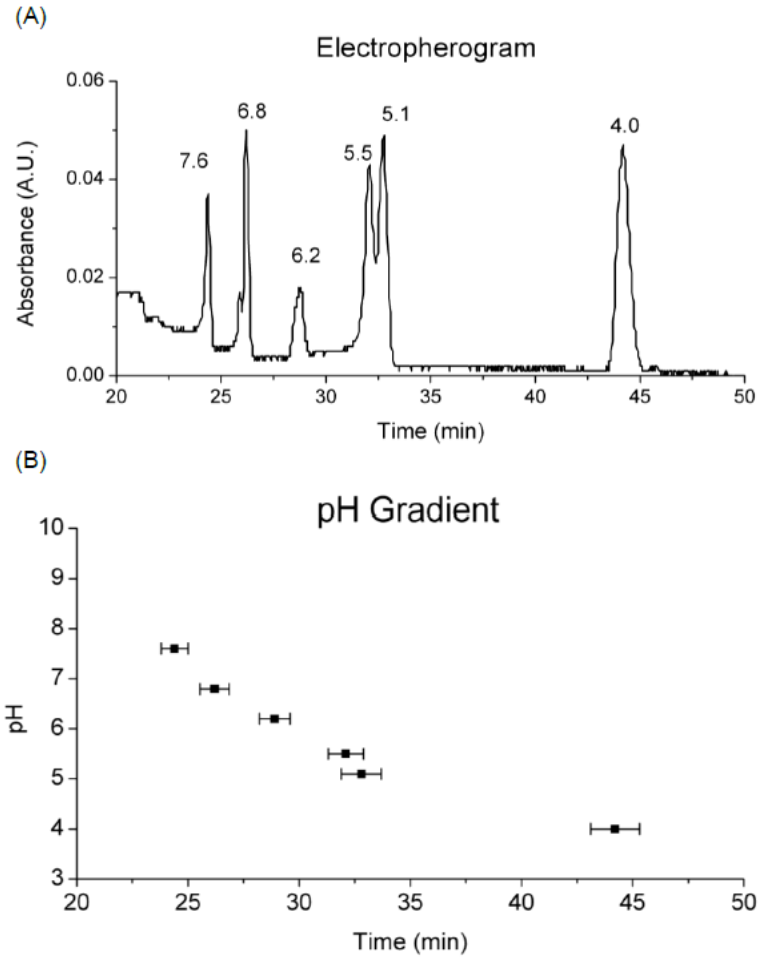

Figure 3.2. cIEF Results from pI markers. (A) cIEF elution UV absorbance trace (315 nm) showing the separation of six pI markers (pI labeled above each peak) in pH 3-10. (B) Corresponding pH gradient plot with standard deviation over several trials (n=90) as error bar.

The resultant MALDI-MS spectra obtained for all of the collected fractions reveal good separation between each protein species (Fig. 3.3A-B). Each of the proteins was found in two to three fractions and thus the peak widths are 1-

1.5 minutes which is comparable to the pI markers. The myoglobin signal (pI 7.1; MW 16,950 Da) is well resolved from the two β-lactoglobulin species. Baseline resolution between β-lactoglobulin A (pI 5.0; MW 18,360 Da) and β-lactoglobulin B (pI 5.3; MW 18,270 Da) was only observed when using the shallower pH gradient 5-8. The MS signals likely are subject to ampholyte suppression although the extent to which was not examined [6, 13]. Overall, MALDI-MS protein detection extends the applicability of cIEF by improving detection limits relative to absorbance measurement.

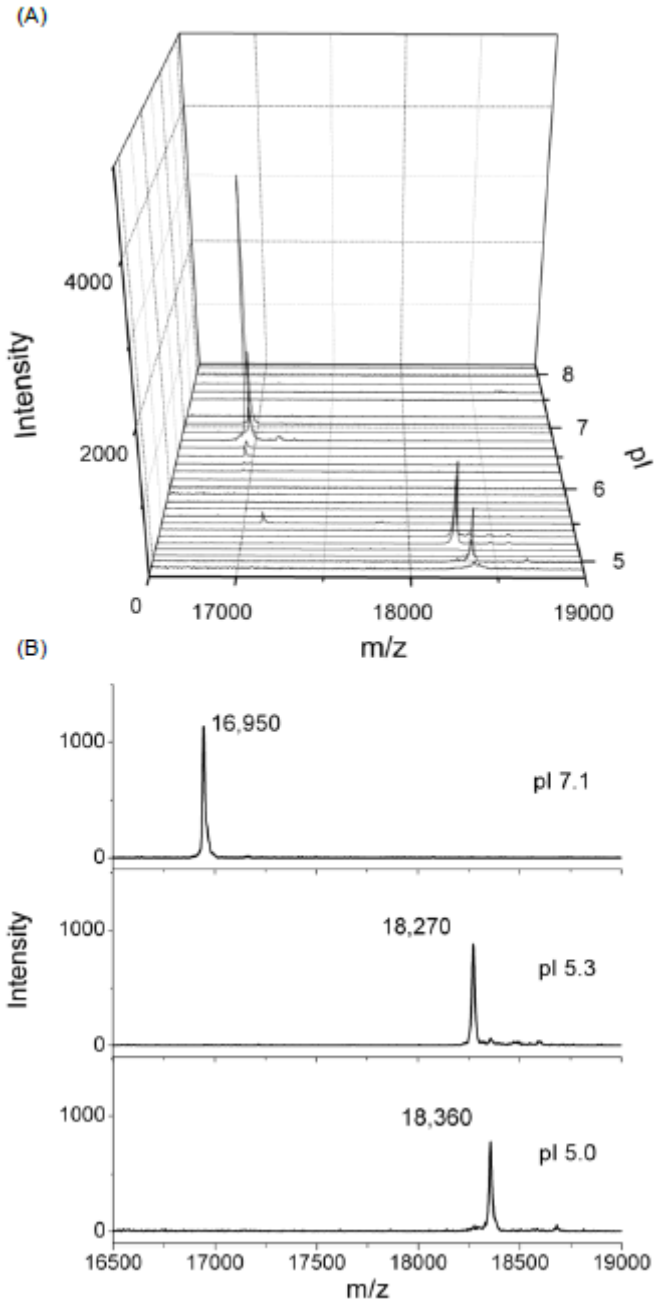

Figure 3.3. cIEF-MALDI-MS results from standard proteins. (A) All MALDI-MS spectra of fractions collected from a cIEF separation of myoglobin (pI 7.1; MW 16,950 Da), β-lactoglobulin A (pI 5.0, 18,360 Da), and β-lactoglobulin B (pI 5.3, 18,270 Da). (B) Individual spectra of the main pI fractions for each protein.

3.4 Concluding remarks

Syringe pump mobilization is found to be compatible in coupling cIEF with MALDI-MS for protein analysis. In this investigation, problematic or null cIEF experiments were primarily the result of bubbles entrapped in the system. Through careful attention to hardware components and interfaces, bubbles were eliminated and the syringe pump mobilization method was shown to have competitive reproducibility of pI markers and accurate pI determination of standard proteins. There does not appear to be significant cIEF resolution loss due to the fraction collection as the β-lactoglobulin A & B species were baseline resolved although differing by only two amino acids.

3.5 References

[1] Foret, F., Muller, O., Thorne, J., Gotzinger, W., Karger, B. L., *J. Chromatogr. A* 1995, *716*, 157-166.

[2] Chartogne, A., Gaspari, M., Jespersen, S., Buscher, B., Verheij, E., van der Heijden, R., Tjaden, U., van der Greef, J., *Rapid Commun. Mass Spectrom.* 2002, *16*, 201-207.

[3] Crowley, T. A., Hayes, M. A., *Proteomics* 2005, *5*, 3798-3804.

[4] Yu, W., Li, Y., Deng, C., Zhang, X., *Electrophoresis* 2006, *27*, 2100-2110.

[5] Lechner, M., Seifner, A., Rizzi, A. M., *Electrophoresis* 2008, *29*, 1974-1984.

[6] Silvertand, L. H. H., Toraño, J. S., de Jong, G. J., van Bennekom, W. P., *Electrophoresis* 2009, *30*, 1828-1835.

[7] Rodriquez-Diaz, R., Wehr, T., Zhu, M., *Electrophoresis* 1997, *18*, 2134-2144.

[8] Minarik, M., Groiss, F., Gas, B., Blaas, D., Kenndler, E., *J. Chromatogr. A* 1996, *738*, 123-128.

[9] Tang, Q., Harrata, A. K., Lee, C. S., *J. Mass Spectrom.* 1996, *31*, 1284-1290.

[10] Huang, T. L., Richards, M., *J. Chromatogr. A* 1997, *757*, 247-253.

[11] Suratman, A., Wätzig H., *J. Sep. Sci.* 2008, *31*, 1834-1840.

[12] Righetti, P. G., *J. Chromatogr. A* 2004, *1037*, 491-499.

[13] Silvertand, L. H. H., Toraño, J. S., de Jong, G. J., van Bennekom, W. P., *Electrophoresis* 2008, *29*, 1985-1996.

Chapter 4

Examining Serum Amyloid P Component Microheterogeneity Using Capillary Isoelectric Focusing and MALDI-MS

4.1 Introduction

The developments in coupling capillary isoelectric focusing (cIEF) and matrix assisted laser desorption/ionization mass spectrometry (MALDI-MS) presented in Chapter 3 are used to examine the heterogeneity of human serum amyloid P component (SAP). SAP is a member of the pentraxin protein family and is well known for its calcium dependent binding properties and presence in amyloid plaques [1]. It is a decameric/pentameric glycoprotein composed of monomers (M.W. ~ 25 kDa) each having a single complex biantennary N-linked glycosylation [2]. Interestingly, there are several conflicting findings regarding the source and number of existing SAP isoforms [2-6]. Two predominant themes are found in the literature regarding SAP microheterogeneity. One theme, based on mass spectrometry, suggests that SAP is relatively homogeneous and observed glycan variance is primarily a result of different numbers of sialic acid residues [2, 6]. Both studies observed varying degrees of sialylation (three forms corresponding to disialo, monosialo, and asialo), but different conclusions were drawn in terms of the endogenous nature of these species. The second theme suggests that SAP has much broader heterogeneity as determined by gel IEF or 2D gel electrophoresis (2DE) visualized by protein staining [3-5]. In each of these gel separation studies a different number of isoforms were identified (4 to 8) with differing isoelectric points (pI) (4.7 to 6.1, Table 1). Even more

incongruous, each of these studies concluded uneven sialylation was not the cause of the multiple bands.

Table 4.1. Literature pI values and isoforms for human SAP

Reference	[Urea]	pI	# of Isoforms	Technique, Sample, Purification Method
[25]	0 M	4.1	N/A	Chromatofocusing, Pool, Sepharose 4B
[5]	0 M	5.6-6.2	N/A	Gel IEF, Individual, Sepharose 4B
[7]	8 M	6	1	Gel IEF, Both, PE Sepharose
[26]	6 M	5.7-5.8	1	Gel IEF, Pool, Sepharose 6B
[3]	9.6 M	5.95-6.08	4	Gel IEF, Pool, Agarose
[4]	8 M	5.65-5.87	6	Gel IEF, Individual, Sepharose 4B
[5]	8 M	4.7-5.7	6 to 8	Gel IEF, Individual, Sepharose 4B

In terms of the second theme, there exists a large amount of experimental and statistical uncertainty. It is difficult to discern quantitative and analytically significant information from these specific gel-based separations for several reasons. In a general sense, the interpretation of the patterns and the intensities of these gels were limited to the broad estimation error associated with manual qualitative assessment. This, along with potential experimental difficulties and a lack of further characterization, may account for the significant differences in data and interpretation. In fact, one study even suggested the additional bands observed in gel IEF characterization to be the result of experimental error associated with impurities or the staining process [7].

No matter the limitations of previous works, pI based separations of SAP have frequently revealed multiple bands suggesting mass spectrometric studies may not have completely identified all isoforms (e.g., unresolved peaks). Therefore, it would be insightful to separate SAP using a more controlled IEF method, characterize separated fractions with mass spectrometry, provide sufficient sampling to apply statistical significance, and examine both pooled and individual samples. Such a comprehensive, quantitative analysis will provide new information to either support existing theories or elucidate novel isoforms.

cIEF was chosen for this study as a useful technique to examine SAP microheterogeneity since it is less reliant on manual manipulation (gels require manual preparation, loading, staining, and visualization), known to have comparable resolution to carrier ampholyte gels, and still compatible with mass spectrometry coupling [8]. As a very brief background for IEF, in general, a uniform electric field and pH gradient are applied to the separation length which is most often a gel or capillary. This causes amphoteric species and proteins to change charge states while migrating electrokinetically due to acid/base reactions. Positively charged proteins migrate towards the cathode or higher pH region until becoming neutral and vice versa for negatively charged proteins. The pH where the protein reaches a net neutral state and ceases to electromigrate is defined as the pI. A more comprehensive comparison of gel and capillary separations can be found elsewhere [9].

After steady state focusing is achieved in cIEF, the capillary contents are typically mobilized allowing for detection of concentrated bands by absorbance or

fluorescence [8]. These detection modes have limited applicability since absorbance detection requires high protein concentrations (LOD ~10 μM) and can suffer from ampholyte/background interference while fluorescence detection often requires the use of linked fluorophores. Additionally, they make it difficult to interpret complex electropherograms, lacking alternative information aside from pI.

A less developed but more universal approach is to interface cIEF with MS [10]. This offers improved detection limits (LOD ~10 fmol or ~10 nM for 1 uL capillary volume) relative to absorbance detection while providing orthogonal separation by molecular weight, similar to traditional 2DE. Additionally, the accurate and precise determination of molecular weight allows for improved characterization. Electrospray ionization (ESI) and MALDI are the two most compatible ionization modes for MS analysis of proteins. With respect to cIEF coupling, ESI receives more attention probably owing to its online coupling ability [11]. On the other hand, cIEF-MALDI-MS has only been demonstrated a few times and its full potential has yet to be realized [12-18]. MALDI-MS uses offline coupling providing semi-permanent sample storage for multiple analyses and can generate simpler spectra. Technically, this increases analysis time and if not performed properly can result in additional band broadening.

In the current work, a quantitative examination of SAP microheterogeneity with pooled and individual samples is undertaken. This work clarifies the microheterogeneity profile of SAP isolated from a pooled serum sample by direct MALDI-MS and with cIEF-MALDI-MS. Only sialic acid variants are observed

and SAP is found to be highly homogenous. Additionally, SAP preparations isolated from several hundred individuals were analyzed using mass spectrometric immunoassay (MSIA). Included in this population study were samples from individuals having type-2 diabetes, myocardial infarction, congestive heart failure, and cancer. No significant population heterogeneity was observed amongst healthy and disease state individuals, which supports the uniform microheterogeneity model concluded from the pooled sample.

4.2 Materials and methods

4.2.1 Chemicals and materials

Acetonitrile (ACN), ammonium hydroxide, phosphoric acid, sinapinic acid, sodium chloride, sodium phosphate, and trifluoracetic acid (TFA) were obtained from Sigma-Aldrich (St. Louis, MO, USA). Pharmalyte brand carrier ampholyte with a pH range of 4-6.5 was obtained from Amersham Biosciences (Amersham, UK). Fluorescent pI markers 5.1 & 4.0 were obtained from Fluka (Buchs, Switzerland). Neuraminidase and sodium citrate buffer were obtained from New England Biolabs (Ipswich, MA, USA). Polyimide coated fused silica capillaries (75 μm inner diameter) with an internal coating for electro-osmotic flow suppression were obtained from Microsolv (Long Branch, NJ, USA). Stock serum amyloid p component purified from pooled human plasma using a proprietary modification to a published method was obtained from Calbiochem/EMD Biosciences (La Jolla, CA, USA) [19]. Slide-a-Lyzer mini dialysis units were obtained from Pierce (Rockford, IL, USA). Individual plasma samples were obtained from ProMedDX (Norton, MA, USA) under Institutional

Review Board approval. Affinity pipette tips for mass spectrometric immunoassay (MSIA) were obtained from Intrinsic Bioprobes (Tempe, AZ, USA). Anti-SAP polyclonal antibody was obtained from DakoCytomation (Carpinteria, CA, USA). Deionized water was generated using a Nanopure UV ultra pure water system from Barnstead/Thermolyne (Dubuque, IA, USA).

4.2.2 Mass spectrometric immunoassay

SAP was analyzed from 374 individual plasma samples to carry out a population based study. In addition to healthy individuals, the cohort including the following disease states: type-2 diabetes (T2D), congestive heart failure (CHF), history of myocardial infarction (hMI), and cancer. The sample distribution is as follows: 133 healthy, 29 healthy (serum), 87 T2D, 25 CHF with T2D, 25 CHF and hMI, 29 with CHF, 17 CHF with hMI and T2D, and 29 cancer (9 prostate, 9 breast, and 11 colon cancer).

SAP was isolated from these plasma samples using MSIA tips derivatized with anti-SAP as previously described [20]. The tips were removed from storage in buffer (0.01 M HEPES, 0.15 M sodium chloride) at 4 °C and loaded onto a Beckman Multimeck 96 robotic workstation (Fullerton, CA, USA) capable of processing 96 tips in parallel. Samples for affinity capture were prepared by mixing 67 µL of plasma and 33 µL of a detergent/buffer solution (4.5 % Tween 20, 0.15 M octyl-β-glucopyranoside, 1.5 M ammonium acetate, 0.67 M sodium phosphate, and 1 M sodium chloride). Each MSIA tip was washed with 30 µL of the sample 1000 repetitions: where one repetition equals one aspirate and dispense cycle. After immuno-precipitation was complete, the tips were rinsed (5

repetitions of 150 µL) with the following solutions in the order listed: PBS (0.1 M sodium phosphate, 0.15 M sodium chloride, pH 7.2), HBS-P (0.01 M HEPES, 0.15 M NaCl, 0.05% v/v Surfactant P20, pH 7.4), water, 0.1 M Tris-HCl (pH 4.6). The tips were rinsed a final time with water (10 repetitions of 150 µL) before they were dried by blotting with a towel. Captured SAP was eluted from the tips by aspirating 4 µL of matrix solution (saturated sinapinic acid in 0.5% TFA/ACN (3/2, v/v)) and dispensing it onto a seeded plate. The spotted protein preparations were quickly crystallized under vacuum for MALDI-MS analysis. The thin layer of matrix or seeded plate was prepared by gently rubbing 100 µL of a matrix solution (sinapinic acid in isopropanol/acetonitrile/water (9/2/1 v/v)) across the plate with a towel until dry.

For ESI analysis, MSIA tips were used to extract SAP from plasma and rinsed as described above along with HBS, distilled water, 2 M ammonium acetate/acetonitrile (3:1 v/v), and distilled water. Captured SAP was manually eluted from the tips by aspirating 5.5 µL of a mixture of 100% formic acid/acetonitrile/distilled water (9/5/1 v/v/v), mixing for 20–30 seconds, and dispensing into a 96-conical well polypropylene autosampler tray. An additional 5.5 µL of distilled water was aspirated into the pipette tip which was used to dilute the eluted sample.

4.2.3 Capillary isoelectric focusing

cIEF was performed on a lab-built instrument using a 40 cm x 75 µm id internally coated capillary for electroosmotic flow suppression. For all cIEF runs 10 mM phosphoric acid and 20 mM ammonium hydroxide were used as the

anolyte and catholyte reservoirs, respectively. The instrument was configured to allow for online absorbance detection and fraction collection for offline MALDI-MS detection. Absorbance was monitored at 220 nm in capillary flow cell using a deuterium light source (Mikropack DH2000), fiber optic cables, and spectrometer (Ocean Optics USB 4000). A sheath flow arrangement, as described previously, allowed for fraction collection without disrupting either the focusing voltage or pH gradient [18]. Briefly, the capillary was threaded through an 18 gauge stainless steel tube (1 mm protrusion) where the ground contact was made. At the time of mobilization, catholyte solution was pumped at a steady rate through the steel tube in order to create catholyte droplets at the capillary tip.

Sample solutions prepared with volumes as low as 5 μL contained 100 ng/μL SAP, 2% (w/v) pharmalyte (pH 4-6.5), and 20 ng/μL pI markers 5.1 & 4.0. The sample mixture was pressure injected through the entire capillary volume (1.8 μL) using 10 psi nitrogen. Then the anodic end of the capillary was threaded into the anolyte vial using Upchurch fittings to create an airtight junction and the cathodic end was submerged into the catholyte vial. Focusing was conducted with an applied voltage of 12 kV for 10 min using a Spellman (Hauppauge, NY, USA) high-voltage power supply and the current decreased from 30 to 5 μA. Subsequently, the catholyte vial was removed and a syringe pump was used for pressure mobilization of capillary contents at 0.15 μL/min and delivery of catholyte sheath flow at 5.25 μL/min. This generated droplets at the capillary tip (5.4 μL/min) where the sheath and capillary flows combined. A MALDI target plate was lightly contacted to droplets in 10-30 second intervals in order to

capture them in discrete fractions (0.9-2.7 μL) for MALDI-MS analysis. This led to fractions differing in pI by approximately 0.1 pH units. The matrix solution (saturated sinapinic acid in 0.5% TFA/ACN (2/1, v/v)) was added immediately after collecting fractions on the plate, since adding it to the sheath flow can cause resolution loss during the spotting process [17].

4.2.4 Desialylation of SAP

A reaction mixture of stock SAP (250 ng/μL), neuraminidase (1.25 units/mL), and pH 6 sodium citrate buffer (50 mM) were incubated at 37°C for 1 hour to remove terminal sialic acid residues. Afterwards the sample was dialyzed against 1 L of deionized water at room temperature for 1 hour to remove buffer components found to be problematic for cIEF. Successful desialylation was confirmed by directly characterizing on MALDI-MS. In one experiment, desialyated SAP was combined with stock SAP in order to enrich the asialo variant to create a mixed sample for cIEF-MS.

4.2.5 Mass spectrometry

For the MSIA population study, MALDI-MS analysis was performed using a Bruker (Billerica, MA, USA) Ultraflex instrument operating in the positive ion, delayed-extraction, and linear mode with the following parameters: ion source 1 at 25.00 kV, ion source 2 at 23.10 kV, lens at 9.00 kV, 90 ns delayed extraction, and deflection signal suppression up to m/z 8000. A 96 spot gold target was used to collect the eluted proteins. Ten thousand laser-shots were accumulated for each mass spectrum. The spectra were externally calibrated with a mixture of proteins supplied by Bruker (Cat. No. 206355 and 207234), baseline

subtracted, and smoothed using the Gauss algorithm (width 1 m/z, cycles 1) within Flex Analysis software.

For ESI analysis, 8 μL of sample was loaded for pre-concentration/solvent exchange before eluting into a Bruker MicrOTOF-Q mass spectrometer following the parameters described previously [21]. For data analysis, approximately 1 min of recorded spectra were averaged across the chromatographic peak maximum followed by spectral deconvolution within 1000 Da to all identified peaks using Bruker data analysis v3.4 software.

For analyzing the cIEF fractions, a 96 spot ground steel target was used for all experiments. Immediately after collecting each cIEF fraction, 2 μL of matrix solution was added to allow for dried droplet deposition. Protein standards without cIEF separation (SAP and desialyated SAP, 500 ng each) were spotted directly onto the target plate and 2 μL of matrix solution was immediately added. Droplets on the target plate were allowed to air dry at room temperature and pressure. All MALDI-MS spectra were generated on either a Bruker Microflex or Autoflex mass spectrometer generated by accumulating 500 shots. The instrument was operated in positive ion mode with a 20 kV extraction voltage and 300 ns delay time. The spectra were calibrated externally using equine myoglobin, baseline subtracted, and smoothed using the Gauss algorithm (width 1 m/z, cycles 1) within Flex Analysis software.

4.3 Results and discussion

4.3.1 Pooled SAP sample assessed via MALDI-MS

The heterogeneity of pooled SAP was analyzed by directly placing samples on a MALDI target plate and subjecting them to mass spectrometric analysis (Fig. 4.1A). The primary signal was at 25,460 m/z which is in good agreement with the theoretical molecular weight of the SAP monomer with two sialic acid residues (disialo) [22]. A peak at 25,170 m/z was observed and assigned to the loss of a single sialic acid residue (-290 Da). Additional peaks were observed (25,670 and 25,380 m/z) with a mass shift of +220 Da and are consistent with matrix adducts of sinapinic acid (224 g/mol) of the disialo and monosialo species. To prepare for and be consistent with experiments noted below, relatively high laser power for desorption and ionization was used, resulting in a small additional peak consistent with the asialo form at 24,880 m/z. This is caused by the sialic acid groups being somewhat labile in response to the ablation process, and is considered to be an artifact of the ionization process. In ESI-MS analysis, only the disialo and monosialo signals were observed confirming that the asialo species is virtually non-existent in native SAP preparations and is likely an artifact in MALDI-MS (Fig. 4.1B). Furthermore, the asialo signal dominates the overall spectra when using much higher laser powers (data not shown).

Supporting this interpretation of the mass spectra is data collected from pooled SAP samples treated with neuraminidase (which selectively and quantitatively removes sialic acid), where signals at 25,460 m/z, assigned to the

disialo, and 25,170 m/z, assigned to monosialo, are minimized and the signal consistent with asialo (24,880 m/z) is significantly enhanced (Fig. 4.1C). Additional peaks are consistent with matrix adducts. These quantitative results are significantly different than the much broader heterogeneity observed in the gel IEF analyses [3-5]. One possible explanation for the difference between these findings and previous results is that direct mass spectrometric analysis may not completely resolve all isoforms and another separation mode is warranted.

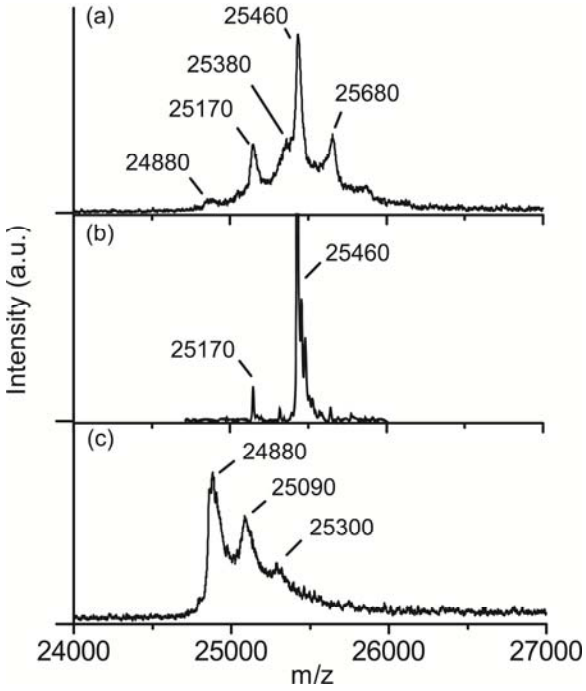

Figure 4.1. MALDI-MS results from pooled SAP. (A) Representative mass spectra of SAP from MALDI-MS, (B) SAP from ESI-MS with y-axis zoomed to show details, and (C) MALDI-MS of SAP after 1 hour incubation with neuraminidase at 37°C. For native SAP, the peaks at 25,460, 25,170, and 24,880 m/z represent the disialo, monosialo, and asialo SAP monomers, respectively. Additional peaks in (A) and (C) represent matrix adducts with a shift of 210-220 Da corresponding to sinapinic acid (224 g/mol).

4.3.2 Pooled SAP sample assessed via cIEF-MALDI-MS

According to gel IEF studies of pooled and individual SAP, multiple bands were interpreted to be isoforms that differ in pI by at least 0.02 and as much as 1.0 pH units which can not be explained in light of mass spectrometry analysis (Table 1) [3-5]. The use of modern capillary-based isoelectric focusing allows for resolution of ΔpH units as small as 0.05 and is compatible with MALDI-MS with minimal separation efficiency loss [17, 23]. In support of effective cIEF and MALDI-MS coupling, baseline resolution of variants β-lactoglobulin A and B (ΔpI 0.3) was demonstrated in Chapter 3, although differing by only two amino acids [18].

Only a single band along the pI dimension resulted from quantitative cIEF-MALDI-MS of pooled SAP, in both native and denaturing conditions (8 M urea), in distinct contrast to some gel IEF results (Fig. 4.2A-B) [3-5]. The single band had a pI 4.2 ± 0.1 (n=4) for the native form and 5.0 ± 0.1 (n=4) for the denatured one. In all cases, the sialic acid variants were found at the same pI and no other mass spectral signals were found in any other pI zones. Higher laser powers were used to ensure optimal detection limits for potentially dilute isoforms, and thus, a weak signal for the asialo protein was observed apparently from fragmentation. The pI shift in the presence of urea is likely due to SAP denaturing and thus disassociating into monomers. The pI was determined by calibrating the pH gradient with the use of pI markers 5.1 and 4 which were detected by online absorbance detection at 220 nm (Fig. 4.3) [24].

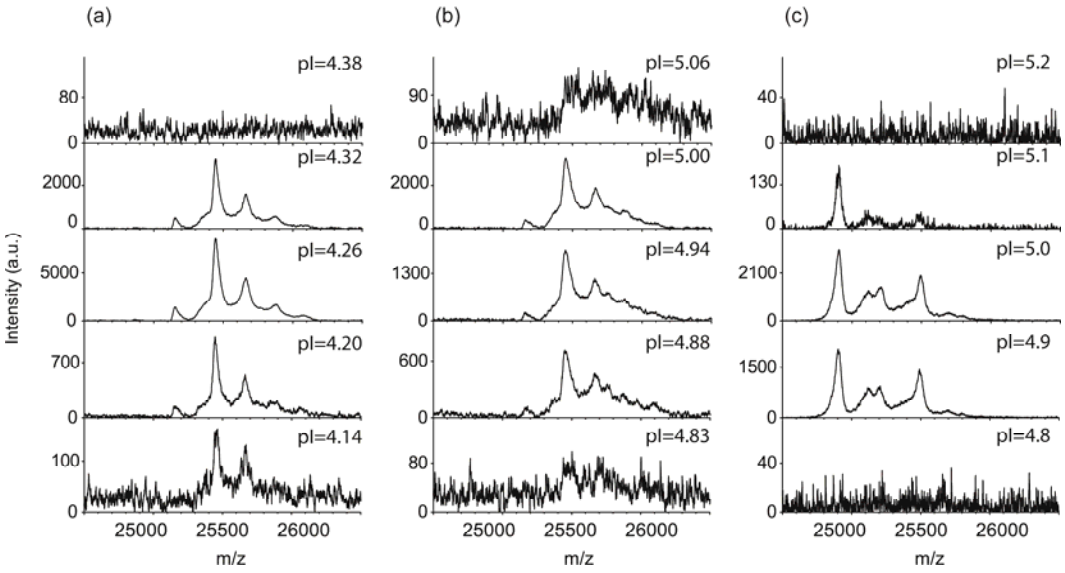

Figure 4.2. cIEF-MALDI-MS results from pooled SAP samples. (A) SAP, (B) SAP with 8 M urea, and (C) a mixture of SAP & desialylated SAP with 8 M urea. Desialylated SAP generated by incubating SAP with neuraminidase at 37 °C for 1 hour. No spectral signals were observed in any other fractions not shown.

For pooled SAP without urea, the experimental pI agrees with the pI value of 4.1 as determined by chromatofocusing [25] but differs from the pI value of 5.6-6.2 observed in gel IEF [5]. In the later case, it is possible that SAP was denatured in the sample preparation or in the acrylamide gel during focusing since this pI value agrees with pI of denatured SAP in other gel IEF experiments [3-5]. For denatured pooled SAP in presence of 8 M urea, the pI is significantly lower than the average pI of 5.8 (± 0.3) from several gel IEF experiments [3-5, 7, 26], and can likely be attributed to the contrasting conditions of the medium, exposure of gel to atmosphere, or difference in temperature. The pooled SAP focused close to the pI markers, suggesting possible interaction between the protein and markers. However, experiments with and without markers produced identical results.

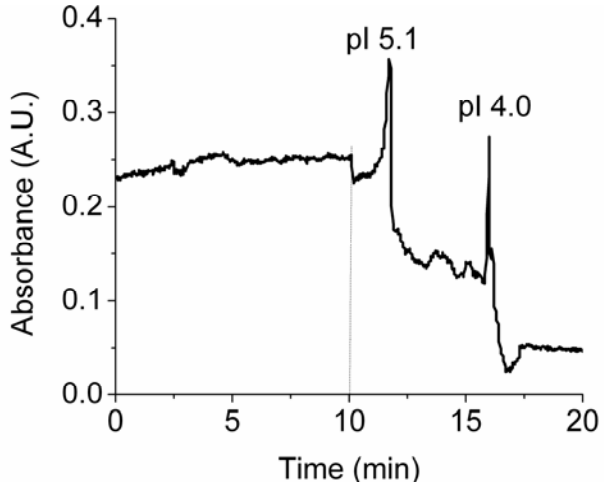

Figure 4.3. Electrophorogram of pI markers. Representative absorbance profile (220 nm) of cIEF run illustrating detection of pI markers (5.1 & 4.0) and steady decay of background absorbance due to ampholyte mixture. The dashed line (10 min) indicates the time at which mobilization is initiated.

The single band observed in all cIEF experiments is in precise agreement with the uneven sialylation peaks identified in direct MS. Sialic acid residues cause a subtle change in pI, on the order of 0.1 pH units for a different protein [27]. SAP sialo-forms are not expected to be resolved by pI since the fraction interval of 0.1 pH unit encompasses the expected pI difference. Additionally, the situation is further complicated by artifacts from the ionization process causing some disialo species to be detected as mono or asialo ones (and mono detected as asialo). The subtle pI difference is further supported in an experiment where the asialo species is enriched using neuraminidase and not completely resolved from disialo (Fig. 4.2C). It is clear, however, that the species are partially resolved since the asialo species provides a unique signal for the pH 5.1 fraction. Nonetheless, the lack of pI resolution amongst SAP sialo-forms was not

concerning since they are easily separated by mass in the spectra. Overall, these findings support the simple model that uneven sialylation is the main source of isoforms previously suggested using MS [2, 6].

These cIEF MALDI-MS results do not support the level of heterogeneity interpreted from previous gel IEF studies [3-5] and a number of experimental details can account for these discrepancies. Individual bands are not resolved from one another in Kubak et al., but data were interpreted as identifying three isoforms within 0.15 pH units (a fourth was observed in 2DE) [3]. Similarly, Serensen et al. reports significant problems with the profile and width of the pI markers suggesting considerable run-to-run variance, yet identifies six isoforms within just 0.22 pH units from only two data sets [4]. Nybo et al. details that the protein markers (carbonic anhydrase and ovalbumin) create multiple bands in the presence of urea, yet claim as many as seven SAP isoforms within 1 pH unit without discussing the obvious experimental problems [5]. Not surprisingly, there is considerable disagreement amongst these results and with other gel IEF studies which did not observe SAP isoforms [7, 26]. Although different, the pooled SAP data shown here using cIEF-MALDI-MS is more reliable than the aforementioned gel IEF studies since it is quantitative and relied on minimal manual manipulation.

4.3.3 Mass spectrometric immunoassay of individual SAP samples

Within the pooled samples, an individual's heterogeneous SAP variant may be diluted such that it is no longer detectable. If there is a large variation among individuals, then the provenance of the samples in the previous studies

could provide an explanation for the varied results. To determine the extent of heterogeneity across the population, SAP preparations isolated from 374 different individuals were analyzed using mass spectrometric immunoassay [6]. The MALDI-MS instrument was operated at a lower laser power to maximize peak resolution. With the exception of one, identical spectra were obtained for all individuals, regardless of health state (Fig. 4.4). The disialo and monosialo signals were consistent with direct and cIEF separated pooled SAP samples. The one individual which is an exception showed an additional peak at 25,780 m/z (+ 320 Da relative to disialo). Currently, it is unclear what this peak represents and additional studies are needed. The spectral uniformity was confirmed quantitatively as shown by the average relative peak areas and standard deviations across the population: disialo (25,460 m/z) 89 ± 1%, monosialo (25,170 m/z) 3.8 ± 0.8%, disialo matrix adduct (25,680 m/z) 4.0 ± 0.2%, and monosialo matrix adduct (25,385 m/z) 3.3 ± 0.5%. The process of matrix adduct formation is poorly understood [28], and thus it is unclear why the relative matrix adduct signals are not proportional to their parent ions. Overall, these results suggest that there is no significant population heterogeneity or any protein modifications specific to the disease states examined (unpublished results). Thus, it is unlikely that previous conflicting findings of SAP isoforms are due to differences in sampling.

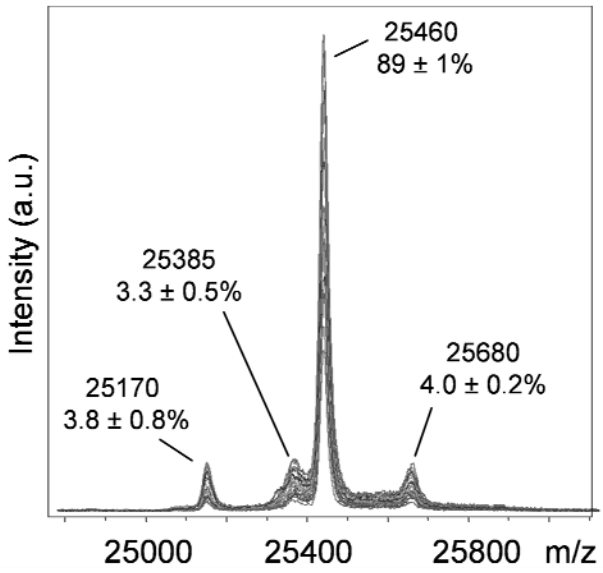

Figure 4.4. Mass spectrometric immunoassay results of individual SAP samples. Representative MALDI mass spectra of SAP preparations from 20 individuals overlaid. The primary peaks are at 25,460 m/z (disialo) and 25,170 m/z (monosialo), and the other peaks represent matrix adducts (25,680 and 25,385 m/z). These spectra are representative of 373 out of 374 samples tested from individuals as supported by the relative peak areas and standard deviations shown above each signal.

4.4 Concluding remarks

Through this work, a comprehensive examination of SAP microheterogeneity is undertaken using pooled and individual preparations in order to clarify the inconsistent findings across SAP literature. Only sialic acid variation was observed when analyzing pooled SAP with direct MALDI-MS and cIEF-MALDI-MS. Here SAP isoforms disialo (25,460 Da) and monosialo (25,170 Da) were identified and found to have similar pIs of 4.2 ± 0.1 and 5.0 ± 0.1 in its native and urea denatured states, respectively. However, the relative amounts of these two species may be biased depending on the extent of sialic acid loss resulting from the laser induced fragmentation process. Considering the

quantitative and instrumental advantages of the methods used, this data provides new information in support of the previous theory suggesting uneven sialylation is the primary microheterogeneity source. Thus, it is concluded that SAP has no isoforms, frequent amongst the population, which were previously thought to exist but were uncharacterized. The SAP population study supports this conclusion since 373 of 374 individual SAP preparations, across an array of disease states, generated essentially identical mass spectral data.

4.5 References

[1] Pepys, M. B., Booth, D. R., Hutchinson, W. L., Gallimore, J. R., Collins, P. M., Hohenester, E., *Amyloid* 1997, *4*, 274-295.

[2] Pepys, M. B., Rademacher, T. W., Amatayakul-Chantler, S., Williams, P., Noble, G. E., Hutchinson, W. L., Hawkins, P. N., Nelson, S. R., Gallimore, J. R., Herbert, J., Hutton, T., Dwek, R. A., *Proc. Natl. Acad. Sci. USA* 1994, *91*, 5602-5606.

[3] Kubak, B. M., Gewurz, H., Potempa, L. A., *Int. Arch. Allergy Appl. Immunol.* 1988, *87*, 194-203.

[4] Serensen, I. J., Andersen, O., Nielsen, E. H., Svehag, S. E., *Int. Arch. Allergy Immunol.* 1995, *106*, 25-31.

[5] Nybo, M., Hackler, R., Kold, B., Nielsen, E. H., Steinmetz, A., Svehag, S. E., *Scand. J. Immunol.* 1998, *48*, 350-356.

[6] Kiernan, U. A., Nedelkov, D., Tubbs, K. A., Niederkofler, E. E., Nelson, R. W., *Proteomics* 2004, *4*, 1825-1829.

[7] Hawkins, P. N., Tennent, G. A., Woo, P., Pepys, M. B., *Clin. Exp. Immunol.* 1991, *84*, 308-316.

[8] Rodriguez-Diaz, R., Wehr, T., Zhu, M., *Electrophoresis* 1997, *18*, 2134-2144.

[9] Hille, J. M., Freed, A. L., Watzig, H., *Electrophoresis* 2001, *22*, 4035-4052.

[10] Silvertand, L. H. H., Torano, J. S., van Bennekom, W. P., de Jong, G. J., *J. Chromatogr. A* 2008, *1204*, 157-170.

[11] Wehr, T., *LCGC North America* 2004, *22*, 998-1004.

[12] Foret, F., Muller, O., Thorne, J., Gotzinger, W., Karger, B. L., *J. Chromatogr. A* 1995, *716*, 157-166.

[13] Chartogne, A., Gaspari, M., Jespersen, S., Buscher, B., Verheij, E., Heijden, v. d., Tjaden, U., van der Greef, J., *Rapid Commun. Mass Spectrom.* 2002, *16*, 201-207.

[14] Crowley, T. A., Hayes, M. A., *Proteomics* 2005, *5*, 3798-3804.

[15] Yu, W., Li, Y., Deng, C., Zhang, X., *Electrophoresis* 2006, *27*, 2100-2110.

[16] Lechner, M., Seifner, A., Rizzi, A. M., *Electrophoresis* 2008, *29*, 1974-1984.

[17] Silvertand, L. H. H., Torano, J. S., de Jong, G. J., van Bennekom, W. P., *Electrophoresis* 2009, *30*, 1828-1835.

[18] Weiss, N. G., Zwick, N. L., Hayes, M. A., *J. Chromatogr. A* 2010, *1217*, 179-182.

[19] Debeer, F. C., Pepys, M. B., *J. Immunol. Methods* 1982, *50*, 17-31.

[20] Niederkofler, E. E., Tubbs, K. A., Kiernan, U. A., Nedelkov, D., Nelson, R. W., *J. Lipid Res.* 2003, *44*, 630-639.

[21] Borges, C. R., Jarvis, J. W., Oran, P. E., Rogers, S. P., Nelson, R. W., *J. Biolmol. Tech.* 2008, *19*, 167-176.

[22] Prelli, F., Pras, M., Frangione, B., *J. Biol. Chem.* 1985, *260*, 12895-12898.

[23] Minarik, M., Groiss, F., Gas, B., Blaas, D., Kenndler, E., *J. Chromatogr. A* 1996, *738*, 123-128.

[24] Righetti, P. G., *J. Chromatogr. A* 2004, *1037*, 491-499.

[25] Ohkubo, I., Sahashi, W., Namikawa, C., Tsukada, K., Takeuchi, T., Sasaki, M., *Clin. Chim. Acta* 1986, *157*, 95-102.

[26] Urbanyi, Z., Medzihradszky, D., *J. Chromatogr.* 1992, *578*, 130-133.

[27] Yang, L., Tang, Q., Harrata, A. K., Lee, C. S., *Anal. Biochem.* 1996, *243*, 140-149.

[28] Loboda, A. V., Chernushevich, I. V., *Int. J. Mass Spectrom.* 2005, *240*, 101-105.

Chapter 5

MALDI-MS Studies Using Photolithographically Patterned Silicon Nanowire Superhydrophobic Surfaces

5.1 Introduction

Mass spectrometry (MS) offers a number of advantages for biomolecular detection including low detection limits (on the order of 100's of fmol), high sensitivity, and large molecular weight dynamic range (1,000 to 100,000 amu). As demonstrated in the previous chapters, MS can improve biomolecule detection for capillary separations by overcoming the limitations of absorbance and fluorescence. Either electrospray ionization (ESI) or matrix assisted laser desorption/ionization (MALDI) are predominantly used as ionization modes for interfacing mass spectrometry with separation techniques. These techniques have complimentary advantages and disadvantages, and thus no single method is universally employed [1]. The emphasis of this dissertation is on MALDI-MS.

Although MALDI-MS can improve detection, it has its own set of limitations. For instance, it is universally recognized to produce non-quantitative responses and often require optimized sample deposition specific to each sample [2]. This point is illuminated when considering many different deposition strategies have been developed to improve the performance of MALDI-MS: dried droplet [3], slow matrix crystallization [4], thin film matrix layer [5], fast evaporation [6], and various probe modifications [7]. Clearly, the crystal morphology and distribution of analyte in matrix plays a critical role in a MALDI-MS experiment [8], but there are a limited number of studies which

explore these dependencies and almost no quantitative physical investigations. Furthermore, a universal mechanistic role of the matrix is questionable as different analytes and matrices have been shown to produce contrasting results [9, 10].

One potential limitation in MALDI-MS is the mismatch in typical spot size (1-2.5 mm) and laser size (~100 μm). Thus, the laser only samples a heterogeneous portion of the deposited material at a given time [11]. The use of miniaturized deposition techniques has emerged as one tactic to help overcome this limitation [12]. It is hypothesized that a smaller spot size will increase the analyte density resulting in more sensitive detection and improve sampling homogeneity leading to better signal precision. Various strategies have been developed including electrical droplet manipulations [13, 14], incorporation of small channels or vials [15, 16], and the use of hydrophobic materials [17-19].

The work of Schuerenberg et al. is probably the most well-known contribution utilizing hydrophobic surfaces to miniaturize MALDI sample deposition [18]. They developed and commercialized a Teflon-coated plate with 200 μm diameter gold, hydrophilic spots (AnchorChip^{TM} plates) which improved MALDI-MS sensitivity and detection limit. This and most other efforts report miniaturized deposition improves MALDI-MS sensitivity because of analyte enrichment. Although logical, this is fairly presumptuous since there lacks sufficient control experiments to corroborate such a hypothesis. The analyte density is increased through miniaturized deposition, but the effects of the altered crystallization and deposition conditions are unknown and arguably equally

influential [20]. Additionally, broad generalizations are not valid because different analytes and matrices do not undergo the same ionization mechanisms [9, 10]. An improved understanding of how various factors in the sample deposition step affect the MALDI-MS signal is needed.

As the analyte-matrix-solvent sample evaporates during deposition, the matrix nucleates, crystallizes, and envelops the analyte in conditionally dependent fashions. Therefore, the inter-woven and non-linear processes of evaporation, mass transport, nucleation, and crystallization must be understood for each analyte/matrix/solvent system in order to completely optimize the sample deposition step [21]. Influencing factors include, but are not limited to: spot size, surface morphology, solvent evaporation rate, solvent composition, droplet contact angle, solubility, temperature, convection, diffusion, and nucleation/crystallization rates of matrix (Fig. 1).

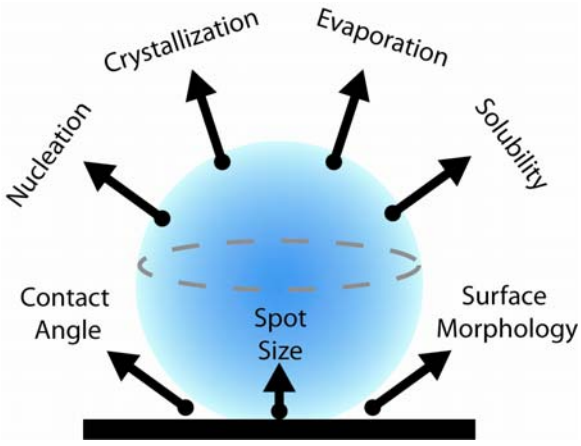

Figure 5.1. Schematic illustration of the physiochemical influences on MALDI sample deposition.

Many of these physiochemical influences were investigated in the dissertation of Melissa McLauchlin, Ph.D. using silicon nanowire (SNW) superhydrophobic surfaces with laser ablated pinning sites [22, 23]. A brief summary of the findings from a sinapinic acid matrix/acetonitrile/water experimental framework are presented here. Kinetic effects were found to dictate the matrix crystallization and rates of crystallization were found to have considerable importance. In addition, spot morphology was found to play an important role when comparing CO_2 and Nd:Yag laser ablation methods. Finally, signal improvements were observed although they were often inconsistent suggesting crystallization effects had strong influence. The current chapter here is an extension of the dissertation in mention.

It can be hypothesized from the previous work that the heterogeneous, roughened nature of the laser ablated pinning sites negatively impacts the deposition process. Therefore, a goal of the current work is to investigate this by using more uniform spots produced through photolithography. In addition, analyte density, matrix density, and spot size are carefully investigated. Collectively, new insights about the resultant MALDI-MS signals are deduced that suggest crystallization processes outweigh the effect of analyte enrichment for a protein/sinapinic acid matrix system.

5.2 Materials and methods

5.2.1 Preparation of silicon nanowire superhydrophobic surfaces

Circular pinning sites between 0.25 and 2.25 mm on SNW based superhydrophobic substrates were fabricated using standard photolithography on a

microscope slide. Microscope slides were cleaned in piranha solution (2:1 sulfuric acid:hydrogen peroxide) before processing. Substrates were coated with 2 nm gold through thermal evaporation to form self-assembled catalytic nanodot seeds for nanowire growth. A photolithographic lift-off method using positive resist AZ 3312 was used to pattern gold onto the microscope slides to create nanowire free pinning sites (0.25-2.25 mm diameters in 0.25 mm increments). SNW were grown on the catalytic gold surface as previously described [23]. Finally, the SNW substrates were incubated in a 0.1% 1H, 1H, 2H, 2H-perfluorooctyltrichlorosilane (PFOS) solution in distilled toluene for 30 minutes to render them superhydrophobic.

5.2.2 Substrate characterization and contact angle

An inverted microscope and 4x objective were used for substrate imaging (Olympus, Center Valley, PA, USA). Images were collected using a miniVID USB video camera and ScopePhoto software (LW Scientific, Lawrenceville, GA,USA). Droplets of varying volume were manually pipetted onto the patterned pinning sites. Still images were collected and the contact angle of the droplet was measured every 2 min using a Goniometer model 100-00 and Drop Image Standard software (Rame-Hart, Inc., Succasunna, NJ, USA) until evaporation was complete.

5.2.3 MALDI-MS analysis

Myoglobin solutions ranging from 40-170 ng/μL (2-10 μM) were prepared using skeletal horse myoglobin (Sigma Aldrich, St. Louis, MO, USA) dissolved in distilled water. Sinapinic acid matrix solutions ranging from 0.08 to

8 μg/μL were prepared in a 70% water/30% acetonitrile solvent. The matrix and protein solutions were combined in a 1:1 volume ratio to prepare working samples for experimentation. Sample drops ranging in volume from 1 to 10 μL were manually pipetted onto a MALDI target plate and allowed to evaporate in air under ambient conditions. The standard reference plate was a ground steel target having a 96 array of 2.5 mm diameter spots (Bruker Daltonics, Billerica, MA, USA). Drops were also deposited onto the fabricated SNW plate.

Analysis of the samples was performed using a Bruker Autoflex MALDI-MS instrument. Spectra were collected by averaging the signal of 1,000 laser shots while randomly scanning the laser probe across the spotted deposit. Three separate spectra were produced for each spot to assess precision. Images of the crystal formations were collected from the instrument's internal camera used for aiming the laser. Flex Analysis software was used to identify the peak height of each of the myoglobin spectra. In some experiments the mean peak height (signal) produced on the fabricated plate are normalized by the mean peak height (signal) on the standard reference plate. In other experiments the mean peak height (signal) is normalized by the analyte density (mass of analyte per spot surface area).

5.3. Results and discussion

5.3.1 Photolithographic plate characteristics

In an earlier study, pining sites on a SNW superhydrophobic coated substrate were fabricated via Nd:Yag laser ablation [22]. In contrast here, photolithography was used for spot fabrication. The evident advantages of

photolithography compared to laser ablation are ease of engineering, spot size precision, and spot uniformity. An array of various pinning site sizes (0.25-2.25 mm) on a superhydrophobic SNW coated microscope slide were produced (Fig. 5.2A). Using optical microscopy, photolithography was observed to produce well-defined pinning sites characterized by a uniform depth and structure within spots (Fig. 5.2B). On the other hand the morphology of the laser ablated sites was described previously as having a crater-like structure with melted material at the edges [23].

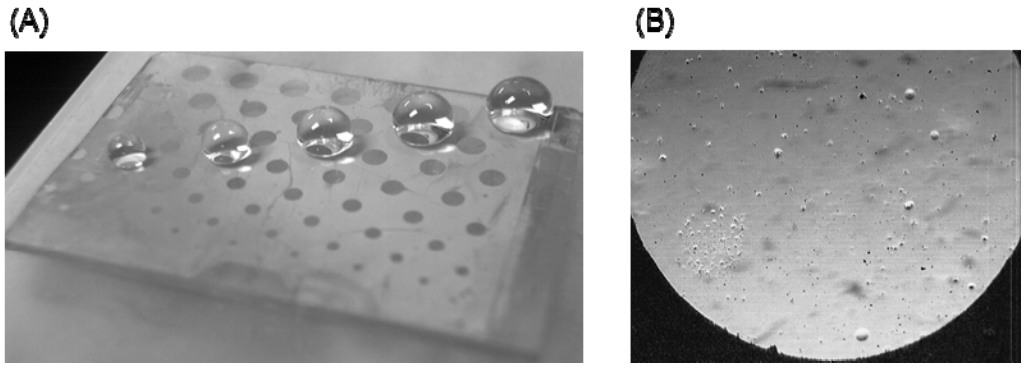

Figure 5.2. Photolithographic plate images. (A) Photolithographically patterned superhydrophobic substrate with an array of various size spots (2.25 mm back row to 0.25 mm front row). (B) Microscopy image of pinning site showing coated glass (light) and SNW (dark).

Initially, the surface wettability characteristics of the superhydrophobic surface were studied. Contact angles between 130 and 165 ° were readily observed for drops pinned within the fabricated sites. Higher contact angles were observed on smaller spot sizes because more SNW surface area interacted with the drop volume. For the largest spot sizes (1.5-2.25 mm) the drop contact angle is largely dictated by the properties of the less hydrophobic coated glass surface

which produces a nominal contact angle of 120 °. It is particularly important to understand how the contact angle changes during evaporation because this impacts the crystal deposition process. High contact angles above 150 ° for a 6 µL drop on a 0.25 mm spot were steadily maintained for most of the evaporation process (Fig. 5.3A-B). In the last few minutes of drop evaporation, a rapid decrease in contact angle is observed because the drop size is small enough that no SNW surface area interacts with the resting drop. All spot sizes produced a similar trend although the starting contact angle varied. This finding suggests that as crystallization ensues the crystalline material will settle within the predetermined drop contact area.

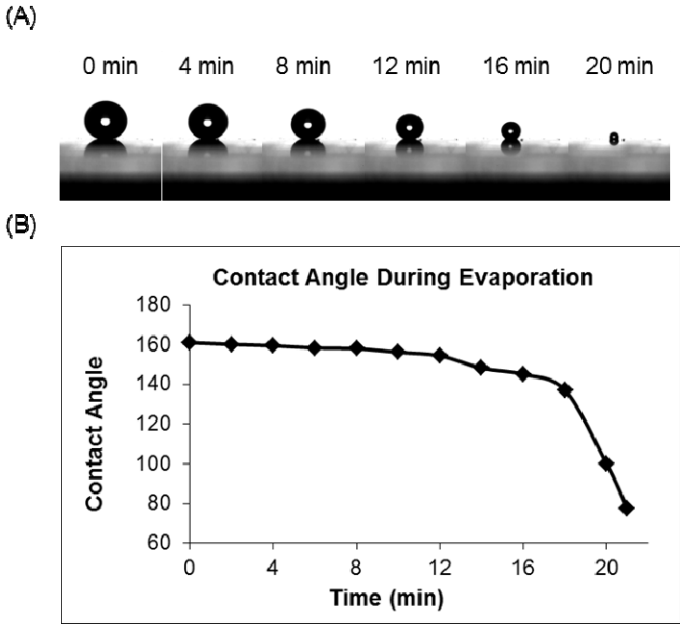

Figure 5.3. Contact angle of an evaporating droplet. (A) Still images of a 6 µL evaporating drop on a 0.25 mm site in four minute intervals. (B) Water drop contact angles during the evaporation process.

Photolithographic spots produced similar contact angles and evaporation rates as the previously employed laser ablated sites. This is expected since the two surfaces are virtually identical with the exception of the structure of the pinning site. Additionally, the photolithographic pinning sites showed strong confinement of crystalline material. Even when high levels of matrix were employed the crystals were confined within the photolithography spots except for the smallest site of 0.25 mm (Fig. 5.4). This suggests that the liquid/solid contact diameter is larger than 0.25 mm such that solids settle outside of the site. Complete matrix confinement to the 0.25 mm site is possible when using reduced matrix concentrations or drop volumes to allow the contact diameter to shrink before crystallization commences. Overall, the photolithographic sites demonstrate an improved confining ability over laser ablated sites where the crystals were observed to deposit outside of the 0.5 mm spot. Most likely, this is a result of the photolithographic sites being more uniform and having a well-defined interface.

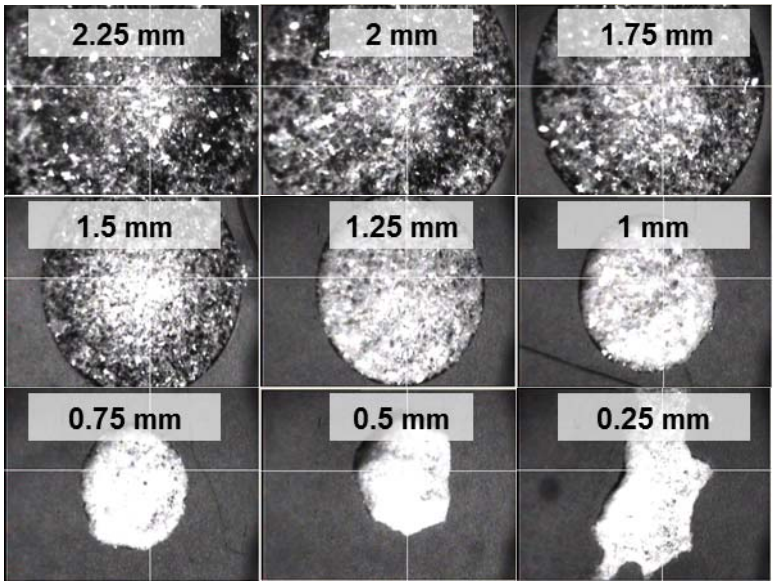

Figure 5.4. Matrix confinement images. Each spot contains 20 μg crystalline matrix deposits produced from the evaporation of 5 μL droplets.

5.3.2 MALDI-MS performance of superhydrophobic plates

The superhydrophobic surfaces were designed with the goal of improving the detection limit, sensitivity, and/or precision of MALDI-MS. A common presumption is that confining equivalent amounts of analyte to smaller surface areas will result in more frequent and uniform sampling by the laser and thus improved signal. As already introduced, however, there are many competing variables involved in the deposition process which have to be considered and in fact may dominate behaviors in any given set of conditions [8]. Spot size, analyte density, and matrix density were studied in effort to better understand the nature of the MALDI-MS signal.

In general, a more sensitive and precise signal was observed using superhydrophobic substrates compared to a standard MALDI-MS plate under typical conditions (Fig. 5.5). However, the signal enhancements were far less

than expected based on the analyte density enrichment upwards of 100-fold. On average, the superhydrophobic plate signal was roughly 3 times that of a standard stainless steel plate (2.5 mm spots) and had a relative standard deviation of 40% instead of around 70%. Interestingly, the 2 μL drops produced larger enhancements than the 3 and 5 μL drops for unknown reasons. The greatest signal enhancement observed was roughly 10 fold in all the experiments conducted. Overall, the MALDI-MS performance of the photolithographic plate is equivalent to the Nd:Yag laser ablated plate. Therefore, the spot morphology or uniformity for these surfaces fails to explain the shortcoming in performance.

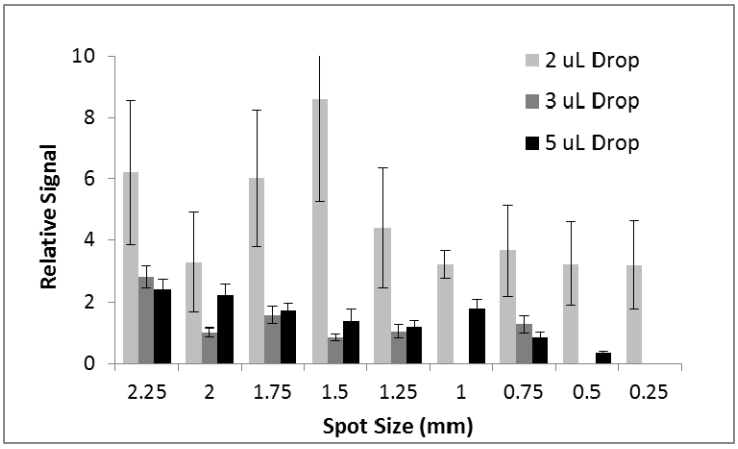

Figure 5.5. Typical MALDI-MS signal enhancements. A plot of mean and standard deviation spectral peak heights (normalized to the reference plate) from various size spots and different volume drops. All samples contained 10 μM myoglobin and 4 μg/μL sinapinic acid matrix in 70% water/ 30% acetonitrile mixture. Data was not collected where the data bars are not present.

Ultimately, a global generalization about performance of the fabricated plates is difficult since the MALDI-MS signal is very dependent on conditions (Fig. 5.1). For instance, there are probably conditions that would favor the

standard plate given the significant differences in dynamics between the two [2]. This is even apparent within some of the data sets presented (Fig. 5.5). Nonetheless, improvements are typically observed although the origin of which is not entirely clear. Analyte density alone is insufficient to understand the behaviors observed. The following section examines this in greater detail.

5.3.3 Examining analyte and matrix density

A systematic increase in signal with decreasing spot size was expected since increasing analyte amounts should be sampled by the laser. However, a consistent trend between signal and spot size was not observed under any experimental conditions tested (Fig. 5.5). In fact, the only apparent trend is that signal may decrease with decreasing spot size, but this is a weak observation since the variances are large. These results are somewhat surprising since contact angles, evaporation rates, and crystallization dynamics were seemingly identical between spot sizes. However, one clearly evident difference between spots is the matrix density (amount of matrix per spot area) because each spot received a fixed amount of matrix resulting in different size deposits (Fig 5.4). The matrix density (amount of matrix per spot area) was duly suspected to be an influencing factor.

It is important to note that this definition of matrix density is not always a surface area description, but rather a normalization of the mass-of-matrix per spot area. This means densities above a threshold value (approximately 10 $\mu g/mm^2$) produce multi-layer deposits (Fig. 5.4). In the case of multi-layer deposits, the surface area sampled by laser is not necessarily fully enriched in analyte because

the analyte becomes distributed vertically and the laser has a limited probe depth. Although this is an insightful consideration it fails to completely account for limitations because weak signals were observed with monolayer deposits as well. In summary, the amount of matrix dictates the deposit thickness and becomes a critical variable, but does not fully account for the shortfall in signal enhancement. This suggests other factors must have greater influence in the MALDI process (Fig. 5.1).

In general though, highly dense and disperse deposits did appear to reduce the ionization efficiency. Therefore, most likely every analyte/matrix system has an optimal matrix density. This was further examined for myoglobin/sinapinic acid by carrying out a broad range of experiments and normalizing signals to their respective analyte densities. Four different concentrations were used at eight different spot sizes to produce a large data set across a wide range of matrix densities. Results are variable, but there does appear to be an optimal matrix density between 2-4 $\mu g/mm^2$ (Fig. 5.6). It is important to note though this only applies to the fabricated plate and other plates including the standard reference plate may have a unique optimum.

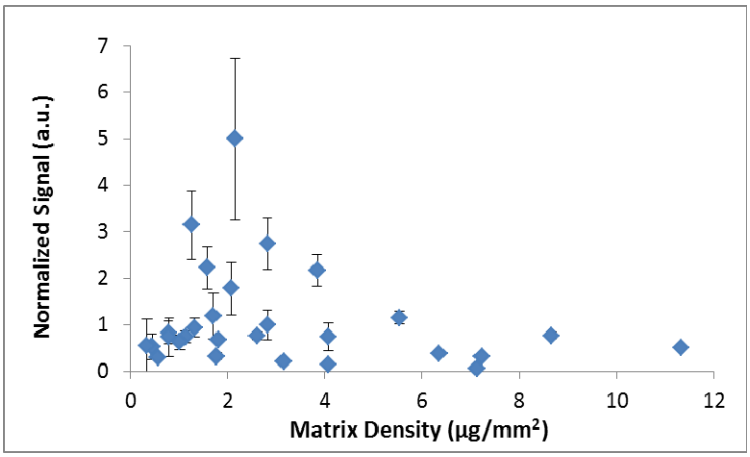

Figure 5.6. Effect of matrix density. Average and standard deviation peak height signals normalized by analyte density are plotted against matrix density. Drops were 2 µL containing 3 µM myoglobin and various matrix concentrations (0.7, 1.6, 2.5, and 3.4 µg/µL). Drops were spotted at all spot sizes (0.25, 0.5, 0.75, 1, 1.25, 1.5, 1.75, 2, and 2.25 mm)

To isolate the role of analyte density more clearly, experiments were carried out while the matrix density was fixed. The starting matrix concentration was adjusted individually (between 0.08 and 8 µg/µL) such that the resultant matrix density at each spot size was 5 µg/mm^2. This density was chosen to prevent multi-layer deposit formation and is seemingly ideal (Fig. 5.6). However, results from these experiments still did not produce a systematic trend with spot size as expected (data not shown). While there are likely many contributing factors, one consideration is that each spot experienced altered nucleation/crystallization dynamics because each spot started with a different matrix concentration. Rates of crystallization are expected to be very different between spot sizes. In fact, unique crystal morphologies were observed on the various size spots suggesting this is a critical factor (Fig. 5.7). This illustrates the

interwoven system dependencies and the difficulty in isolating variables individually. All starting conditions impact more than one variable.

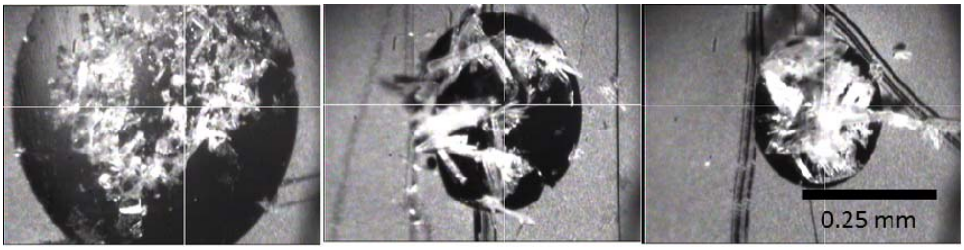

Figure 5.7. Variation in crystal morphology. Images of crystal deposits on 0.75, 0.5, and 0.25 mm spots where the starting matrix concentration was adjusted to 0.74, 0.33, and 0.08 µg/µL, respectively. The drop volumes were 3 µL and produced an ending matrix density of 5 µg/mm^2.

5.3.4 Alternative paradigms

One possible limitation of this work is that relatively high protein concentrations were employed. Therefore, it is plausible that results did not meet expectations because the conditions were near the signal saturation limit. More dilute concentrations could potentially improve the findings; however, brief efforts in doing produced equally inconsistent trends. Further studies are needed though before completely ruling this out. Another possibility is that protein MALDI is very different from peptide MALDI. Most miniaturized sample depositions utilize peptides for proof-of-principle experiments [13, 16-19]. Perhaps the desorption/ionization of peptides is much more efficient and linear such that they produce better results and are subject to greater benefit from surface enrichment strategies. Instead of these hypotheses, it is suspected that this works greatest limitation is the difficulty in isolating variables individually and

carrying out control experiments. Overall though, more data sets and more conditions need investigation before complete conclusions can be drawn.

A better approach might be to carry out many experiments over a broad range of conditions while carefully tracking all outcomes and variables: crystal morphology, evaporation rates, sample composition, matrix density, spot size, analyte density, contact angle and diameter. Using multivariate or chemometric methods large volumes of data could be analyzed to individually isolate variables [24]. This could lead to the development of crude, quantitative models of MALDI-MS. Initial models would initiate a feedback loop where the experimental framework is improved, new data sets are collected, and more accurate and complex models are constructed.

5.4 Concluding remarks

Superhydrophobic surfaces with photolithographically patterned pinning sites were used to investigate some fundamental MALDI-MS behaviors of a protein/sinapinic acid matrix system. Findings suggest that increasing analyte density does not sufficiently explain observed signal improvements, and that similar studies need to carefully examine this presumption before suggesting otherwise. Results also show that subtle crystallization dynamics represent an equally if not more important variable. Differences in spot morphology between photolithographic sites and Nd:Yag sites have negligible impact on MALDI-MS signals. This work reinforces the same questions that are yet to be fully understood for MALDI-MS. How do the interwoven dynamics of evaporation,

nucleation, and crystallization affect the analyte and matrix distributions? Is there a quantitative relationship between analyte distribution and ionization efficiency?

5.5 References

[1] Stutz, H., *Electrophoresis* 2005, *26*, 1254-1290.

[2] Kussmann, M., Nordhoff, E., Rahbek-Nielsen, H., Haebel, S., Rossel-Larsen, M., Jakobsen, L., Gobom, J., Mirgorodskaya, E., Kroll-Kristensen, A., Palm, L., Roepstorff, P., *J. Mass Spectrom.* 1997, *32*, 593-601.

[3] Karas, M., Hillenkamp, F., *Anal. Chem.* 1988, *60*, 2299-2301.

[4] Xiang, F., Beavis, R. C., *Org. Mass Spectrom.* 1993, *28*, 1424-1429.

[5] Xiang, F., Beavis, R. C., *Rapid Commun. Mass Spectrom.* 1994, *8*, 199-204.

[6] Vorm, O., Roepstorff, P., Mann, M., *Anal. Chem.* 1994, *66*, 3281-3287.

[7] Xu, Y., Bruening, M. L., Watson, J. T., *Mass Spectrom. Rev.* 2003, *22*, 429-440.

[8] Cohen, S. L., Chait, B. T., *Anal. Chem.* 1996, *68*, 31-37.

[9] Gluckmann, M., Pfenninger, A., Kruger, R., Thierolf, M., Karas, M., Horneffer, V., Hillenkamp, F., Stupat, K., *Int. J. Mass Spectrom.* 2001, *210*, 121-132.

[10] Chang, W. C., Huang, L. C. L., Wang, Y.-S., Peng, W.-P., Chang, H. C., Hsu, N. Y., Yang, W. B., Chen, C. H., *Anal. Chim. Acta* 2007, *582*, 1-9.

[11] Garden, R. W., Sweedler, J. V., *Anal. Chem.* 2000, *72*, 30-36.

[12] Tu, T., Gross, M. L., *Trends Analyt. Chem.* 2009, *28*, 833-841.

[13] Tu, T., Sauter Jr, A. D., Sauter, A. D., Gross, M. L., *Am. Soc. Mass Spectrom.* 2008, *19*, 1086-1090.

[14] Bogan, M., J., Agnes, G. R., *J. Am. Soc. Mass Spectrom.* 2004, *15*, 486-495.

[15] Little, D. P., Cornish, T. J., O'Donnell, M., J., Braun, A., Cotter, R. J., Koster, H., *Anal. Chem.* 1997, *69*, 4540-4546.

[16] Ekström, S., Ericsson, D., Önnerfjord, P., Bengtsson, M., Nilsson, J., Marko-Varga, G., Laurell, T., *Anal. Chem.* 2001, *73*, 214-219.

[17] Gundry, R. L., Edward, R., Kole, T. P., Sutton, C., Cotter, R. J., *Anal. Chem.* 2006, *77*, 6609-6617.

[18] Schuerenberg, M., Luebbert, C., Elckhoff, H., Kalkum, M., Lehrach, H., Nordhoff, E., *Anal. Chem.* 2000, *72*, 3436-3442.

[19] Wang, J., Chen, R., Ma, M., Li, L., *Anal. Chem.* 2008, *80*, 491-500.

[20] Choi, C. H., Kim, C.-J., *Langmuir* 2009, *25*, 7561-7567.

[21] Baird, J. K., *J. Cryst. Growth* 1999, *204*, 553-562.

[22] McLauchlin, M. L., *Chemistry and Biochemistry*, Arizona State University, Tempe 2007, p. 138.

[23] McLauchlin, M. L., Yang, D., Aella, P., Garcia, A. A., Picraux, S. T., Hayes, M. A., *Langmuir* 2007, *23*, 4871-4877.

[24] Brandt, H., Ehmann, T., *Anal. Chem.* 2010, *82*, 8169-8175.

Chapter 6

Isoelectric Focusing in a Drop

6.1 Introduction

Chapters 3 and 4 presented examples of high resolution separations where subtle variations were targeted. There also exists a need for low-resolution separations capable of high-throughput, crude sample purification. Moreover, devices that perform these separations with low-volume sample size are of growing interest. Miniaturized devices that address these needs can provide lower cost, higher productivity, and more effective decision-making. The miniaturization of this technology (along with other design elements) allows it to be broadly deployed to the sampling locations, rather than the current paradigm of transportation to a central laboratory with complex and expensive instrumentation. Various microfluidic systems have been developed in this vein over the past ten years [1-6].

Microfluidic systems can be categorized either as flow, digital, or hybrid depending upon whether the fluid of interest is fed continuously through microchannels, moved as discrete drops, or is manipulated as discrete drops within a continuous immiscible liquid, respectively [7]. In any case, the ability to conduct molecular separations of complex samples is a desirable feature of such microfluidic systems. Flow and hybrid systems typically require the use of microchannels which can create some challenges. These range from difficult integration of sample pre-processing and surface fouling to channel blockages resulting from bubbles or particulates. Digital microfluidic systems overcome

most of these obstacles by allowing discrete fluidic processing in open environments and minimizing surface area contact. Perhaps the most daunting challenge in the digital system, however, is the implementation of a molecular separation step [8].

A few strategies for performing separations within drops have been explored recently. Electrophoretic [9] and dielectrophoretic [10,11] forces were exploited to create binary separations of particles 1-10 μm which increased their concentration about two-fold. Methods for collecting magnetic particles [12,13] and for extracting proteins by precipitation [14] have also been developed in drops. In an alternative approach, a microchannel based separation was integrated onto a digital platform [15]. Although such sophisticated efforts open up new opportunities for digital microfluidics, the interest here is in exploring a separation mechanism which could separate more than two analytes and be carried out in the digital state. Such a separation would maintain simplicity, avoid unwanted effects of microchannels, and be capable of integrating into any digital microfluidic platform regardless of actuation method (electric [8] or magnetic [16]). Here the idea of performing a molecular separation within an open drop using droplet-based isoelectric focusing (dIEF) is explored.

Isoelectric focusing, traditionally carried out in gels and more recently capillaries [17,18], is a type of gradient separation which separates molecules based on their isoelectric point (pI) or pH of net neutral charge. A uniform electric field and a pH gradient are applied along the separation length which causes molecules to focus in the region of net neutrality which is specific to their

chemical composition. The term focusing comes from the fact that diffusion is counter-balanced by electrophoresis once a steady state is reached. A molecule that diffuses out of the neutral zone towards the anode (lower pH region) will assume a positive charge and migrate back towards the focus point and vice versa if it diffuses towards the cathode. Thus, the steady state concentration distribution of a 1D system is given by the following [19]:

$$C(x) = C_o\, e^{\frac{-(\rho E (x - x_{pI})^2)}{2D}} \tag{1}$$

where C is the concentration of a component, C_o is the concentration maximum, $\rho = d\mu/dx$ is the slope of the electrophoretic mobility (μ): assumed to be constant within the focused zone, E is the electric field strength, x is the coordinate along the direction of current, x_{pI} is the isoelectric point, and D is the diffusion coefficient. This is a Gaussian concentration profile with standard deviation given by:

$$x_\sigma = \pm\sqrt{\frac{D}{\rho E}} \tag{2}$$

Eqs. (1-2) are insightful because they identify the important parameters for generating narrow bands of material and can be used to model more complex systems. Proteins are particularly well suited for IEF because they have large mobility slopes (ρ) and small diffusion coefficients (D). Applying these concepts within an open drop gives rise to the technique of dIEF.

In addition to visualization, non-invasive light scattering measurements are used to confirm protein focusing in dIEF. Dynamic light scattering (DLS) was

originally developed to study the fluid dispersions of colloidal (size ≤1 μm) particles [20]. The ability of DLS to detect early changes in the molecular morphology of proteins has the potential to help develop new treatments to combat various ocular and systemic diseases prior to the onset of irreversible changes [21]. In a DLS experiment, a constantly fluctuating speckle pattern is seen in the far field when light passes through an ensemble of small particles suspended in a fluid [20]. This speckle pattern is the result of interference in the light paths and it fluctuates as the particles in the scattering medium perform random movements on a time scale of ≥1 μs due to the collisions between themselves and the fluid molecules (Brownian motion). In the absence of particle-particle interactions (dilute dispersions) light scattered from small particles fluctuates rapidly while light scattered from large particles fluctuates more slowly. Generally speaking, an increase in particle sizes (from nanometers to a few microns) and an increase in the number or density of these particles result in an increase in total scattered light intensity (static light scattering). The experiments reported here utilize this feature.

Superhydrophobic surfaces (SHS) provide some unique opportunities for manipulating fluids in the digital state [22-25], and much progress has been made in fabrication over the years [26,27]. An important realization is that aqueous drops take up well-defined shapes and do not spread on a SHS. Thus, if manipulated properly the drop can be positioned and stabilized in shapes necessary for carrying out a separation without the need for a supporting chamber (e.g., channel, capillary, etc.). With the interest of developing low cost, simple

devices a roughened polyethylene SHS is utilized to allow manipulation of drops [16,28,29]. This paper presents a preliminary yet detailed study of the dIEF principles. Through this work the generation of stable pH gradients, well behaved protein focusing, and accurate quantitative modeling is demonstrated. These findings suggest that dIEF could be applied for sample purification of complex biological mixtures or integration into digital microfluidic devices.

6.2 Materials and methods

6.2.1 Chemicals and materials

Unless mentioned otherwise all chemicals and materials were obtained from Sigma-Aldrich (St. Louis, MO, USA). Pharmalyte brand ampholyte (pH 3-10) was obtained from Amersham Biosciences (Postcataway, NJ, USA). A stock universal indicator solution was prepared with 400 ppm phenolphthalein, 50 ppm thymol blue, 300 ppm bromothymol blue, and 150 ppm methyl red in 10% ethanol (v/v). Electrodes were made from 0.5 mm diameter platinum wire which was shaped into 5 mm diameter loops. A digital power supply was used for applying voltages and measuring current (SMU2064, Signametrics, Seattle WA).

Superhydrophobic polyethylene surfaces were prepared as previously described [23]. Briefly, low density polyethylene was allowed to crystallize on a polyethylene substrate in the presence of a solvent and nonsolvent by slow heating and evaporation. A USB camera (MiniVid, LW Scientific, Lawernceville GA) was used to capture all movies and images of the DIEF experiments.

6.2.2 Droplet-based isoelectric focusing

For pH gradient visualization the samples contained 2 % (w/v) ampholyte pH 3-10 and 10 % (v/v) stock universal indicator. For preliminary protein studies the samples contained 2 % (w/v) ampholyte pH 3-10 and 0.25 mg/mL myoglobin. Drops ranging in volume from 50-200 μL were pinned and stretched 0.5-2 cm between two loop electrodes on a superhydrophobic surface (Fig. 6.1). This led to drops with an allantoidal shape where the drop body is cylindrical with rounded ends where it pinned to the electrodes. Depending on the experiment, a low voltage was applied ranging from 5-30 V resulting in currents 0.1-1 mA. Voltages were applied for durations up to an hour. Over this period the current decreased to about 40% of its initial value; a result typical of a loss of charge carriers in IEF. The nominal electric field strength is estimated by dividing the applied voltage by the drop length. Video footage was collected to characterize pH gradient formation. For protein separation experiments, the drop was split as described below.

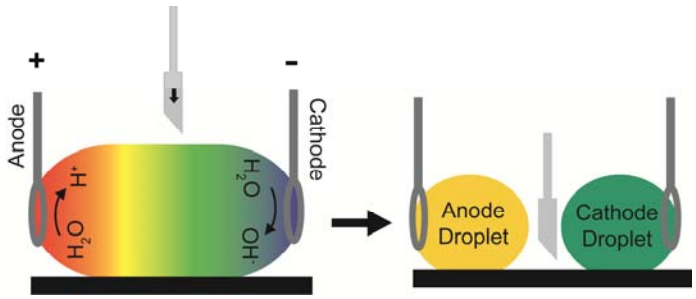

Figure 6.1. Schematic illustration of isoelectric focusing in a drop. An allantoidal drop is supported on a superhydrophobic substrate and pinned between two loop electrodes. Upon applying a voltage the electrolysis of water produces H^+ and OH^- at the anode and cathode, respectively. Then the drop is split by lowering a superhydrophobic 'guillotine' to generate two new drops.

6.2.3 Drop splitting and protein quantification

Drops were split using a thin superhydrophobic substrate to penetrate and separate the drop into two. Initially, this surface was mounted on a slide positioned above the drop (Fig. 6.1). When the dIEF experiment was complete the slide was lowered splitting the drop into two sections. This action is capable of physically splitting a water drop to generate two new daughter drops. When proteins or other surfactants are present, the superhydrophobic surface becomes wettable and the drop no longer has the necessary surface energy to independently form two new drops. Nonetheless, the penetrated surface provides a barrier to separately collect the split portions without mixing. Thus, after lowering the superhydrophobic 'guillotine' in these experiments the two separated portions were collected by pipette, weighed to determine volume, and stored for quantification.

Myoglobin was quantified by absorbance measurements (λ = 405 nm, ε405nm = 245,000 M-1 cm-1) using a small-volume flow-cell built in house. This consisted of a 320 μm internal diameter capillary threaded into a CE flow cell with fiber optics delivering light from a DH-2000 deuterium lamp to a USB 4000 bench top spectrometer (Ocean Optics, Dunendin, FL, USA). This apparatus only requires 15 μL of sample while providing a reasonable path length and is well suited for quantifying the <100 μL fractions collected after drop splitting.

6.2.4 Light scattering detection

A compact fiber-optic light scattering probe was used to measure aggregation in the protein sample as the DC voltage was applied (Fig. 6.2). It was mounted roughly 5 cm from the drop surface and scanned laterally across the length of the drop at a rate of 50 μm/s using a programmable stage motor. The total time to collect a single scan (6 mm length) was 2 minutes. Allowing time for the probe to return to its starting position, scans were collected every 2.5 minutes for the duration of the dIEF experiment. To successfully capture the progression, light scattering intensity was continuously recorded for the entire experiment duration. The setup comprises a semiconductor laser (λ=639.4 nm, power=80 μW), a photodetector (avalanche photodiode based photon counting module), a DLS probe built at NASA for both static and dynamic light scattering configurations (scattering angle=163.0 degrees, focal length=16 mm, scattering volume ~50 μm^3), a translation stage with a motorized actuator, for accurate positioning, (to which the DLS fiber optic probe is mounted on a multi axis translation stage), and a Pentium based computer containing a digital correlator card (BI-9000) for data acquisition. This system has been previously used in protein crystal growth experiments [30], particle sizing applications in flowing dispersions [31], in protein characterization of ocular tissues in live animals [32], and in clinical ophthalmic applications for the early detection of cataract [33]. Only the static (total intensity) light scattering measurements were made in the experiments reported here.

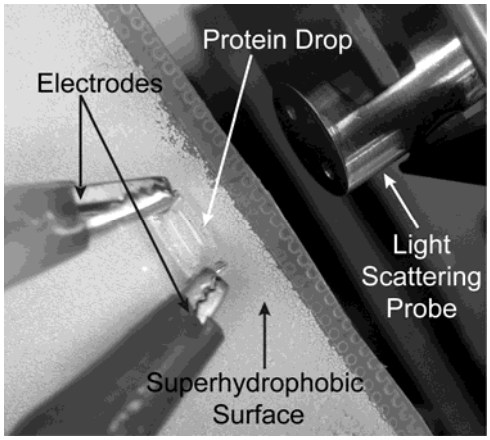

Figure 6.2. Experimental setup used for light scattering detection.

6.3 Results and discussion

6.3.1 pH gradient formation

Electrolytic pH gradient generation has been demonstrated theoretically and experimentally for microfluidic systems [34,35], and it is hypothesized a similar process could take place within open drops. It is based on the principle of oxidizing water at the anode to form H^+ ions and reducing water at the cathode to form OH^- ions. As time evolves, these ions can be transported throughout the solution through diffusion, electromigration, fluid flow, and exchange with buffering ions. Thus, a pH profile can develop across the solution and dynamically change until reaching an equilibrium state defined by the solution and electrical properties. Buffering of the solution has a critical role in generating smooth, stable gradients since electrolysis of non-buffered solutions typically leads to a step-like pH profiles across the system length [36]. Therefore, the first phase of experimentation was to examine the possibility of forming smooth,

stable pH gradients by electrolyzing water in drops after positioning and stretching them on a SHS.

A universal indicator dye sensitive to a pH range of 3-10 was used for visual characterization of gradient formation (Fig. 6.3I). Not surprisingly, when 25 mM phosphate is used step-like pH profiles develop rather than uniform gradients (data not shown). In these experiments, extreme pH zones slowly evolve over time from the electrodes, pH<3 for the anode and pH>10 for the cathode, until a very narrow pH transition region remains. This pH profile is likely formed because the rate of electrolysis exceeds mass transport and exchange with buffering ions (i.e., source exceeds sink). Next, a common IEF ampholyte mixture (Pharmalyte pH 3-10) was used and this generated stable, uniform pH gradients as indicated by the color profile of the dye. Still images show the formation of a pH gradient ranging from pH ~ 4 (light red, anode side) to pH ~ 9 (blue, cathode side) (Fig. 6.3A-D). The gradient was formed in about 10 minutes and was found to be stable over longer periods of applied voltage (at least 45 minutes). This is an indication that the ampholyte buffers are distributed across the drop such that they buffer the pH and efficiently transport the continual generation of H^+ and OH^- ions. The pH gradient was reversed by switching electrode polarity (Fig. 6.3E-H). It took about 15 minutes for the gradient to reverse, but similarly a stable profile was observed over prolonged applications of voltage. For comparison, reference pH solutions and their universal indicator color response are shown (Fig. 6.3I).

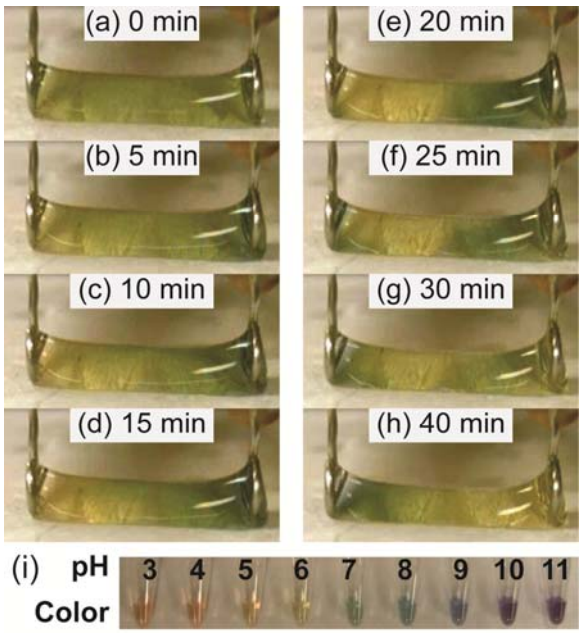

Figure 6.3. Visualizing droplet pH gradients with a universal indicator. (A-D) Still images over time showing the generation of a stable pH gradient using 2% pharmalyte 3-10 as the buffer. (E-H) The polarity of the electrodes is switched at t=15 min causing a reversal of the pH gradient. (I) Reference pH solutions and their corresponding color response.

Traditional IEF theory predicts individual ampholyte species will focus into steady state zones, stacked in order of pIs, and will control local pH [37]. Experimental investigations have demonstrated that ampholytes are often distributed in a much more random fashion [38]. Thus, it is uncertain how ampholyte components are distributed in these drop experiments. An exponential reduction in current is observed over time characteristic of a decrease in conductivity from ampholyte focusing. Overall these results demonstrate that pH gradients within drops can be generated, held stable with appropriate buffers, and reversed by switching polarity.

6.3.2 Characterizing protein focusing

The next phase of experiments involved characterizing the dIEF focusing behavior of a single protein and comparing the results to 1D steady state theory. Myoglobin (pI 7.2) was selected as a target since it has a chromophore allowing easy detection and its IEF properties were previously studied [39]. Assuming a linear pH gradient and defining the anode as pH 3 at x=0 and the cathode as pH 10 at x=1.5 cm means that myoglobin would focus at x_{pI}=0.9 cm. Several trials were conducted where 5-20 V was applied across 150 μL drops for twenty minutes. Subsequently, the drops were split at an average position of x=0.7 cm and the protein content in the two resultant droplets, defined as anode and cathode droplets, was quantified by absorbance measurements.

Two clear observations arose from these experiments (Table 1). The first is that the protein became more isolated to the cathode droplet side with increasing electric field. This is an expected result since bandwidth becomes narrower with increasing field (Eq. (2)) and myoglobin's pI lies on the cathode side of the droplet. Thus, more protein is predicted to be isolated on the cathode side as the field increases. The second observation is that the protein recovery decreased with increasing field strength, presumably as a result of an increasing current. This suggests that significant protein oxidation and/or reduction is occurring as a result of direct contact with the electrodes which renders the protein undetectable. In support of this interpretation is data collected where high protein recoveries were observed (>95%) when isolating the electrodes to reservoirs separated from the drop by dialysis membranes.

Table 6.1. Experimental and theoretical findings for myoglobin at various electric fields in droplet isoelectric focusing.

	Experimental: Relative Myoglobin Mass		Theoretical: Relative Myoglobin Mass		
E (V/cm)	Anode	Cathode	Anode	Cathode	% Recovery
4.3	42%	58%	41%	59%	77%
8.9	40%	60%	38%	62%	70%
12.7	28%	72%	35%	65%	65%

To construct an appropriate model of myoglobin focusing in a drop numerical values are substituted into Eq. (1). The ratio of ρ/D, defined as α, can be determined by rearranging Eq. (2) and using experimental data to solve:

$$\alpha = \frac{\rho}{D} = \frac{1}{E\, x_{\sigma}^{\,2}} \tag{3}$$

Previously, myoglobin focused into a band with a standard deviation of 0.6 cm in a 40 cm capillary while applying 10 kV [39]. Thus, when the separation length is 40 cm then α=0.01 V^{-1} cm^{-1} for myoglobin. In the case of a 1.5 cm drop using the same ampholyte mixture, α=0.27 V^{-1} cm^{-1} since ρ is 27 times greater due to the different length scales (40 cm to 1.5 cm) and noting the D is unchanged. Substituting α and x_{pI} into Eq. (1) and normalizing the function so the peak area is 1 gives the following relation:

$$C(x) = \sqrt{\frac{0.27\,E}{2\,\pi}}\, e^{\frac{-\left(0.27\,E\,(x-0.9)^2\right)}{2}} \tag{4}$$

Plots of the model presented in Eq. (4) at various field strengths provide a quantitative sense of the expected steady state distributions of myoglobin in dIEF (Fig. 6.4). The relative extent of protein isolation is determined by integrating Eq. (4) with respect to the split position and infinity. Splitting the drop at x=0.7 cm results in 59-65% of myoglobin being isolated to the cathode droplet when the electric field is 4-13 V/cm. Thus, the model is consistent with the experimental results collected at equivalent field strengths (Table 6.1). Although the model is expected to be more accurate with narrowing bandwidth (finite size effects), the differences between the experimental and theoretical findings are attributed to the limited precision (~10% RSD) of the drop splitting mechanism. This along with evaporative and redox effects makes it difficult to assess the model's accuracy from the experimental results alone. Nonetheless, the results suggest that dIEF approaches a steady state, under the conditions employed, similar to that predicted from 1D theory. Furthermore, this simple model can be used to make predictions for other proteins with known α and x_{pI} values.

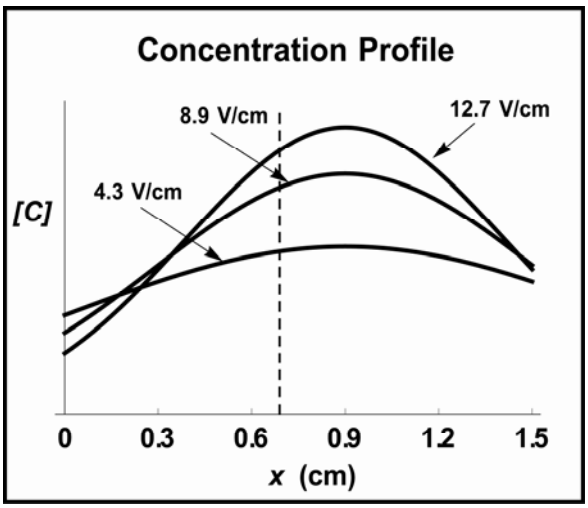

Figure 6.4. Modeling steady state protein concentration. Concentration profiles of myoglobin focusing in dIEF at different field strengths (Eq. 4). Dashed line indicates position where drop was split (0.7 cm).

To improve the separation efficiency of a particular protein either the electric field could be increased or the drop could be split further away from its pI. For example, when 300 V/cm is applied (more typical of electrokinetic techniques) Eq. (4) predicts myoglobin would be 99.5% isolated to the cathode droplet when split at the same position (0.7 cm). Experimentally, fields greater than 15 V/cm were not applied since high currents and excessive bubbling occurred. Electrodes can be isolated to separate reservoirs to minimize these effects as is common practice in traditional electrophoretic techniques, with the caveat that the isolated zones must be relatively small volume and the electrodes a short diffusional/transport distance from the separations drop. On the other hand, when splitting the drop at x=0.3 cm while applying a low field strength (13 V/cm) 95% of myoglobin would be isolated to the cathode droplet. Ultimately, this

approach requires precise engineering control over drop splitting and it would reduce the volume which is purified.

6.3.3 Protein focusing detected by light scattering

Visible, unlabelled proteins such as myoglobin or cytochrome c often are precipitated in dIEF at the necessary concentrations for good visualization. Additionally, it is difficult to image the drop directly due to the non-linear optical reflective and refractive effects resulting from the drop's curved surface. Therefore, light scattering was used to provide more direct characterization of protein focusing in dIEF, where the signal is due to aggregation of the target protein when the local concentration is very high. In these experiments a light-scattering probe, containing optical fibers to deliver light from source and to detector, was scanned across the drop. For simplicity and speed, a smaller drop was used (50 μL and 5 mm length) and the SHS was removed allowing the drop to be suspended in the air.

When a voltage is applied to a drop containing protein an intense scattering signal near 2.75 mm was observed after 18 minutes in three different trials (Fig. 6.5A). The scattering signal was roughly 100 times greater than what is expected from the calibration curve generated by protein standards without applying a voltage (data not shown). Considering its magnitude, this intense response is interpreted as the result of protein focusing which stimulates aggregation and leads to larger particles scattering more light. Regardless of the exact mechanism, this scattering signal is not observed in control experiments

where either the protein or voltage is removed (Fig. 6.5B-C); confirming that it is a direct result of the protein's presence while applying a voltage.

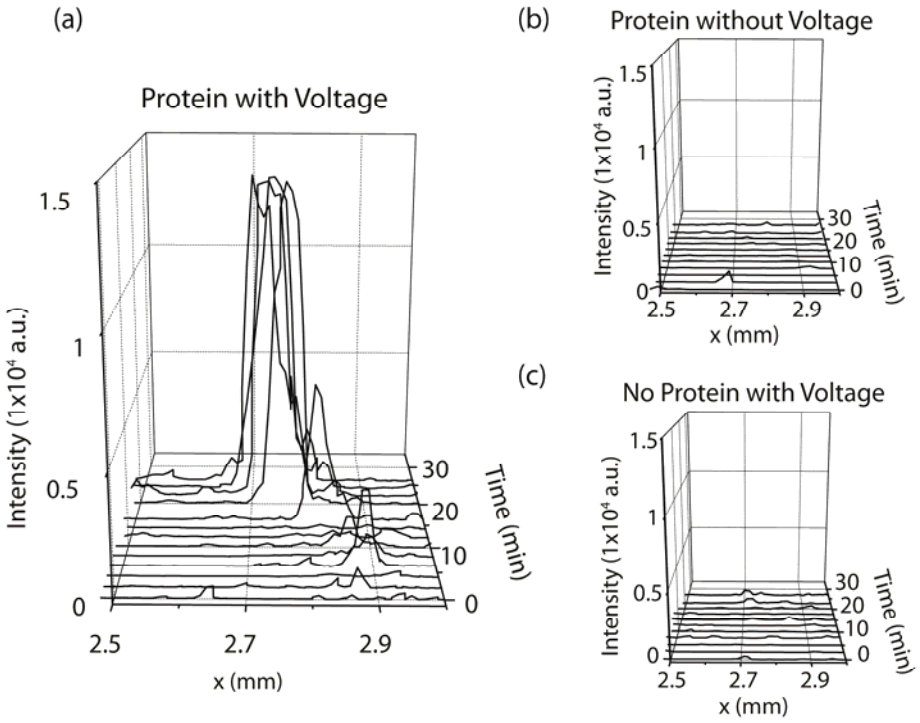

Figure 6.5. Light scattering detection of protein focusing. Whole drop light scattering detection scans taken in 2.5 minute intervals (A) applying voltage to drop containing protein, (B) control experiment where protein is present without voltage, and (C) control experiment where voltage is applied without the protein's presence.

The light scattering data provides direct evidence of protein focusing in dIEF. The consistent observation of a scattering signal near 2.75 mm confirms that myoglobin is focusing near pH 7.2. It is difficult to assess the bandwidth of the focused zone since the scattering signal is a result of protein aggregation and not protein concentration alone. Additionally, this means the timescale for which the signal is observed, requiring time for aggregation, does not necessarily reflect

that for actual protein focusing. Although it is difficult to say for certain, the protein achieves a steady-state focus after approximately 10 minutes since this is when the current stabilizes and the pH gradient is fully established (Fig. 6.3C).

6.4 Concluding remarks

A preliminary investigation of isoelectric focusing within a drop is undertaken here in an effort to develop a separation mechanism compatible with digital microfluidics. Through electrolysis and the use of ampholyte buffers stable pH gradients can be generated in drops on the order of 10 minutes. Furthermore, light scattering data provides evidence that proteins focus about their pI within the established pH gradient as expected. Combining protein focusing with drop splitting leads to a mechanism for preparative separation. Characterizations using myoglobin reveal that differential protein concentrations are sustained after drop splitting, up to 70%:30% with an electric field of 13 V/cm and by splitting near its pI. These results are found to correlate well to predictions based on quantitative modeling of IEF theory suggesting that dIEF is well behaved and reaches a steady state. Ultimately, these results support the idea that dIEF can be used for purifying protein samples upwards of 99% and that it can be integrated into digital microfluidic systems. This could also be very useful in container less processing of materials in space.

6.5 References

[1] Cesaro-Tadic, S., Dermick, G., Juncker, D., Bourman, G., Kropshofer, H., Michel, B., Fattinger, C., Delamarche, E., *Lab Chip* 2004, *4*, 563-569.

[2] Blazej, R. G., Kumaresan, P., Mathies, R. A., *PNAS* 2006, *103*, 7240-7245.

[3] Fu, J., Schoch, R. B., Stevens, A. L., Tannenbaum, S. R., Han, J., *Nat. Nanotechnol.* 2007, *2*, 121-128.

[4] Srisa-Art, M., Dyson, E. C., deMello, A. J., Ede, J. B., *Anal. Chem.* 2008, *80*, 7063-7067.

[5] Unger, M. A., Chou, H.-P., Thorsen, T., Scherer, A., Quake, S. R., *Science* 2000, *288*, 113-116.

[6] Srinivasan, V., Pamula, V. K., Fair, R. B., *Lab Chip* 2004, *4*, 310-315.

[7] Teh, S.-Y., Lin, R., Hung, L.-H., Lee, A. P., *Lab Chip* 2008, *8*, 198-220.

[8] Fair, R. B., *Microfluid. Nanofluidics* 2007, *3*, 245-281.

[9] Cho, S. K., Zhao, Y., Jin, C., Kim, C., *Lab Chip* 2007, *7*, 490-498.

[10] Fan, S.-K., Huang, P.-W., Wang, T.-T., Peng, Y.-H., *Lab Chip* 2008, *8*, 1325-1331.

[11] Zhao, Y., Yi, U.-C., Cho, S. K., *J. Microelectromech. Syst.* 2007, *6*, 1472-1481.

[12] Sista, R. S., Eckhardt, A. E., Srinivasan, V., Pollack, M. G., Palanki, S., Pamula, V. K., *Lab Chip* 2008, *8*, 2188-2196.

[13] Wang, Y., Zhao, Y., Cho, S. K., *J. Micromech. Microeng.* 2007, *17*, 2148-2156.

[14] Wheeler, A. R., Jebrail, M. J., *Anal. Chem.* 2009, *81*, 330-335.

[15] Abdelgawad, M., Watson, M. W. L., Wheeler, A. R., *Lab Chip* 2009, *9*, 1046-1051.

[16] Schneider, J., Egatz-Gomez, A., Melle, S., Lindsay, S. A., Dominguez-Garcia, P., Rubio, M. A., Marquez, M., Garcia, A. A., *Colloids Surf. A Physiochem. Eng. Asp.* 2008, *323*, 19-27.

[17] Righetti, P., Drysdale, J., *J. Chromatogr.* 1974, *98*, 271-321.

[18] Rodriguez-Diaz, R., Wehr, T., Zhu, M., *Electrophoresis* 1997, *18*, 2134-2144.

[19] Svensson, H., *Acta Chem. Scand.* 1961, *15*, 325-341.

[20] Chu, B., *Laser Light Scattering: Basic Principles and Practice*, Academic Press, New York 1991.

[21] Ansari, R. R., *J. Biomed. Optics* 2004, *9*, 22-37.

[22] Egatz-Gomez, A., Melle, S., Garcia, A. A., Lindsay, S. A., Marquez, M., Dominguez-Garcia, P., Rubio, M. A., Picraux, S. T., Taraci, J. L., Clement, T., Yang, D., Hayes, M., Gust, D., *Appl. Phys. Lett.* 2006, *89*, 034106.

[23] Garcia, A. A., Egatz-Gomez, A., Lindsay, S. A., Dominguez-Garcia, P., Melle, S., Marquez, M., Rubio, M. A., Picraux, S. T., Yang, D., Aella, P., Hayes, M. A., Gust, D., Loyprasert, S., Vazquez-Alvarez, T., Wang, J., *J. Magn. Magn. Mater.* 2007, *311*.

[24] Lindsay, S. A., Vazquez-Alvarez, T., Egatz-Gomez, A., Loyprasert, S., Garcia, A. A., Wang, J., *Analyst* 2007, *132*, 412-416.

[25] McLauchlin, M. L., Yang, D., Aella, P., Garcia, A. A., Picraux, S. T., Hayes, M. A., *Langmuir* 2007, *23*, 4871-4877.

[26] Li, X.-M., Reinhoudt, D., Crego-Calama, M., *Chem. Soc. Rev.* 2007, *36*.

[27] Roach, P., Shirtcliffe, N. J., Newton, M. I., *Soft Matter* 2008, *4*.

[28] Erbil, H. Y., Demirel, A. L., Avci, Y., Mert, O., *Science* 2003, *299*, 1377-1380.

[29] Lu, X., Zhang, C., Han, Y., *Macromol. Rapid Commun.* 2004, *25*, 1606-1610.

[30] Ansari, R. R., Suh, K. I., Arabshai, A., Wilson, W., Bray, T. L., DeLucas, L. J., *J. Cryst. Growth* 1996, *168*, 216-226.

[31] Leung, A. B., Suh, K. I., Ansari, R. R., *Appl. Opt.* 2006, *45*, 2186-2190.

[32] Simpanya, M. F., Ansari, R. R., *J. Photochem. and Photobiol.* 2008, *84*, 1589-1595.

[33] Datiles, M. B., Ansari, R. R., Suh, K. I., Vitale, S., Reed, G. F., Zigler, J. S., Ferris, F. L., *Arch. Ophthalmol.* 2008, *126*.

[34] Macounova, K., Cabrera, C. R., Holl, M. R., Yager, P., *Anal. Chem.* 2000, *72*, 3745-3751.

[35] Cabrera, C. R., Finlayson, B., Yager, P., *Anal. Chem.* 2001, *73*, 658-666.

[36] Klimov, A., Pollack, G. H., *Langmuir* 2007, *23*, 11890-11895.

[37] Mosher, R. A., Thormann, W., *Electrophoresis* 1990, *11*, 717-723.

[38] Sebastiano, R., Simo, C., Mendieta, M. E., Antonioli, P., Citterio, A., Cifuentes, A., Peltre, G., Righetti, P., *Electrophoresis* 2006, *27*, 3919.

[39] Weiss, N. G., Zwick, N. L., Hayes, M., *J. Chromatogr. A* 2010, *1217*, 179-182.

Chapter 7

Dielectrophoretic Mobility Determination in DC Insulator-Based Dielectrophoresis

7.1 Introduction

Particles are ubiquitous in our bodies and our environment. This class of materials includes cells, organelles, nanoparticles, aerosols, large proteins and DNA strands, bacteria, and viruses—among other organic and inorganic debris. Dielectrophoresis (DEP) has emerged as an important technique for manipulating micro to nano scale particles [1, 2]. The nature of this force, described over 50 years ago by Pohl, depends on a particle's polarizability in a non-uniform electric field (Eq. (1)) [3]. The dielectrophoretic force experienced by a spherical particle is described as follows:

$$F = 4\pi\varepsilon_f r_p^{\,3} Re(f_{cm})(E\cdot\nabla)E = 2\pi\varepsilon_f r_p^{\,3} Re(f_{cm})\nabla E^2$$
$$Re(f_{cm}) = \frac{\sigma_p - \sigma_f}{\sigma_p + 2\sigma_f} \qquad f < 100 \text{ kHz} \tag{1}$$

where ε_f is the permittivity of the fluid, r_p is the particle radius, $Re(f_{cm})$ is the real part of the Clausius-Mossoti factor defined by the particle and fluid conductivities (σ) at low frequency (f), and E is the electric field. At higher frequencies the conductivities are replaced with frequency dependent permittivities. According to this relationship, to have a DEP force on a non-charge-containing species there must be a non-uniform field and a particle that has a different conductivity/permittivity relative to the fluid.

It is important to note that DEP can be operated in AC or DC modes using either shaped conductors or insulators to generate field gradients [4]. The emphasis in this work is on DC insulator-based dielectrophoresis (DC iDEP). The initial and most popular design for DC iDEP is a microfluidic channel employing an array of insulating structures (Fig. 7.1A) [5-19]. Channels with obstructions (Fig. 7.1B) [20-26], serpentine features [27, 28], and converging-diverging or saw-tooth features (Fig. 7.1C) [29-33] have also been established in DC iDEP. Similar iDEP designs employ AC fields (10 Hz – 10 MHz) to gain additional DEP control through frequency modulation of the Clausius-Mossoti factor [34-38]. Additionally, a contactless AC iDEP approach where the sample is completely isolated from the electrodes has been shown [39, 40]. In all of the designs an insulating material (e.g., glass, polymer, etc.) is used to create regions where the electric field is constricted to generate a field gradient and a DEP force. These devices deflect, stream, or trap particles in a composition-dependent manner for separation or concentration.

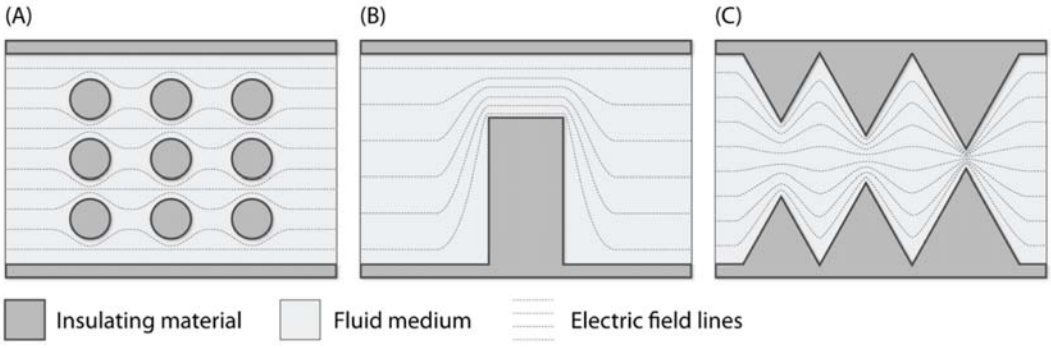

Figure 7.1. Schematic illustrations of the most common iDEP devices. Examples shown include the (A) array of insulators [5-19, 35-38], (B) obstructed channel [20-26, 34], and (C) converging-diverging or saw-tooth [29-33].

While Eq. (1) is widely accepted, it is usually only considered qualitatively when considering actual experimental data. Most discussions of real data rarely advance beyond an analysis of positive (towards stronger fields) versus negative (towards weaker fields) DEP. This is somewhat odd since there is extensive quantitative theory and modeling of DEP [31-34, 41, 42]. One detailed study did indicate some unique deviations from Eq. (1) from ionic effects [43]. Dielectrophoretic techniques are growing in popularity and with this interest it becomes increasingly important to develop detailed and quantitative metrics for the field.

It is often unreasonable to accurately calculate the DEP force that is exerted on a particle from first principles and this provides, perhaps, one explanation for the relative paucity of quantitative application of theory to experimental data. The difficulty arises from the uncertainties in the permittivity, particle size/shape, deformability, and local field gradients. Furthermore, Eq. (1) assumes a spherical particle having a permanent or induced dipole and fails to describe complex shapes or multipolar states [44]. A practical solution to determining the DEP properties of particles is to experimentally determine the relative dielectrophoretic velocity in a known gradient. This is analogous to the electrophoretic or electroosmotic mobility that is routinely measured in electrophoresis with a known electric field. Previously, methodologies have been developed for measuring a dielectrophoretic mobility in AC-DEP [43, 45-47]. Although useful for AC applications, these approaches are limited because they define the DEP mobility parameter to be dependent on the device-specific electric

field properties (device parameters actually appear in the definitions of the mobility). Thus, the mobility constants are specific to the particular device geometries used and cannot be ported to iDEP systems. To quantify dielectrophoretic effects from the complex geometries of current iDEP designs (Fig. 7.1A-C) and allow detailed investigations resulting in accurate models, a universal quantitative metric of the DEP particle properties is needed. Moreover, if the DEP properties are known the electric field profile necessary for a particular outcome can be determined. With the aid of modeling software, iDEP systems can be rationally designed to generate the necessary electric field to target specific analytes (e.g., bacteria or virus).

In this work, a strategy to quantitatively determine dielectrophoretic properties of particles in iDEP settings is initiated by defining the dielectrophoretic mobility and demonstrating an approach to measure it in a converging microfluidic channel. This method relies on streak-based velocimetry to generate the spatial velocity profile of particles. From this the dielectrophoretic and electrokinetic mobilities of polystyrene particles are simultaneously determined.

7.2 Materials and methods

7.2.1 Device fabrication

A microfluidic channel was fabricated using standard soft lithography using the elastomer PDMS from a Slygard 184 kit (Dow/Corning, Midland, MI, USA). PDMS was cast over a master wafer that contained an AZ 4620 photoresist pattern (AZ Electronic Materials, Branchburg, NJ, USA) to create

channel impressions. The resist thickness was characterized with a Tencor P2 Profilometer and found to have a depth of 10 μm. After casting the PDMS over the master wafer it was cured at 70 °C for 1 hour and subsequently access holes were punched. An oxygen plasma was used to render the channels hydrophilic and generate a self-sealing surface. Finally, a clean glass microscope slide was used as a cover plate to enclose the microfluidic PDMS channel.

7.2.2 Dielectrophoresis experiments

The microfluidic channel was initially filled with buffer solution and allowed to equilibrate at rest for 10 minutes. The buffer consisted of 5 mM aspartic acid pH 3.1 and had a conductivity of 250 μS/cm or specific resistivity of 4,000 Ω•cm (Sigma Aldrich, St Louis, MO, USA). Solution conductivities were measured using an Orion 3 Star conductivity meter (Thermo Fischer, Walthan, MA, USA). Sulfated polystyrene particles 1 μm in size and fluorescently labeled (Invitrogen, Carlsbad, CA, USA) were diluted to a concentration of approximately 5 x 10^6 particles/mL in the working buffer and sonicated for 15 minutes. Particles were introduced into the device using hydrostatic pressure initiated by a height difference in the two reservoirs. At the start of an experiment the pressure was equilibrated to stop hydrodynamic flow, and then 1,500 V was applied from a Bertran Series 225 power supply (Bertran, Brooklyn, NY, USA) using two platinum electrodes dipped into the reservoirs with anode in region 1 and cathode in region 3. Particle motion was imaged using an Osram mercury short arc H30 103 w/2 light source and a 4x objective on an inverted microscope (Olympus, Center Valley, PA, USA). Movies were collected using a QICAM

CCD camera (Q Imaging Inc., Surrey, British Columbia, Canada) and Streampix III software (Norpix, Montreal, Quebec, Canada). Depending on the experiment, the field of view was approximately 1.6 x 1.2 mm in region 1 or 2 (Fig. 7.2A) and the exposure time was adjusted to 30, 60 or 90 ms corresponding to 19.1, 16.6 or 11.1 frames per second, respectively.

7.2.3 Velocimetry and data analysis

The velocity data is automatically generated from the streaked particle images using an algorithm. The details of the method have been described elsewhere but the main steps are briefly described here [48]. Frames captured during the imaging process serve as the algorithm input. A 20 pixel strip is cropped from the center of the image frame and the streaks are identified from the background by image thresholding. Velocities are estimated by dividing the streak length, identified as the distance between the starting and ending points of a streak, by the exposure time. These velocities are then spatio-temporally averaged over the entire cropped region to generate the centerline velocity.

Manual tracking of particles was done using ImageJ software (http://rsbweb.nih.gov/ij/). The image stack was cropped to a region 20 pixels wide along the channel centerline. The brightness and contrast was increased to allow for better visualization of particles and streaked images. The x coordinates of a single particle were tracked as it moved through the region of view by manually selecting the center of the particle's fluorescence. There was no problem with particles defocusing since the channel depth is on the order of 10 μm. Dilute particle concentrations and optimal camera conditions provided well

resolved and continuous particle trajectories. Therefore, particles were confidently identified in consecutive frames manually without need for a nearest neighbor algorithm. For each experiment, at least 50 different particles were tracked in the same manner. The x-component particle velocity as it moved from x_a to x_b was assigned to the mean position of x_a and x_b and was calculated as follows:

$$v\left(\frac{x_a + x_b}{2}\right)_x = \frac{x_b - x_a}{\Delta t} \tag{2}$$

The elapsed time, Δt, between consecutive frames is the inverse of the frame rate (16.6 fps).

The mean velocity $<v_p>$ is determined from several hundred streak based velocity measurements from a single 90 ms exposure experiment within region 1 (Fig. 7.2A). The longer exposure time produced particle streak images allowing for streak velocity assessment. In region 1 the electric field is uniform and the electrokinetic mobility (μ_{EK}) is calculated using the following convention:

$$\mu_{EK} = \left(\mu_{EO} + \mu_{EP}\right) = \frac{< v_{p,x} >}{E} \tag{3}$$

where μ_{EP} is the electrophoretic mobility and μ_{EO} is the electroosmotic mobility. A linear best fit was obtained from the velocimetry data in region 2 (Fig. 7.2A, 7.3B, and 7.4A-B).

7.3 Results and discussion

7.3.1 Particle motion and device design

In contrast to works based on AC-DEP [43, 45-47], the DEP mobility (μ_{DEP}) is defined independent of the electric field and thus becomes a universal

parameter, consistent with electrophoretic and electroosmotic mobilities, and follows the typical convention in iDEP (Eq. (4)) [6, 7, 12, 13, 16, 17, 31, 40]. In other words this definition of DEP mobility is intrinsic to the particle and represents the relative DEP velocity per unit electric field gradient squared as shown:

$$v_{DEP} = \mu_{DEP} \nabla E^2$$
$$\mu_{DEP} = \frac{\varepsilon_f r_p^{\,2} Re(f_{CM})}{3\eta} \quad (4)$$

where v_{DEP} is the DEP velocity and η is the fluid viscosity. Furthermore, an ideal method for quantifying iDEP ought to simultaneously quantify other electrokinetic effects (electroosmosis and electrophoresis). This is particularly important considering electroosmotic flow can vary by more than 10% [6]. A clear approach to quantifying the dielectrophoretic velocity emerges by examining the equations of motion.

The motion of a spherical particle with negligible particle-particle interactions under the influence of a DC electric field in iDEP is extensively described by Chen et al. [31]. The velocity along the x direction ($v_{p,x}$), the axis of the applied current, is given by:

$$v_{p,x} = E\left(\mu_{EO} + \mu_{EP} + \mu_{DEP}\frac{\partial E}{\partial s}\right)\cos\theta - \frac{\mu_{DEP}E^2}{R}\sin\theta \quad (5)$$

where s is the arc length along the field line, θ is the angle between the tangent of the field line and the x-axis, and R is the radius of curvature of the field line. At the centerline of a symmetrical channel, the field lines are parallel to the x-axis. In other words θ=0 which simplifies Eq. (5) to:

$$v_{p,x} = E\left(\mu_{EK} + \mu_{DEP} \frac{\partial E}{\partial x} \right) \quad (6)$$

where the combined electrokinetic mobility is defined as $\mu_{EK} = \mu_{EO} + \mu_{EP}$. According to Eq. (6), μ_{DEP} can be calculated by measuring the x-component of the particle velocity along the channel centerline. Traditionally, positive μ_{EK} is defined as movement towards the negative electrode and positive μ_{DEP} is defined as movement towards high field strength. The same convention is followed here since the experiments are carried out with these two conditions aligned.

The microfluidic channel consists of a wide uniform area segment (region 1), a constricting taper segment (region 2), and a narrow uniform area segment (region 3) (Fig. 7.2A). The taper was designed to create a linearly increasing electric field, or a constant gradient, since this would generate the simplest DEP force (Eq. (6) and Fig. 7.2B-C). This is similar in design to a conductive polymer used for equilibrium gradient focusing [49]. Given a constant channel height (h) determined by the photoresist thickness, the channel cross-sectional area (A) varies inversely with x as:

$$A(x) = h \times w_2(x) = h \frac{w_1}{(1 + kx)} \quad 0 \le x \ge 2.5 \text{ mm} \quad (7)$$

where w_2 is the channel width of region 2, the taper starts and ends at x=0 and x=2.5 mm, respectively, w_1 is the width of region 1, and k is the rate at which the channel tapers. The electric field is defined along the length of the channel ($E(x)$) is calculated by substituting Eq. (5) into the current density ($J(x)$) relation:

$$E(x) = J(x)\rho$$
$$E(x) = \gamma(1 + kx) \qquad \gamma = \frac{i\rho}{w_1 h} \qquad 0 \le x \ge 2.5 \text{ mm} \tag{8}$$

Substituting Eq. (8) into Eq. (6) gives the velocity profile along the centerline ($v_{p,x}(x)$):

$$v_{p,x}(x) = \gamma(1 + k\,x)(\mu_{EK} + \gamma\, k\, \mu_{DEP})$$
$$v_{p,x}(x) = (\gamma^2\, k^2\, \mu_{DEP} + \gamma\, k\, \mu_{EK})x + (\gamma^2\, k\, \mu_{DEP} + \gamma\, \mu_{EK}) \tag{9}$$

Thus, particles experience a linear velocity increase as they move through the taper region. The slope of the velocity profile depends on both a dielectrophoretic and electrokinetic term in Eq. (7). Therefore, according to this logic, the velocity slope will be steeper in the case of positive DEP and shallower in the case of negative DEP compared to that predicted if there is no DEP force (Fig. 7.2D). For these experiments w_1= 2 mm, k= 12.93 mm^{-1}, h=0.01 mm, γ= 8 V/mm and the taper ended at x=2.5 mm.

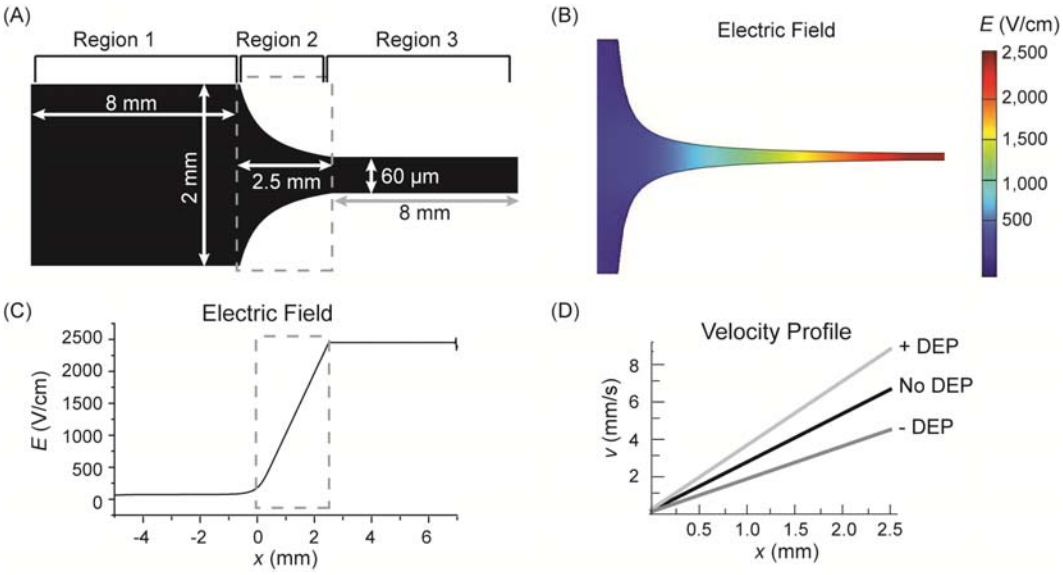

Figure 7.2. Design, electric field, and principles of mobility device. (A) Diagram and dimensions of iDEP device used consisting of wide uniform segment (region 1), taper segment (region 2), and narrow uniform segment (region 3). (B-C) COMSOL simulation of electric field of iDEP device. Dashed box indicates region 2. (D) Theoretical velocity profile in region 2 based on Eq. (9) in the case of positive, zero, or negative DEP using hypothetical mobility and electric field values.

7.3.2 Streak-based velocimetry

One challenge in estimating particle velocities in iDEP devices is the wide range of velocities frequently encountered, which generate streaked particle images. For example, the spatial field gradients typically employed can create up to a 100-fold increase in the electroosmotic transport velocity. This led to the pursuit of a streak-based velocimetry approach rather than traditional micro-particle image velocimetry techniques [50].

Streak-based velocimetry operates by associating the length and trajectory of a streak in a blurred image with the exposure time to estimate the velocity field. As particles move from a weak to strong electric field they accelerate, and thus,

the distance traveled in a single exposure becomes greater as observed by streak lengths in a captured image (Fig. 7.3A). An automated algorithm detects, processes, and determines the velocities traveled by the particles at all pixels across the image sequence. The particle velocity linearly increases along the x-axis and remains relatively constant along the y-axis (RSD 5%) within the depicted centerline strip (Fig. 7.3B). This is consistent with the expectation that the electric field is parallel to the x-axis (Eq. (6)) and it linearly increases in magnitude (Eq. (8)) within this region. The *x*-dimension has been cropped to exclude the beginning and ending portions of the taper where particles travel either too slow or fast for precise streak velocimetry assessment, respectively. Overall, Eq. (9) is considered to accurately describe the velocity profile. Furthermore, the constant velocity along the y-axis allows spatiotemporal averaging to improve the centerline velocity estimation.

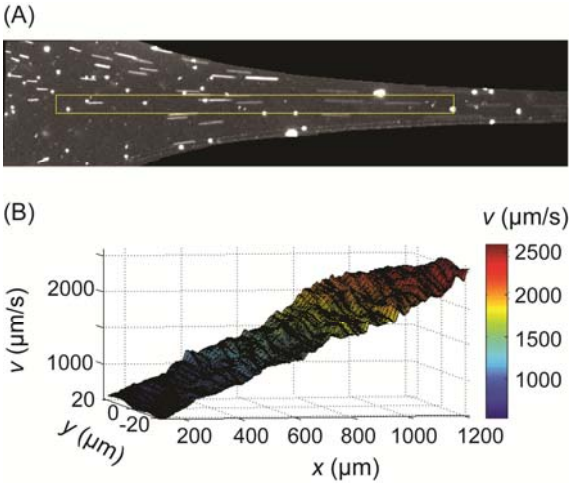

Figure 7.3. Streak velocimetry processing and results. (A) An overlaid image sequence showing particle streak images and (B) the resultant spatial velocity estimation deduced from streak analysis. The region where data was analyzed and processed is highlighted by the light bounding box in (A).

In addition to streak-based analysis, particle velocities were assessed using manual tracking for comparison. Clearly, the automated streak analysis is more precise compared to the manual particle tracking (Fig. 7.4A-B), and thus there is greater confidence in the slope determined by streak analysis. This difference in precision is associated with the elongation of the imaged particles as they accelerate. Substantial uncertainty is introduced when manually tracking a particle's center of mass if the particle motion produces a streaked image. Automated streak tracking avoids this problem since it relies on the blurred streak images for velocity estimation.

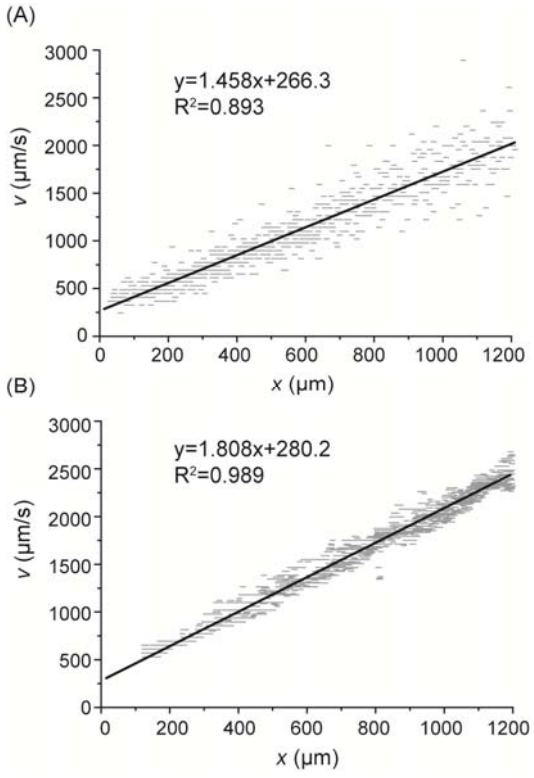

Figure 7.4. Velocimetry results for 1 μm polystyrene particles. Comparison of velocimetry result between (A) manual particle tracking and (B) automated streak analysis (before averaging). In each case several hundred velocity estimations were made across the device and linear best fits were generated.

7.3.3 Electrokinetic and dielectrophoretic mobilities

As defined in Eq. (4), the dielectrophoretic mobility describes a non-charge containing particle's polarizability in a particular fluid medium and primarily depends on a particle's size and Clausius-Mossoti factor. Thus, there will be a broad spectrum of dielectrophoretic mobilities given the diversity of particle sizes, charges, and ionic properties. In fact the richness of this term suggests that within a single particle type there could be significant microheterogeneity to create sub-populations with unique mobility constants. Supporting this idea is the observation that charge properties of particles have been found to be much broader compared to molecules [51, 52].

The streak-based velocity estimations were used to calculate the system properties. Using 1 μm polystyrene particles the electrokinetic mobility was estimated to be 3.5×10^{-4} $cm^2/(V \bullet s)$ as calculated by Eq. (3) using the velocity data from region 1. This is considered a reasonable result and is likely dominated by electroosmotic flow considering its similarity to other electroosmotic mobility estimations [6, 53]. The dielectrophoretic mobility of polystyrene particles was found to be $-2 \pm 0.4 \times 10^{-8}$ $cm^4/(V^2 \bullet s)$ from the slope in Eq. (9). The statistics are from three separate experiments which involved over one thousand velocity measurements each. This result agrees with the general finding that polymeric particles exhibit negative dielectrophoresis under similar conditions [5, 8, 11]. Subtle variations in electroosmotic flow, particle heterogeneity, and variance in the velocity estimation likely contribute to the 20% RSD observed.

Under these particular conditions the electrokinetic velocity is about twice the magnitude of the dielectrophoretic velocity based on calculations of the individual terms in Eq. (9). The relative DEP velocity could be increased by increasing the applied voltage, reducing electroosmotic flow, or utilizing steeper field gradients. However, particle motion rapidly changes direction in these regimes complicating velocity associations. For optimal quantitative analysis, the DEP motion must be observable but not predominant.

7.4 Concluding remarks

An approach to simultaneously quantifying the electrokinetic and dielectrophoretic properties of particles in iDEP is discussed. Critical to the success of such analysis is the accurate and precise estimation of particle velocities. Presently, streak-based velocimetry was found to be more precise than manual particle tracking and has the advantage of automation. From this approach polystyrene particles were found to have a dielectrophoretic mobility of $-2 \pm 0.4 \times 10^{-8}$ $cm^4/(V^2 \cdot s)$. Quantitative approaches like this one enable an unprecedented evaluation of iDEP and provide a metric for standardization. Ideally, discussions will eventually evolve from subjective descriptions of particle behaviors to more objective quantitative responses.

7.5 References

[1] Lapizco-Encinas, B. H., Rito-Palomares, M., *Electrophoresis* 2007, *28*, 4521-4538.

[2] Zhang, C., Khoshmanesh, K., Mitchell, A., Kalantar-zadeh, K., *Anal. Bioanal. Chem.* 2010, *396*, 401-420.

[3] Pohl, H. A., *J. Appl. Phys.* 1951, *22*, 869-871.

[4] Pethig, R., *Biomicrofluidics* 2010, *4*, 022811.

[5] Cummings, E. B., Singh, A. K., *Anal. Chem.* 2003, *75*, 4724-4731.

[6] Martinez-Lopez, J. I., Moncada-Hernandez, H., Baylon-Cardiel, J. L., Martinez-Chapa, S. O., Rito-Palomares, M., Lapizco-Encinas, B. H., *Anal. Bioanal. Chem.* 2009, *394*, 293-302.

[7] Kwon, J.-S., Maeng, J.-S., Chun, M.-S., Song, S., *Microfluid. Nanofluid.* 2008, *5*, 23-31.

[8] Lapizco-Encinas, B. H., Simmons, B. A., Cummings, E. B., Fintschenko, Y., *Anal. Chem.* 2004, *76*, 1571-1579.

[9] Baylon-Cardiel, J. L., Lapizco-Encinas, B. H., Reyes-Betanzo, C., Chavez-Santoscoy, A. V., Martinez-Chapa, S. O., *Lab Chip* 2009, *9*, 2896-2901.

[10] Mela, P., van den Berg, A., Fintschenko, Y., Cummings, E. B., Simmons, B. A., Kirby, B. J., *Electrophoresis* 2005, *26*, 1792-1799.

[11] Ozuna-Chacon, S., Lapizco-Encinas, B. H., Rito-Palomares, M., Martinez-Chapa, S. O., Reyes-Betanzo, C., *Electrophoresis* 2008, *29*, 3115-3122.

[12] Cummings, E. B., *IEEE Engineering in Medicine and Biology Magazine* 2003, *Nov/Dec*, 75-84.

[13] Lapizco-Encinas, B. H., Simmons, B. A., Cummings, E. B., Fintschenko, Y., *Electrophoresis* 2004, *25*, 1695-1704.

[14] Lapizco-Encinas, B. H., Davalos, R. V., Simmons, B. A., Cummings, E. B., Fintschenko, Y., *J. Microbiol. Methods* 2005, *62*, 317-326.

[15] Ozuna-Chacon, S., Lapizco-Encinas, B. H., Rito-Palomares, M., Collado-Arredondo, E., Martinez-Chapa, S. O., *Revista Mexicana De Ingenieria Quimica* 2007, *6*, 329-335.

[16] Lapizco-Encinas, B. H., Ozuna-Chacon, S., Rito-Palomares, M., *J. Chromatogr. A* 2008, *1206*, 45-51.

[17] Gallo-Villanueva, R. C., Rodriguez-Lopez, C. E., Diaz-de-la-Garza, R. I., Reyes-Betanzo, C., Lapizco-Encinas, B. H., *Electrophoresis* 2009, *30*, 4195-4205.

[18] Moncada-Hernandez, H., Lapizco-Encinas, B. H., *Anal. Bioanal. Chem.* 2010, *396*, 1805-1816.

[19] Davalos, R. V., McGraw, G. J., Wallow, T. I., Morales, A. M., Krafcik, K. L., Fintschenko, Y., Cummings, E. B., Simmons, B. A., *Anal. Bioanal. Chem.* 2008, *390*, 847-855.

[20] Hawkins, B. G., Smith, A. E., Syed, Y. A., Kirby, B. J., *Anal. Chem.* 2007, *79*, 7291-7300.

[21] Kang, Y., Li, D., Kalams, S. A., Eid, J. E., *Biomed. Microdevices* 2008, *10*, 243-249.

[22] Kang, K. H., Xuan, X., Kang, Y., Li, D., *J. Appl. Phys.* 2006, *99*, 064702.

[23] Kang, K. H., Kang, Y., Xuan, X., Li, D., *Electrophoresis* 2006, *27*, 694-702.

[24] Barrett, L. M., J., S. A., Singh, A. K., Cummings, E. B., Fiechtner, G. J., *Anal. Chem.* 2006, *77*, 6798-6804.

[25] Barbulovic-Nad, I., Xuan, X., Lee, J. S. H., Li, D., *Lab Chip* 2006, *6*, 274-279.

[26] Lewpiriyawong, N., Yang, C., Lam, Y. C., *Biomicrofluidics* 2008, *2*, 034105.

[27] Zhu, J., Tzeng, T.-R. J., Hu, G., Xuan, X., *Microfluid. Nanofluid.* 2009, *7*, 751-756.

[28] Church, C., Zhu, J., Nieto, J., Keten, G., Ibarra, E., Xuan, X., *J. Micromech. Microeng.* 2010, *20*, 065011.

[29] Pysher, M. D., Hayes, M. A., *Anal. Chem.* 2007, *79*, 4552-4557.

[30] Staton, S. J. R., Chen, K. P., Taylor, T. J., Pacheco, J. R., Hayes, M. A., *Electrophoresis* 2010, *31*, 3634-3641.

[31] Chen, K. P., Pacheco, J. R., Hayes, M. A., Staton, S. J. R., *Electrophoresis* 2009, *30*, 1441-1448.

[32] Ai, Y., Joo, S. W., Jiang, Y., Xuan, X., Qian, S., *Electrophoresis* 2009, *30*, 2499-2506.

[33] Ai, Y., Qian, S., Liu, S., Joo, S. W., *Biomicrofluidics* 2010, *4*, 013201.

[34] Kirby, B. J., Hawkins, B. G., *Electrophoresis* 2010, *31*, 3622-3633.

[35] Jen, C.-P., Huang, C.-T., Shih, H.-Y., *Microsyst. Technol.* 2010, *16*, 1097.

[36] Ros, A., Hellmich, W., Regtmeier, J., Duong, T. T., Anselmetti, D., *Electrophoresis* 2006, *27*, 2651-2658.

[37] Regtmeier, J., Duong, T. T., Eichhom, R., Anselmetti, D., Ros, A., *Anal. Chem.* 2007, *79*, 3925-3932.

[38] Chou, C.-F., Tegenfeldt, J. O., Bakajin, O., Chan, S., S., Cox, E. C., Darnton, N., Duke, T., Austin, R. H., *Biophys. J.* 2002, *83*, 2170-2179.

[39] Shafiee, H., Sano, M. B., Henslee, E. A., Caldwell, J. L., Davalos, R. V., *Lab Chip* 2010, *10*, 438-445.

[40] Shafiee, H., Caldwell, J. L., Sano, M. B., Davalos, R. V., *Biomed. Microdevices* 2009, *11*, 997-1006.

[41] Winter, W. T., Welland, M. E., *J. Phys. D: Appl. Phys.* 2009, *42*, 045501.

[42] Ai, Y., Qian, S., *J. Colloid Interface Sci.* 2010, *346*, 448-454.

[43] Tsukahara, S., Sakamoto, T., Watarai, H., *Langmuir* 2000, *16*, 3866-3872.

[44] Washizu, M., Jones, T. B., *J. Electrostat.* 1994, *33*, 187-198.

[45] Watarai, H., Sakamoto, T., Tsukahara, S., *Langmuir* 1997, *13*, 2417-2420.

[46] Ikeda, I., Monjushiro, H., Watarai, H., *Analyst* 2005, *130*, 1340-1342.

[47] Kuokkanen, M. H., *Cent. Eur. J. Phys.* 2010, *8*, 178-183.

[48] Mahanti, P., Taylor, T., Hayes, M. A., *Microfluid. Nanofluid.* 2011, In Preparation, Available at: http://www.public.asu.edu/~mhayes/.

[49] Humble, P. H., Kelly, R. T., Woolley, A. T., Tollety, D. H., Lee, M. L., *Anal. Chem.* 2004, *76*, 5641-5648.

[50] Yan, D., Yang, C., Nguyen, N.-T., Huang, X., *Electrophoresis* 2006, *27*, 620-627.

[51] Jones, H. K., Ballou, N. E., *Anal. Chem.* 1990, *62*, 2484-2490.

[52] Petersen, S. L., Ballou, N. E., *Anal. Chem.* 1992, *64*, 1676-1681.

[53] Badal, Y. M., Wong, M., Chiem, N., Salimi-Moosavi, H., Harrison, D. J., *J. Chromatogr. A* 2002, *947*, 277-286.

Chapter 8

Dielectrophoretic Mobility Characterizations Using a Symmetrical Channel

8.1 Introduction

Dielectrophoresis (DEP) is a unique approach to separating particle mixtures but has one distinct disadvantage compared to all other separation techniques. DEP is limited because analyte-dependent properties are rarely monitored and assessed quantitatively. In other techniques, for example, retention times (chromatography), electrophoretic mobilities (electrophoresis) [1], and isoelectric points (isoelectric focusing) [2] are analyte-specific properties that can be deduced. Quantitative outcomes like these improve the utility of separations by allowing system calibration [3], unique mechanisms to be elucidated [4], and devices to be intelligently engineered [1]. The DEP mobility is a quantitative metric that offers such benefits to DEP, but there lacks sufficient and robust means to accurately measure it.

A method for DEP mobility determination was introduced in Chapter 7 and proof-of-principle experiments were carried out. Contrary to typical DEP experiments, this approach relied on simple electric field gradients to generate linear velocity profiles. The linearized system allowed velocimetry methods to be feasibly employed and data sets to be confidently fit. The velocity slope was described as follows:

$$m_{p,x} = \left(\frac{dE}{dx}\right)^2 \mu_{DEP} + \left(\frac{dE}{dx}\right)\mu_{EK} = (\gamma k)^2 \mu_{DEP} + (\gamma k)\mu_{EK} \quad (1)$$

where $m_{p,x}$ is the x-component particle velocity slope ($dv_{p,x}/dx$), μ_{EK} and μ_{DEP} are the electrokinetic and DEP mobilities, and dE/dx is the electric field gradient defined by the product of the initial electric field (γ) and the rate of electric field increase (k). The μ_{DEP} was calculated by solving Eq. 1:

$$\mu_{DEP} = \frac{m_{p,x} - \left(\frac{dE}{dx}\right)\mu_{EK}}{\left(\frac{dE}{dx}\right)^2} = \frac{m_{p,x} - \gamma k \mu_{EK}}{(\gamma k)^2} \tag{2}$$

Although this methodology is sufficient for rough measurements, there are some limiting factors that hinder the precision in the results.

First, the uncertainty of the calculated DEP mobility (μ_{DEP}) is relatively high. Each of the dependent variables has some inherent uncertainty because they are either experimentally measured or computed based on the device geometry. Therefore, the propagated uncertainty is on the order of 50-75% given the number of dependencies. This is inevitable because there no reference standards for DEP and the electric field is approximated from the theoretical device design alone [1]. Not only do these factors impact the results here, they are also endemic problems in all DEP experiments. In some instances the system uncertainty can be so large that one cannot confidently state a DEP force is influencing the particle motion. Other devices have much more complex designs and the uncertainty in electric field gradients alone can exceed 100%. These and other considerations likely explain the deficiency in quantitative characterizations of DEP motion.

The approach from Chapter 7 is also limited because it relies on a number of assumptions that could introduce errors in the analysis: flow and electric field

lamina are identical within the field of analysis, the *y*-component forces are zero within the field of analysis, only electrokinetic forces impact particle motion, and pressure, temperature, and conductivity gradients are non-existent or negligible. In other words, the model used to analyze particle motion may be incomplete and thus the calculated results may be biased. There are insufficient means to perform control experiments and validate these assumptions using the previous DEP mobility device.

There exists a clear need to improve the methodology of DEP mobility determination to account for the limitations of the device used in Chapter 7. Ideally a new approach would minimize the systematic uncertainty and validate or rely on fewer assumptions. The purpose of the current chapter is to demonstrate a new method for DEP mobility determination that makes some of these improvements. Using a symmetrical channel, particle motion is cross-referenced to directly isolate DEP motion. It is clear from this approach that other unanticipated forces, such as surface interactions, create noisy data sets that overwhelm the DEP signal. Although the resultant data is currently difficult to interpret, the cross-referencing approach demonstrates vast improvement over the method from Chapter 7 because propagated uncertainty is reduced and assumptions can be experimentally tested. From this, an assessment of DEP mobility for red blood cells (RBCs) is deduced.

8.2 Materials and methods

Materials, methods, equipment, and procedures are the same as described in Chapter 7 with some minor changes indicated here. Polydimethylsiloxane

(PDMS) channels were cast from photolithographically patterned templates, and glass slides were bonded to enclose channels after plasma oxidation. Red blood cell (RBC) samples were employed in experiments. Whole blood was collected, washed, and cells were isolated by centrifugation. Cells were washed in triplicate with phosphate buffer (115 mM, pH 7.4) containing ethylenediaminetetraacetic acid (EDTA) before fluorescently labeling using an Invitrogen staining kit. The protocol consisted of a 15 minute incubation of 0.5% hematocrit in 5 μM Vybrant DiO dye at 37 °C [5]. The stained cells were pelleted and washed in duplicate to remove unbound dye before being diluted 100 fold volumetrically in phosphate buffer (130 mM, pH 7.4) for working samples. In some instances bovine serum albumin (BSA) was added to samples at a concentration of 8 mg/mL. Samples were introduced into the microfluidic device via gravity flow. An inverted fluorescence microscope and camera were used to record movies of particle motion. The imaged area was approximately 2 mm by 0.5 mm centered about the middle of the symmetrical channels (Fig. 8.1). Manual particle tracking was carried out using ImageJ software to collect spatial velocity information.

8.3 Results and discussion

8.3.1 Symmetrical channel design and methodology

The linear field (constant gradient) was the most essential feature of the previous design and thus is retained for the new approach. However, the new design employs a spatially symmetrical linear field. A symmetrical channel taper is used to engineer this new feature where the field increases on one side and decrease on the other at equal rates (Fig. 8.1).

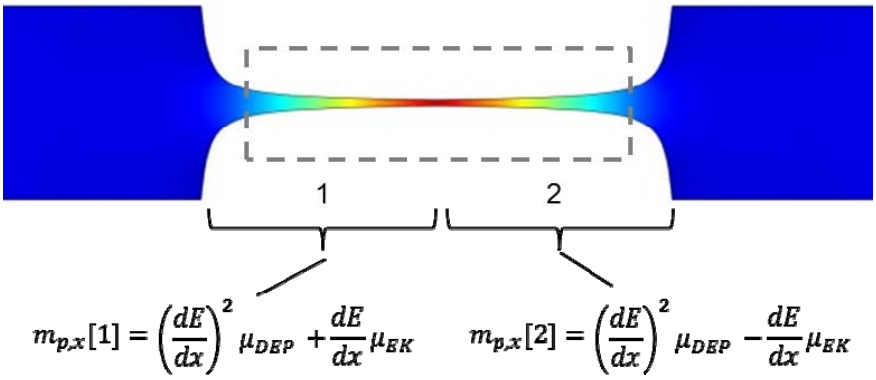

Figure 8.1. Illustration of symmetrical channel device. The new DEP mobility device features a symmetrical channel taper to produce a symmetrical electric field (field strength indicated by color). The equations of motion for the two sides (labeled 1 and 2) are shown. Dashed box indicates imaged region for velocimetry analysis.

The reversal of the field gradient is important because the DEP velocity becomes asymmetrical while the electrokinetic velocity is symmetrical. Additionally, many other unforeseen influences on particle motion (e.g., pressure, temperature, or conductivity gradients) would also behave symmetrically. Therefore, the data sets from the two sides can be cross-referenced to allow more direct isolation of the DEP mobility. Combining Eq. 1 with other unknown, symmetrical influences (A_1, A_2, *etc.*) the particle motion is described on the two sides as follows:

$$m_{p,x}[1] = \left(\frac{dE}{dx}\right)^2 \mu_{DEP} + \left(\frac{dE}{dx}\right)\mu_{EK} + A_1 + A_2 \ldots \qquad \text{Side 1} \qquad (3)$$

$$m_{p,x}[2] = \left(\frac{dE}{dx}\right)^2 \mu_{DEP} - \left(\frac{dE}{dx}\right)\mu_{EK} - A_1 - A_2 \ldots \qquad \text{Side 2} \qquad (4)$$

where all terms have the same magnitude on either side. The DEP mobility can be directly isolated by summing Eqs. 3 and 4 to remove the symmetrical terms:

$$\mu_{DEP} = \frac{m_{p,x}[1] + m_{p,x}[2]}{2\left(\frac{dE}{dx}\right)^2} \tag{5}$$

A positive value or negative value corresponds with positive or negative DEP, respectively.

Thus, if pressure, temperature, conductivity or other symmetrical effects impact particle motion they will be removed without biasing the DEP mobility determination. Also, any over- or under-estimation from the velocimetry techniques will also act symmetrically and be removed. Most importantly the data is not influenced by electrokinetic heterogeneity or variations between lamina paths when Eq. 5 is applied to individual particles rather than averaged data sets. The only requirement for this cross-referencing elimination is that the particle follows the same lamina on both sides or that the lamina within the field of analysis are not significantly different. Finally, the propagated uncertainty is significantly reduced (fewer dependent terms) and this approach improves the confidence in DEP mobility determinations. A hypothetical data set for positive DEP is presented and characterized by a net bias for all particles amongst some degree of noise (Fig. 8.2).

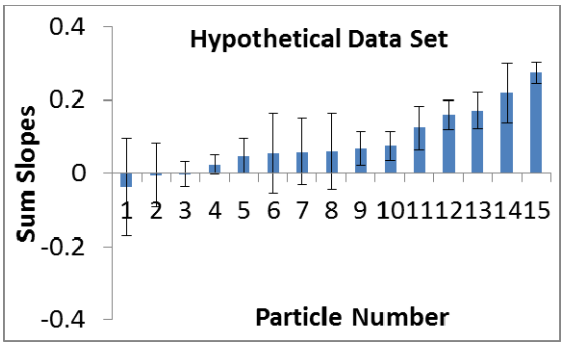

Figure 8.2. Hypothetical velocity results within symmetrical channel. On average, a net positive bias is observed although some particles experience equal magnitude velocity slopes on the two sides.

8.3.2 Validating device symmetry and methodology

Control experiments were first carried out using only hydrodynamic flow to ensure the geometric symmetry of the system and validate the methodology of Eq. 5. For a pressure differential of 100 Pa the average velocity slopes were 0.28 and -0.29 s^{-1} for the two sides (Fig. 8.3A). Therefore, on average RBCs experienced equal magnitude velocity slopes within reasonable error. This is strong evidence that channel geometries are symmetrical and supports the methodology of Eqs. 3-5. Furthermore, this suggests a pressure gradient can be applied without interfering with the DEP mobility determination. This is a useful finding because it allows adjustable means to transport particles towards the region of interest and is decoupled from the electric field unlike electroosmosis.

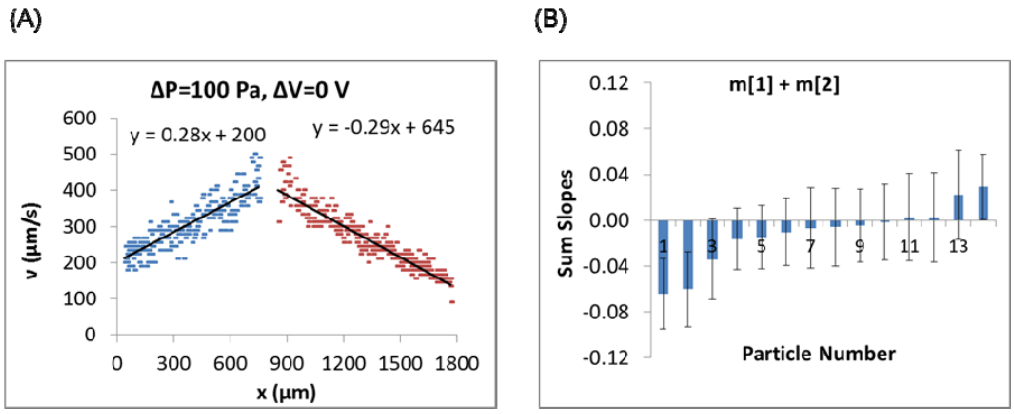

Figure 8.3. Velocity results with pressure flow. (A) The average velocity slopes for a population of RBCs in the symmetrical gradient device. (B) The sum of the slopes for individual RBCs with propagated uncertainty for error bars.

However, when individual particles are examined around 30% of them are observed to slightly deviate from this expected result (Fig. 8.3B). In these instances a non-zero result is obtained between ±0.05 s when the two slopes are summed. Furthermore, this net-bias is statistically significant when considering the propagated error of the slopes. In other words, certain particles experience different velocity slopes on the two sides. There is still strong evidence for device symmetry because both positive and negative biases are observed with equal frequency. Instead this suggests there are other non-symmetrical influences that can occur randomly. Some possible sources of this could be surface interactions, inter-particle interactions, or cross-over between different flow lamina. Regardless of the origin, however, this systematic noise must be considered and overcome for DEP mobilities to be confidently deduced. These unknown influences could also be exacerbated when electric fields are applied.

8.3.3 Red blood cell characterizations

After validating the geometric symmetry, experiments were carried out with applied electric fields and hydrodynamic flow. One immediately distinct observation is the range of RBC velocities and slopes becomes much broader under these conditions (Fig. 8.4A). The variation in particle behaviors makes it difficult to make generalizations at the population level and precise best fits were not obtained. Additionally, the variance in population data sets becomes greater with increasing field strengths. Instead, particles were assessed on an individual basis because good linearity was obtained for most particles ($R^2 > 0.9$). Approximately 50% of particles experience a net bias, although both positive and negative biases (from -0.1 to 0.1 s^{-1}) are observed with equal frequency (Fig. 8.4B). One interpretation of these results is that the RBCs have broad DEP heterogeneity that spans both positive and negative Clausius-Mossotti factors. This is a reasonable possibility considering both positive and negative DEP trapping behaviors of blood cell materials (e.g., fragments, lysed cells) has been previously observed [5]. However, another explanation could be that the data sets are unreliable because of unknown assymetrical influences which compromise the approach of Eq. 5. These effects were observed in control experiments (Fig. 8.3B) and could be exacerbated in the presence of electric fields.

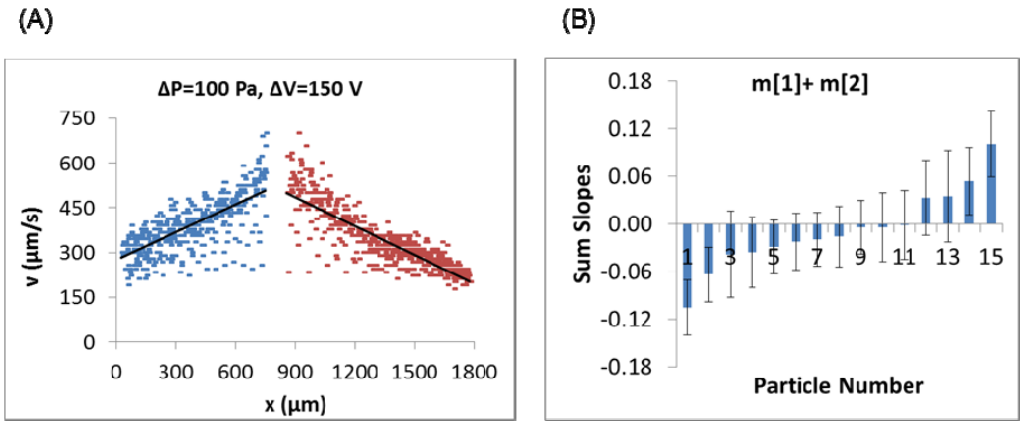

Figure 8.4. Velocity results with electric field and pressure flow. (A) The average velocity slopes for a population of RBCs in the symmetrical gradient device. (B) The sum of the slopes for individual RBCs with propagated uncertainty for error bars.

The range of signals observed (summed slopes) is from -0.1 to 0.1 s^{-1} while the standard deviation in signal is on the order of ±0.1 s^{-1}. Therefore, the variability in individual particles makes it difficult to make a global conclusion about the DEP mobility of RBCs. Nonetheless, this data set can provide an upper limit of DEP mobility by solving Eq. 5 from the maximum signals observed. The electric field gradient is (*dE/dx*) is computed from COMSOL to be 3×10^3 V cm^{-2} under these conditions. From this the magnitude of the DEP mobility of RBCs is no larger than 6×10^{-9} cm^4 V^{-2} s^{-1} – although the sign is unknown or varies. Again, it is unclear if data variations are from particle heterogeneity or from systematic noise. Nonetheless, this magnitude is a reasonable result compared to that observed in Chapter 7 for polystyrene particles (2×10^{-8} cm^4 V^{-2} s^{-1}).

A stronger field gradient and/or reduced system noise is needed to more clearly elucidate the DEP signal. In essence, higher fields could be employed, but the need for isotonic buffers (~130 mM) means that high currents (> 100 μA) and

excessive joule heating would result. Additionally, high fields push the limits by which imaging and velocimetry techniques could be feasibly employed to monitor particle motion. More studies are needed to identify the origin of and reduce system noise, but likely culprits are surface interactions, inter-particle interactions, and inter-lamina cross overs.

The limitations of the approach from Chapter 7 are clearly elucidated from the new symmetrical experimental design. It was previously assumed that only electrokinetic and DEP forces impact particle motion; however, other influences or biases are clearly apparent when cross-referencing data from the symmetrical device. Although the resultant data sets are still difficult to interpret, the experimental validity is improved and the propagated uncertainty of the calculated DEP mobility is reduced with the symmetrical device.

8.3.4 Reducing surface interactions

From the previous results there was clear indication that surface interactions were a strongly influencing particle motion. This is reasonable considering the channel depth is on the order of 10 μm while the RBCs have a diameter on the order of 5 μm, surface adsorption of RBCs was clearly evident over prolonged periods, and the depth of field of the microscope is on the order of 30 μm. Experiments were carried out using BSA as a dynamic coating agent that was added to all solutions at 8 mg/mL. This was suspected to block RBC-channel interactions because RBC surface adsorption was significantly reduced. As expected, control experiments using only pressure flow showed better performance. The number of particles whose motion differed in magnitude

between the two sides was reduced from 30% to 20%. Additionally, the velocity linearity improved as indicated by an average increase in R^2 values.

Considering the reduction in systematic noise using BSA, it was expected that DEP signals would be more clearly elucidated. Experiments were carried out across a range of voltages and multiple different particles were tracked. Better linearity was obtained in the velocity slopes, but equally broad behaviors were observed (Fig. 8.5). Furthermore, the average propagated uncertainty in the slopes increased with increasing voltage from 0.03 to 0.07 s^{-1} using 500 to 800 V, respectively. These voltages correspond to electric field gradients between 2.4×10^3 and 3.8×10^3 V cm^{-2}. This means the velocity results become less linear and Eq. 5 becomes less reliable as DEP forces become stronger. In accord with Eq. 5, the magnitude of the summed slopes increased with increasing voltage. However, this cannot be directly attributed to DEP because of the not all particles were systemically biased and the potential for unknown, asymmetries. It is possible that the higher energy conditions promote unwanted effects such as inter-particle and surface interactions.

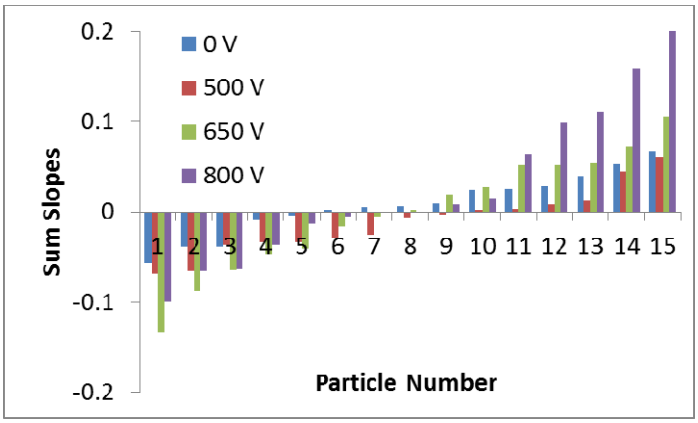

Figure 8.5. Velocity results with dynamic coating. The velocity slopes of individual RBCs are summed. Different voltages are applied and a constant pressure flow of 100 Pa was applied in all experiments. Each data point is a unique RBC and the results are sorted low to high. An equal number of net negative and net positive biases are observed. The propagated uncertainty (not shown for clarity) in the slopes ranges between 0.02 and 0.09 s^{-1}.

It is unclear why the DEP force is so elusive in attempts to quantitatively monitor it, but qualitative observations can provide some insights. Particle motions are observed to become more complex when the DEP force is significant. This is characterized by rapid fluctuations in velocity magnitude and direction. Perhaps dynamic fluctuations in voltage, conductivity, or temperature strongly couple with DEP. Another possibility is that fluctuations in particle properties such as orientation/shape, surface charge, counter-ion clouds, or membrane composition cause fluctuating forces. This fluctuating and unanticipated behavior typical of DEP is illustrated under exaggerated conditions (Fig. 8.6B). In comparison to low voltage conditions which produce linear predictable profiles (Fig. 8.6A), higher voltages produce a significant DEP force where particle motion can be arrested and it can unpredictably fluctuate directions (Fig. 8.6B). Only a few of these particles are immobilized to the surface, while the rest are

trapped in potential energy well from a balance of DEP, pressure, and electrokinetic forces. Although these conditions are exaggerated beyond typical velocimetry experiments, similar 'unsteady' effects could be occurring that explain the imprecise data sets observed.

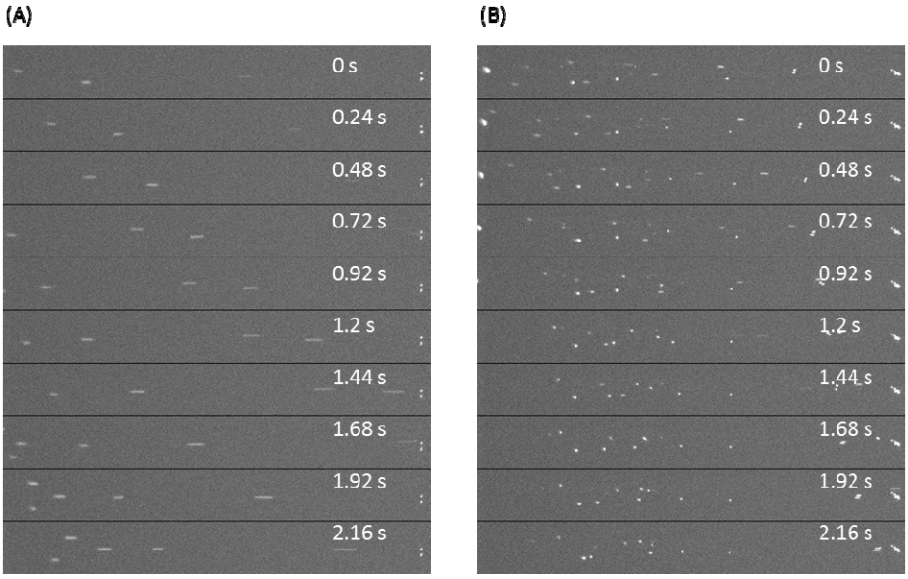

Figure 8.6. Still image sequence of particle motion. (A) Particle motion at lower voltages when DEP force is weaker. The particles follow very linear predictable paths. (B) Particle motion at higher voltages when DEP force is strong and particle motion fluctuates unpredictably.

8.4 Concluding remarks

Although reliable DEP mobilities for RBCs were not obtained, some unique insights were observed. The magnitude of RBC DEP mobility is less than 1×10^8 although the direction was undetermined because other influences overwhelm DEP signals. The experiments conducted illustrate the difficulty in isolating DEP forces from background noise and shed light onto future directions.

Attempts to increase the strength of DEP force with increasing voltage produced more noise. However, this could be the result of excessive joule heating from the resulting high currents. The present design tapers from 2 mm to 0.05 mm in width over 1.75 mm in length. An alternative approach would be to redesign the channel geometry to have a steeper geometric gradient, smaller cross-sections, and shorter lengths. For instance, a channel taper from 0.5 mm to 0.05 mm in width over 0.2 mm in length could provide better outcomes. The smaller cross section would reduce current and heating loads, the resultant gradient would be twice as steep, and the reduced length significantly diminishes the probability of interference from surface or inter-particle interactions.

Additionally, there are some inevitable limitations of velocimetry techniques that can constrain this approach. For instance, rapid imaging is required but decreased exposure times produce more noise in images. Additionally, velocimetry techniques are limited to larger particles (>400 nm), require fluorescent labels in many cases, and are limited to velocities less than 2 mm/s. An alternative and more universal approach would be to employ fixed point detection and time-based analysis. Similar to electrophoresis, the travel time to a detector is directly dependent on the transporting forces. Through careful design and analysis the DEP motion could be deduced.

The incorporation of a controlled injection apparatus into the microfluidic device could also improve results. This could allow either single particle or ensemble populations to be monitored in a controlled fashion.

In conclusion, with additional redesign of methodologies the DEP mobility measurements can be improved. Ultimately, these metrics will enable particles to be standardized, mechanisms to be elucidated, and devices to be rationally designed.

8.5 References

[1] Martinez-Lopez, J. I., Moncada-Hernandez, H., Baylon-Cardiel, J. L., Martinez-Chapa, S. O., Rito-Palomares, M., Lapizco-Encinas, B. H., *Anal. Bioanal. Chem.* 2009, *394*, 293-302.

[2] Righetti, P. G., *J. Chromatogr. A* 2004, *1037*, 491-499.

[3] Weiss, N. G., Zwick, N. L., Hayes, M. A., *J. Chromatogr. A* 2010, *1217*, 179-182.

[4] Zenker, A., Galanski, M., Bereuter, T. L., Keppler, B. K., Lindner, W., *J. Chromatogr. B* 2000, *745*, 211-219.

[5] Jones, P. V., Staton, S. J. R., Hayes, M. A., *Anal. Bioanal. Chem.* 2011, *401*, 2103-2111.

Chapter 9

Concluding Remarks

9.1 Isoelectric focusing

High resolution protein analysis requires highly selective techniques and sample enrichment strategies. Isoelectric focusing (IEF) has long been a powerful tool capable of meeting these requirements; however, detection limits, automation, and reproducibility still need improving. These and other limitations necessitate solutions in order for isoelectric focusing to solve new and more difficult problems. Methods for interfacing capillary IEF (cIEF) with matrix assisted laser desorption/ionization mass spectrometry (MALDI-MS) were advanced, validated, and applied to the analysis of serum amyloid P component (SAP) in Chapters 3 and 4. Some fundamental dependencies of MALDI-MS were deduced in Chapter 5 which sheds light onto an optimal deposition strategy when coupling cIEF and MALDI-MS. The cIEF-MALDI-MS platform offers the potential of higher resolution and more automatable protein analysis. In addition, there is also a need for low-resolution, high-throughput sample preparations. Towards this goal, IEF was employed within open drops (dIEF) and the fundamental processes were characterized. From this, it is evident that droplet microfluidic technologies could adopt the dIEF principles to enable inexpensive and rapid sample preparation. Although the principals of IEF are not new, continual improvements of the technique are warranted because it offers the highly valuable combination of high-resolution and analyte enrichment. Many elements within this dissertation contribute towards this goal.

9.2 Dielectrophoresis

Dielectrophoresis (DEP) is an incredibly rich tool for the separation and concentration of particles (>20 nm). More than anything else, DEP is limited by a lack of means for the accurate, quantitative assessment of particle behaviors. Quantifying dielectrophoretic particle behaviors allows devices to be intelligently designed, insights and mechanisms to be deduced, and particles to be standardized. Chapters 7 and 8 promote such quantitative investigations through the development of methods for dielectrophoretic mobility determination. Dielectrophoretic mobilities for 1 μm polystyrene particles and red blood cells are found. More importantly, however, a foundation for quantitative dielectrophoresis is introduced which enables new and improved technologies. Although crude measurements are possible, additional efforts are needed to reduce system noise and increase dielectrophoretic forces.

REFERENCES

CHAPTER 1

[1] Skoog, D. A., Holler, F. J., Crouch, S. R., *Principles of Instrumental Analysis 6th Ed.*, Thomson Brooks/Cole, Belmont 2007.

[2] Goncalves, M. S., *Chem. Rev.* 2009, *109*, 190-212.

[3] Jameson, C. J., *Isotopes in the Physical and Biomedical Sciences*, Elsevier Science Ltd., Amsterdam 1987.

[4] Maeda, M., *J. Pharm. Biomed. Anal.* 2003, *30*, 1725-1735.

[5] Chattopadhaya, S., Bakar, F. B. A., Yao, S. Q., *Curr. Med. Chem.* 2009, *16*, 4527-4543.

[6] Prange, A., Proefrock, D., *J. Anal. At. Spectrom.* 2008, *23*, 432-459.

[7] Giddings, J. C., *Unified Separation Science*, Wiley, New York 1991.

[8] Mancinelli, L., Cronin, M., Sadee, W., *AAPS PharmSci* 2000, *2*.

[9] Meyer, J. M., Ginsburg, G. S., *Curr. Opin. Chem. Biol.* 2002, *6*, 434-438.

[10] Bates, S., *Drug Discov. Today* 2010, *15*, 115-120.

[11] Smith, C. L., Cantor, C. R., *Methods Enzymol.* 1987, *155*, 449-467.

[12] Barron, A. E., Blanch, H. W., *Sep. Purif. Methods* 1995, *24*, 1-118.

[13] Sinville, R., Soper, S. A., *J. Sep. Sci.* 2007, *30*, 1714-1728.

[14] Firestone, G. L., Winguth, S. D., *Methods Enzymol.* 1990, *182*, 688-700.

[15] Paliwal, S. K., DeFrutos, M., Regnier, F. E., *Methods Enzymol.* 1996, *270*, 133-151.

[16] Lilley, K. S., Razzaq, A., Dupree, P., *Curr. Opin. Chem. Biol.* 2002, *6*, 46-50.

[17] Huang, Y. F., Huang, C. C., Hu, C. C., Chang, H. T., *Electrophoresis* 2006, *27*, 3503-3522.

[18] Radisci, M., Iyer, R. K., Murthy, S. K., *Int. J. Nanomedicine* 2006, *1*, 3-14.

[19] Langer, V., Niessner, R., Seidel, M., *Anal. Bioanal. Chem.* 2011, *399*, 1041-1050.

[20] Abdel-Hamid, I., Ivnitski, D., Atanasov, P., Wilkins, E., *Anal. Chim. Acta* 1999, *399*, 99-108.

[21] Clark, M. F., Lister, R. M., Barjoseph, M., *Methods Enzymol.* 1986, *118*, 742-766.

[22] Kozlowski, S., Swann, P., *Adv. Drug Deliv. Rev.* 2006, *58*, 707-722.

[23] Righetti, P. G., Drysdale, J. W., *J. Chromatogr.* 1974, *98*, 271-321.

[24] Pohl, H. A., *J. Appl. Phys.* 1951, *22*, 869-871.

[25] Meighan, M. M., Staton, S. J. R., Hayes, M. A., *Electrophoresis* 2009, *30*, 852-565.

[26] Karas, M., Hillenkamp, F., *Anal. Chem.* 1988, *60*, 2299-2301.

[27] Gluckmann, M., Pfenninger, A., Kruger, R., Thierolf, M., Karas, M., Horneffer, V., Hillenkamp, F., Stupat, K., *Int. J. Mass Spectrom.* 2001, *210*, 121-132.

[28] Chang, W. C., Huang, L. C. L., Wang, Y.-S., Peng, W.-P., Chang, H. C., Hsu, N. Y., Yang, W. B., Chen, C. H., *Anal. Chim. Acta* 2007, *582*, 1-9.

[29] Gross, J., Strupat, K., *Trends Analyt. Chem.* 1998, *17*, 8-9.

[30] He, B., Patankar, N. A., Lee, J., *Langmuir* 2003, *19*, 4999.

[31] Shibuichi, S., Onda, T., Satho, N., Tsujii, K., *J. Phys. Chem.* 1996, *100*, 19512.

[32] Barthlott, W., Neinhuis, C., *Planta* 1997, *202*, 1-8.

[33] Li, X.-M., Reinhoudt, D., Crego-Calama, M., *Chem. Soc. Rev.* 2007, *36*.

CHAPTER 2

[1] Andrews, A. T., *Electrophoresis: theory, techniques, and biochemical and clinical applications*, Oxford University Press, New York 1986.

[2] Schulz, S. F., Sticher, H., *Progr. Colloid. Polym. Sci.* 1994, *97*, 85-88.

[3] Swinney, K., Bornhop, D. J., *Electrophoresis* 2000, *21*, 1239-1250.

[4] Miura, K., *Electrophoresis* 2001, *22*, 801-813.

[5] Rice, C., Whitehead, R., *J. Phys. Chem.* 1965, *69*, 4017-4024.

[6] Giddings, J. C., *Unified Separation Science*, Wiley, New York 1991.

[7] Meighan, M. M., Staton, S. J. R., Hayes, M. A., *Electrophoresis* 2009, *30*, 852-565.

[8] Rodriguez-Diaz, R., Wehr, T., Zhu, M., *Electrophoresis* 1997, *18*, 2134-2144.

[9] Shackman, J. G., Munson, M. S., Ross, D., *Anal. Chem.* 2007, *387*, 155-158.

[10] Burke, J. M., Ivory, C. F., *Electrophoresis* 2008, *29*, 1013-1025.

[11] Meighan, M. M., Keebaugh, M. W., Quihuis, A. M., Kenyon, S. M., Hayes, M. A., *Electrophoresis* 2009, *30*, 3786-3792.

[12] Kenyon, S. M., Meighan, M. M., Hayes, M. A., *Electrophoresis* 2011, *32*, 482-493.

[13] Righetti, P. G., Drysdale, J. W., *J. Chromatogr.* 1974, *98*, 271-321.

[14] Just, W. W., *Methods Enzymol.* 1983, *91*, 281-298.

[15] Righetti, P. G., Bossi, A., *Anal. Biochem.* 1997, *247*, 1-10.

[16] Mao, Q., Pawllszyn, J., Thormann, W., *Anal. Chem.* 2000, *72*, 5493-5502.

[17] Sebastiano, R., Simo, C., Mendieta, M. E., Antonioli, P., Citterio, A., Cifuentes, A., Peltre, G., Righetti, P., *Electrophoresis* 2006, *27*, 3919.

[18] Svensson, H., *Acta Chem. Scand.* 1961, *15*, 325-341.

[19] Lilley, K. S., Razzaq, A., Dupree, P., *Curr. Opin. Chem. Biol.* 2002, *6*, 46-50.

[20] Issaq, H. J., Veenstra, T. D., *Biotechniques* 2008, *44*, 697.

[21] Ogden, R. C., A., A. D., *Methods Enzymol.* 1987, *152*, 61-87.

[22] Righetti, P. G., *Journal of Chromatography A* 2004, *1037*, 491-499.

[23] Hille, J. M., Freed, A. L., Watzig, H., *Electrophoresis* 2001, *22*, 4035-4052.

[24] Harper, S. B., Hurst, W. J., Lang, C. M., *J. Chromatogr. B.* 1994, *657*, 339-344.

[25] Horka, M., Ruzicka, F., Horky, J., Hola, V., Slais, K., *J. Chromatogr. B.* 2006, *841*, 152-159.

[26] Weiss, N. G., Zwick, N. L., Hayes, M. A., *J. of Chromatogr. A* 2010, *1217*, 179-182.

[27] Abdelgawad, M., Wheeler, A. R., *Adv. Mater.* 2009, *21*, 920-925.

[28] Garcia, A. A., Egatz-Gomez, A., Lindsay, S. A., Dominguez-Garcia, P., Melle, S., Marquez, M., Rubio, M. A., Picraux, S. T., Yang, D., Aella, P., Hayes, M. A., Gust, D., Loyprasert, S., Vazquez-Alvarez, T., Wang, J., *J. Magn. Magn. Mater.* 2007, *311*.

[29] Cooney, C. G., Chen, C.-Y., Emerling, M. R., Nadim, A., Sterling, J. D., *Microfluid. Nanofluid.* 2006, *2*, 435-446.

[30] Cho, S. K., Moon, H., Kim, C.-J., *J. Microelectromech. Syst.* 2003, *12*, 70-80.

[31] Sista, R. S., Eckhardt, A. E., Srinivasan, V., Pollack, M. G., Palanki, S., Pamula, V. K., *Lab Chip* 2008, *8*, 2188-2196.

[32] Lindsay, S. A., Vazquez-Alvarez, T., Egatz-Gomez, A., Loyprasert, S., Garcia, A. A., Wang, J., *Analyst* 2007, *132*, 412-416.

[33] Fan, S.-K., Huang, P.-W., Wang, T.-T., Peng, Y.-H., *Lab Chip* 2008, *8*, 1325-1331.

[34] Wang, Y., Zhao, Y., Cho, S. K., *J. Micromech. Microeng.* 2007, *17*, 2148-2156.

[35] Cygan, Z. T., T., C. J., Beers, K. L., Amis, E. J., *Langmuir* 2005, *21*, 3629-3634.

[36] Fair, R. B., *Microfluid. Nanofluidics* 2007, *3*, 245-281.

[37] Kang, Y., Li, D., Kalams, S. A., Eid, J. E., *Biomed. Microdevices* 2008, *10*, 243-249.

[38] Pysher, M. D., Hayes, M. A., *Anal. Chem.* 2007, *79*, 4552-4557.

CHAPTER 3

[1] Foret, F., Muller, O., Thorne, J., Gotzinger, W., Karger, B. L., *J. Chromatogr. A* 1995, *716*, 157-166.

[2] Chartogne, A., Gaspari, M., Jespersen, S., Buscher, B., Verheij, E., van der Heijden, R., Tjaden, U., van der Greef, J., *Rapid Commun. Mass Spectrom.* 2002, *16*, 201-207.

[3] Crowley, T. A., Hayes, M. A., *Proteomics* 2005, *5*, 3798-3804.

[4] Yu, W., Li, Y., Deng, C., Zhang, X., *Electrophoresis* 2006, *27*, 2100-2110.

[5] Lechner, M., Seifner, A., Rizzi, A. M., *Electrophoresis* 2008, *29*, 1974-1984.

[6] Silvertand, L. H. H., Toraño, J. S., de Jong, G. J., van Bennekom, W. P., *Electrophoresis* 2009, *30*, 1828-1835.

[7] Rodriquez-Diaz, R., Wehr, T., Zhu, M., *Electrophoresis* 1997, *18*, 2134-2144.

[8] Minarik, M., Groiss, F., Gas, B., Blaas, D., Kenndler, E., *J. Chromatogr. A* 1996, *738*, 123-128.

[9] Tang, Q., Harrata, A. K., Lee, C. S., *J. Mass Spectrom.* 1996, *31*, 1284-1290.

[10] Huang, T. L., Richards, M., *J. Chromatogr. A* 1997, *757*, 247-253.

[11] Suratman, A., Wätzig H., *J. Sep. Sci.* 2008, *31*, 1834-1840.

[12] Righetti, P. G., *J. Chromatogr. A* 2004, *1037*, 491-499.

[13] Silvertand, L. H. H., Toraño, J. S., de Jong, G. J., van Bennekom, W. P., *Electrophoresis* 2008, *29*, 1985-1996.

CHAPTER 4

[1] Pepys, M. B., Booth, D. R., Hutchinson, W. L., Gallimore, J. R., Collins, P. M., Hohenester, E., *Amyloid* 1997, *4*, 274-295.

[2] Pepys, M. B., Rademacher, T. W., Amatayakul-Chantler, S., Williams, P., Noble, G. E., Hutchinson, W. L., Hawkins, P. N., Nelson, S. R., Gallimore, J. R., Herbert, J., Hutton, T., Dwek, R. A., *Proc. Natl. Acad. Sci. USA* 1994, *91*, 5602-5606.

[3] Kubak, B. M., Gewurz, H., Potempa, L. A., *Int. Arch. Allergy Appl. Immunol.* 1988, *87*, 194-203.

[4] Serensen, I. J., Andersen, O., Nielsen, E. H., Svehag, S. E., *Int. Arch. Allergy Immunol.* 1995, *106*, 25-31.

[5] Nybo, M., Hackler, R., Kold, B., Nielsen, E. H., Steinmetz, A., Svehag, S. E., *Scand. J. Immunol.* 1998, *48*, 350-356.

[6] Kiernan, U. A., Nedelkov, D., Tubbs, K. A., Niederkofler, E. E., Nelson, R. W., *Proteomics* 2004, *4*, 1825-1829.

[7] Hawkins, P. N., Tennent, G. A., Woo, P., Pepys, M. B., *Clin. Exp. Immunol.* 1991, *84*, 308-316.

[8] Rodriguez-Diaz, R., Wehr, T., Zhu, M., *Electrophoresis* 1997, *18*, 2134-2144.

[9] Hille, J. M., Freed, A. L., Watzig, H., *Electrophoresis* 2001, *22*, 4035-4052.

[10] Silvertand, L. H. H., Torano, J. S., van Bennekom, W. P., de Jong, G. J., *J. Chromatogr. A* 2008, *1204*, 157-170.

[11] Wehr, T., *LCGC North America* 2004, *22*, 998-1004.

[12] Foret, F., Muller, O., Thorne, J., Gotzinger, W., Karger, B. L., *J. Chromatogr. A* 1995, *716*, 157-166.

[13] Chartogne, A., Gaspari, M., Jespersen, S., Buscher, B., Verheij, E., Heijden, v. d., Tjaden, U., van der Greef, J., *Rapid Commun. Mass Spectrom.* 2002, *16*, 201-207.

[14] Crowley, T. A., Hayes, M. A., *Proteomics* 2005, *5*, 3798-3804.

[15] Yu, W., Li, Y., Deng, C., Zhang, X., *Electrophoresis* 2006, *27*, 2100-2110.

[16] Lechner, M., Seifner, A., Rizzi, A. M., *Electrophoresis* 2008, *29*, 1974-1984.

[17] Silvertand, L. H. H., Torano, J. S., de Jong, G. J., van Bennekom, W. P., *Electrophoresis* 2009, *30*, 1828-1835.

[18] Weiss, N. G., Zwick, N. L., Hayes, M. A., *J. Chromatogr. A* 2010, *1217*, 179-182.

[19] Debeer, F. C., Pepys, M. B., *J. Immunol. Methods* 1982, *50*, 17-31.

[20] Niederkofler, E. E., Tubbs, K. A., Kiernan, U. A., Nedelkov, D., Nelson, R. W., *J. Lipid Res.* 2003, *44*, 630-639.

[21] Borges, C. R., Jarvis, J. W., Oran, P. E., Rogers, S. P., Nelson, R. W., *J. Biolmol. Tech.* 2008, *19*, 167-176.

[22] Prelli, F., Pras, M., Frangione, B., *J. Biol. Chem.* 1985, *260*, 12895-12898.

[23] Minarik, M., Groiss, F., Gas, B., Blaas, D., Kenndler, E., *J. Chromatogr. A* 1996, *738*, 123-128.

[24] Righetti, P. G., *J. Chromatogr. A* 2004, *1037*, 491-499.

[25] Ohkubo, I., Sahashi, W., Namikawa, C., Tsukada, K., Takeuchi, T., Sasaki, M., *Clin. Chim. Acta* 1986, *157*, 95-102.

[26] Urbanyi, Z., Medzihradszky, D., *J. Chromatogr.* 1992, *578*, 130-133.

[27] Yang, L., Tang, Q., Harrata, A. K., Lee, C. S., *Anal. Biochem.* 1996, *243*, 140-149.

[28] Loboda, A. V., Chernushevich, I. V., *Int. J. Mass Spectrom.* 2005, *240*, 101-105.

CHAPTER 5

[1] Stutz, H., *Electrophoresis* 2005, *26*, 1254-1290.

[2] Kussmann, M., Nordhoff, E., Rahbek-Nielsen, H., Haebel, S., Rossel-Larsen, M., Jakobsen, L., Gobom, J., Mirgorodskaya, E., Kroll-Kristensen, A., Palm, L., Roepstorff, P., *J. Mass Spectrom.* 1997, *32*, 593-601.

[3] Karas, M., Hillenkamp, F., *Anal. Chem.* 1988, *60*, 2299-2301.

[4] Xiang, F., Beavis, R. C., *Org. Mass Spectrom.* 1993, *28*, 1424-1429.

[5] Xiang, F., Beavis, R. C., *Rapid Commun. Mass Spectrom.* 1994, *8*, 199-204.

[6] Vorm, O., Roepstorff, P., Mann, M., *Anal. Chem.* 1994, *66*, 3281-3287.

[7] Xu, Y., Bruening, M. L., Watson, J. T., *Mass Spectrom. Rev.* 2003, *22*, 429-440.

[8] Cohen, S. L., Chait, B. T., *Anal. Chem.* 1996, *68*, 31-37.

[9] Gluckmann, M., Pfenninger, A., Kruger, R., Thierolf, M., Karas, M., Horneffer, V., Hillenkamp, F., Stupat, K., *Int. J. Mass Spectrom.* 2001, *210*, 121-132.

[10] Chang, W. C., Huang, L. C. L., Wang, Y.-S., Peng, W.-P., Chang, H. C., Hsu, N. Y., Yang, W. B., Chen, C. H., *Anal. Chim. Acta* 2007, *582*, 1-9.

[11] Garden, R. W., Sweedler, J. V., *Anal. Chem.* 2000, *72*, 30-36.

[12] Tu, T., Gross, M. L., *Trends Analyt. Chem.* 2009, *28*, 833-841.

[13] Tu, T., Sauter Jr, A. D., Sauter, A. D., Gross, M. L., *Am. Soc. Mass Spectrom.* 2008, *19*, 1086-1090.

[14] Bogan, M., J., Agnes, G. R., *J. Am. Soc. Mass Spectrom.* 2004, *15*, 486-495.

[15] Little, D. P., Cornish, T. J., O'Donnell, M., J., Braun, A., Cotter, R. J., Koster, H., *Anal. Chem.* 1997, *69*, 4540-4546.

[16] Ekström, S., Ericsson, D., Önnerfjord, P., Bengtsson, M., Nilsson, J., Marko-Varga, G., Laurell, T., *Anal. Chem.* 2001, *73*, 214-219.

[17] Gundry, R. L., Edward, R., Kole, T. P., Sutton, C., Cotter, R. J., *Anal. Chem.* 2006, *77*, 6609-6617.

[18] Schuerenberg, M., Luebbert, C., Elckhoff, H., Kalkum, M., Lehrach, H., Nordhoff, E., *Anal. Chem.* 2000, *72*, 3436-3442.

[19] Wang, J., Chen, R., Ma, M., Li, L., *Anal. Chem.* 2008, *80*, 491-500.

[20] Choi, C. H., Kim, C.-J., *Langmuir* 2009, *25*, 7561-7567.

[21] Baird, J. K., *J. Cryst. Growth* 1999, *204*, 553-562.

[22] McLauchlin, M. L., *Chemistry and Biochemistry*, Arizona State University, Tempe 2007, p. 138.

[23] McLauchlin, M. L., Yang, D., Aella, P., Garcia, A. A., Picraux, S. T., Hayes, M. A., *Langmuir* 2007, *23*, 4871-4877.

[24] Brandt, H., Ehmann, T., *Anal. Chem.* 2010, *82*, 8169-8175.

CHAPTER 6

[1] Cesaro-Tadic, S., Dermick, G., Juncker, D., Bourman, G., Kropshofer, H., Michel, B., Fattinger, C., Delamarche, E., *Lab Chip* 2004, *4*, 563-569.

[2] Blazej, R. G., Kumaresan, P., Mathies, R. A., *PNAS* 2006, *103*, 7240-7245.

[3] Fu, J., Schoch, R. B., Stevens, A. L., Tannenbaum, S. R., Han, J., *Nat. Nanotechnol.* 2007, *2*, 121-128.

[4] Srisa-Art, M., Dyson, E. C., deMello, A. J., Ede, J. B., *Anal. Chem.* 2008, *80*, 7063-7067.

[5] Unger, M. A., Chou, H.-P., Thorsen, T., Scherer, A., Quake, S. R., *Science* 2000, *288*, 113-116.

[6] Srinivasan, V., Pamula, V. K., Fair, R. B., *Lab Chip* 2004, *4*, 310-315.

[7] Teh, S.-Y., Lin, R., Hung, L.-H., Lee, A. P., *Lab Chip* 2008, *8*, 198-220.

[8] Fair, R. B., *Microfluid. Nanofluidics* 2007, *3*, 245-281.

[9] Cho, S. K., Zhao, Y., Jin, C., Kim, C., *Lab Chip* 2007, *7*, 490-498.

[10] Fan, S.-K., Huang, P.-W., Wang, T.-T., Peng, Y.-H., *Lab Chip* 2008, *8*, 1325-1331.

[11] Zhao, Y., Yi, U.-C., Cho, S. K., *J. Microelectromech. Syst.* 2007, *6*, 1472-1481.

[12] Sista, R. S., Eckhardt, A. E., Srinivasan, V., Pollack, M. G., Palanki, S., Pamula, V. K., *Lab Chip* 2008, *8*, 2188-2196.

[13] Wang, Y., Zhao, Y., Cho, S. K., *J. Micromech. Microeng.* 2007, *17*, 2148-2156.

[14] Wheeler, A. R., Jebrail, M. J., *Anal. Chem.* 2009, *81*, 330-335.

[15] Abdelgawad, M., Watson, M. W. L., Wheeler, A. R., *Lab Chip* 2009, *9*, 1046-1051.

[16] Schneider, J., Egatz-Gomez, A., Melle, S., Lindsay, S. A., Dominguez-Garcia, P., Rubio, M. A., Marquez, M., Garcia, A. A., *Colloids Surf. A Physiochem. Eng. Asp.* 2008, *323*, 19-27.

[17] Righetti, P., Drysdale, J., *J. Chromatogr.* 1974, *98*, 271-321.

[18] Rodriguez-Diaz, R., Wehr, T., Zhu, M., *Electrophoresis* 1997, *18*, 2134-2144.

[19] Svensson, H., *Acta Chem. Scand.* 1961, *15*, 325-341.

[20] Chu, B., *Laser Light Scattering: Basic Principles and Practice*, Academic Press, New York 1991.

[21] Ansari, R. R., *J. Biomed. Optics* 2004, *9*, 22-37.

[22] Egatz-Gomez, A., Melle, S., Garcia, A. A., Lindsay, S. A., Marquez, M., Dominguez-Garcia, P., Rubio, M. A., Picraux, S. T., Taraci, J. L., Clement, T., Yang, D., Hayes, M., Gust, D., *Appl. Phys. Lett.* 2006, *89*, 034106.

[23] Garcia, A. A., Egatz-Gomez, A., Lindsay, S. A., Dominguez-Garcia, P., Melle, S., Marquez, M., Rubio, M. A., Picraux, S. T., Yang, D., Aella, P., Hayes, M. A., Gust, D., Loyprasert, S., Vazquez-Alvarez, T., Wang, J., *J. Magn. Magn. Mater.* 2007, *311*.

[24] Lindsay, S. A., Vazquez-Alvarez, T., Egatz-Gomez, A., Loyprasert, S., Garcia, A. A., Wang, J., *Analyst* 2007, *132*, 412-416.

[25] McLauchlin, M. L., Yang, D., Aella, P., Garcia, A. A., Picraux, S. T., Hayes, M. A., *Langmuir* 2007, *23*, 4871-4877.

[26] Li, X.-M., Reinhoudt, D., Crego-Calama, M., *Chem. Soc. Rev.* 2007, *36*.

[27] Roach, P., Shirtcliffe, N. J., Newton, M. I., *Soft Matter* 2008, *4*.

[28] Erbil, H. Y., Demirel, A. L., Avci, Y., Mert, O., *Science* 2003, *299*, 1377-1380.

[29] Lu, X., Zhang, C., Han, Y., *Macromol. Rapid Commun.* 2004, *25*, 1606-1610.

[30] Ansari, R. R., Suh, K. I., Arabshai, A., Wilson, W., Bray, T. L., DeLucas, L. J., *J. Cryst. Growth* 1996, *168*, 216-226.

[31] Leung, A. B., Suh, K. I., Ansari, R. R., *Appl. Opt.* 2006, *45*, 2186-2190.

[32] Simpanya, M. F., Ansari, R. R., *J. Photochem. and Photobiol.* 2008, *84*, 1589-1595.

[33] Datiles, M. B., Ansari, R. R., Suh, K. I., Vitale, S., Reed, G. F., Zigler, J. S., Ferris, F. L., *Arch. Ophthalmol.* 2008, *126*.

[34] Macounova, K., Cabrera, C. R., Holl, M. R., Yager, P., *Anal. Chem.* 2000, *72*, 3745-3751.

[35] Cabrera, C. R., Finlayson, B., Yager, P., *Anal. Chem.* 2001, *73*, 658-666.

[36] Klimov, A., Pollack, G. H., *Langmuir* 2007, *23*, 11890-11895.

[37] Mosher, R. A., Thormann, W., *Electrophoresis* 1990, *11*, 717-723.

[38] Sebastiano, R., Simo, C., Mendieta, M. E., Antonioli, P., Citterio, A., Cifuentes, A., Peltre, G., Righetti, P., *Electrophoresis* 2006, *27*, 3919.

[39] Weiss, N. G., Zwick, N. L., Hayes, M., *J. Chromatogr. A* 2010, *1217*, 179-182.

CHAPTER 7

[1] Lapizco-Encinas, B. H., Rito-Palomares, M., *Electrophoresis* 2007, *28*, 4521-4538.

[2] Zhang, C., Khoshmanesh, K., Mitchell, A., Kalantar-zadeh, K., *Anal. Bioanal. Chem.* 2010, *396*, 401-420.

[3] Pohl, H. A., *J. Appl. Phys.* 1951, *22*, 869-871.

[4] Pethig, R., *Biomicrofluidics* 2010, *4*, 022811.

[5] Cummings, E. B., Singh, A. K., *Anal. Chem.* 2003, *75*, 4724-4731.

[6] Martinez-Lopez, J. I., Moncada-Hernandez, H., Baylon-Cardiel, J. L., Martinez-Chapa, S. O., Rito-Palomares, M., Lapizco-Encinas, B. H., *Anal. Bioanal. Chem.* 2009, *394*, 293-302.

[7] Kwon, J.-S., Maeng, J.-S., Chun, M.-S., Song, S., *Microfluid. Nanofluid.* 2008, *5*, 23-31.

[8] Lapizco-Encinas, B. H., Simmons, B. A., Cummings, E. B., Fintschenko, Y., *Anal. Chem.* 2004, *76*, 1571-1579.

[9] Baylon-Cardiel, J. L., Lapizco-Encinas, B. H., Reyes-Betanzo, C., Chavez-Santoscoy, A. V., Martinez-Chapa, S. O., *Lab Chip* 2009, *9*, 2896-2901.

[10] Mela, P., van den Berg, A., Fintschenko, Y., Cummings, E. B., Simmons, B. A., Kirby, B. J., *Electrophoresis* 2005, *26*, 1792-1799.

[11] Ozuna-Chacon, S., Lapizco-Encinas, B. H., Rito-Palomares, M., Martinez-Chapa, S. O., Reyes-Betanzo, C., *Electrophoresis* 2008, *29*, 3115-3122.

[12] Cummings, E. B., *IEEE Engineering in Medicine and Biology Magazine* 2003, *Nov/Dec*, 75-84.

[13] Lapizco-Encinas, B. H., Simmons, B. A., Cummings, E. B., Fintschenko, Y., *Electrophoresis* 2004, *25*, 1695-1704.

[14] Lapizco-Encinas, B. H., Davalos, R. V., Simmons, B. A., Cummings, E. B., Fintschenko, Y., *J. Microbiol. Methods* 2005, *62*, 317-326.

[15] Ozuna-Chacon, S., Lapizco-Encinas, B. H., Rito-Palomares, M., Collado-Arredondo, E., Martinez-Chapa, S. O., *Revista Mexicana De Ingenieria Quimica* 2007, *6*, 329-335.

[16] Lapizco-Encinas, B. H., Ozuna-Chacon, S., Rito-Palomares, M., *J. Chromatogr. A* 2008, *1206*, 45-51.

[17] Gallo-Villanueva, R. C., Rodriguez-Lopez, C. E., Diaz-de-la-Garza, R. I., Reyes-Betanzo, C., Lapizco-Encinas, B. H., *Electrophoresis* 2009, *30*, 4195-4205.

[18] Moncada-Hernandez, H., Lapizco-Encinas, B. H., *Anal. Bioanal. Chem.* 2010, *396*, 1805-1816.

[19] Davalos, R. V., McGraw, G. J., Wallow, T. I., Morales, A. M., Krafcik, K. L., Fintschenko, Y., Cummings, E. B., Simmons, B. A., *Anal. Bioanal. Chem.* 2008, *390*, 847-855.

[20] Hawkins, B. G., Smith, A. E., Syed, Y. A., Kirby, B. J., *Anal. Chem.* 2007, *79*, 7291-7300.

[21] Kang, Y., Li, D., Kalams, S. A., Eid, J. E., *Biomed. Microdevices* 2008, *10*, 243-249.

[22] Kang, K. H., Xuan, X., Kang, Y., Li, D., *J. Appl. Phys.* 2006, *99*, 064702.

[23] Kang, K. H., Kang, Y., Xuan, X., Li, D., *Electrophoresis* 2006, *27*, 694-702.

[24] Barrett, L. M., J., S. A., Singh, A. K., Cummings, E. B., Fiechtner, G. J., *Anal. Chem.* 2006, *77*, 6798-6804.

[25] Barbulovic-Nad, I., Xuan, X., Lee, J. S. H., Li, D., *Lab Chip* 2006, *6*, 274-279.

[26] Lewpiriyawong, N., Yang, C., Lam, Y. C., *Biomicrofluidics* 2008, *2*, 034105.

[27] Zhu, J., Tzeng, T.-R. J., Hu, G., Xuan, X., *Microfluid. Nanofluid.* 2009, *7*, 751-756.

[28] Church, C., Zhu, J., Nieto, J., Keten, G., Ibarra, E., Xuan, X., *J. Micromech. Microeng.* 2010, *20*, 065011.

[29] Pysher, M. D., Hayes, M. A., *Anal. Chem.* 2007, *79*, 4552-4557.

[30] Staton, S. J. R., Chen, K. P., Taylor, T. J., Pacheco, J. R., Hayes, M. A., *Electrophoresis* 2010, *31*, 3634-3641.

[31] Chen, K. P., Pacheco, J. R., Hayes, M. A., Staton, S. J. R., *Electrophoresis* 2009, *30*, 1441-1448.

[32] Ai, Y., Joo, S. W., Jiang, Y., Xuan, X., Qian, S., *Electrophoresis* 2009, *30*, 2499-2506.

[33] Ai, Y., Qian, S., Liu, S., Joo, S. W., *Biomicrofluidics* 2010, *4*, 013201.

[34] Kirby, B. J., Hawkins, B. G., *Electrophoresis* 2010, *31*, 3622-3633.

[35] Jen, C.-P., Huang, C.-T., Shih, H.-Y., *Microsyst. Technol.* 2010, *16*, 1097-1104.

[36] Ros, A., Hellmich, W., Regtmeier, J., Duong, T. T., Anselmetti, D., *Electrophoresis* 2006, *27*, 2651-2658.

[37] Regtmeier, J., Duong, T. T., Eichhom, R., Anselmetti, D., Ros, A., *Anal. Chem.* 2007, *79*, 3925-3932.

[38] Chou, C.-F., Tegenfeldt, J. O., Bakajin, O., Chan, S., S., Cox, E. C., Darnton, N., Duke, T., Austin, R. H., *Biophys. J.* 2002, *83*, 2170-2179.

[39] Shafiee, H., Sano, M. B., Henslee, E. A., Caldwell, J. L., Davalos, R. V., *Lab Chip* 2010, *10*, 438-445.

[40] Shafiee, H., Caldwell, J. L., Sano, M. B., Davalos, R. V., *Biomed. Microdevices* 2009, *11*, 997-1006.

[41] Winter, W. T., Welland, M. E., *J. Phys. D: Appl. Phys.* 2009, *42*, 045501.

[42] Ai, Y., Qian, S., *J. Colloid Interface Sci.* 2010, *346*, 448-454.

[43] Tsukahara, S., Sakamoto, T., Watarai, H., *Langmuir* 2000, *16*, 3866-3872.

[44] Washizu, M., Jones, T. B., *J. Electrostat.* 1994, *33*, 187-198.

[45] Watarai, H., Sakamoto, T., Tsukahara, S., *Langmuir* 1997, *13*, 2417-2420.

[46] Ikeda, I., Monjushiro, H., Watarai, H., *Analyst* 2005, *130*, 1340-1342.

[47] Kuokkanen, M. H., *Cent. Eur. J. Phys.* 2010, *8*, 178-183.

[48] Mahanti, P., Taylor, T., Hayes, M. A., *Microfluid. Nanofluid.* 2011, In Preparation, Available at: http://www.public.asu.edu/~mhayes/.

[49] Humble, P. H., Kelly, R. T., Woolley, A. T., Tollety, D. H., Lee, M. L., *Anal. Chem.* 2004, *76*, 5641-5648.

[50] Yan, D., Yang, C., Nguyen, N.-T., Huang, X., *Electrophoresis* 2006, *27*, 620-627.

[51] Jones, H. K., Ballou, N. E., *Anal. Chem.* 1990, *62*, 2484-2490.

[52] Petersen, S. L., Ballou, N. E., *Anal. Chem.* 1992, *64*, 1676-1681.

[53] Badal, Y. M., Wong, M., Chiem, N., Salimi-Moosavi, H., Harrison, D. J., *J. Chromatogr. A* 2002, *947*, 277-286.

CHAPTER 8

[1] Martinez-Lopez, J. I., Moncada-Hernandez, H., Baylon-Cardiel, J. L., Martinez-Chapa, S. O., Rito-Palomares, M., Lapizco-Encinas, B. H., *Anal. Bioanal. Chem.* 2009, *394*, 293-302.

[2] Righetti, P. G., *J. Chromatogr. A* 2004, *1037*, 491-499.

[3] Weiss, N. G., Zwick, N. L., Hayes, M. A., *J. Chromatogr. A* 2010, *1217*, 179-182.

[4] Zenker, A., Galanski, M., Bereuter, T. L., Keppler, B. K., Lindner, W., *J. Chromatogr. B* 2000, *745*, 211-219.

[5] Jones, P. V., Staton, S. J. R., Hayes, M. A., *Anal. Bioanal. Chem.* 2011, *401*, 2103-2111.

APPENDIX A

PUBLISHED PORTIONS

Chapters 3, 4, 6, and 7 were previously published in the journals referenced below:

Weiss, N. G., Zwick, N. L., Hayes, M. A., *J. Chromatogr. A*, 2010, *1217*, 179-182.

Weiss, N. G., Jarvis, J. W., Nelson, R. W., Hayes, M. A., *Proteomics*, 2011, *11*, 106-113.

Weiss, N. G., Hayes, M. A., Garcia, A. A., Ansari, R. R., *Langmuir*, 2011, *27*, 494-498.

Weiss, N. G., Jones, P. J., Mahanti, P., Taylor, T., Hayes, M. A. *Electrophoresis*, 2011, *32*, 2292-2297.

Published portions were included with the permission of all co-authors.